

# The Bose-Hubbard model with disorder in low-dimensional lattices



SCUOLA INTERNAZIONALE  
SUPERIORE di STUDI AVANZATI  
International School  
for Advanced Studies

Candidate: Juan Felipe Carrasquilla Álvarez  
Supervisors: Dr. Federico Becca and Prof. Michele Fabrizio

A thesis submitted for the degree of

*Doctor Philosophiæ*

October 2010

---

# Contents

<b>Introduction</b>	<b>iii</b>
<b>1 Ultracold atoms on optical lattices and the dirty boson problem</b>	<b>1</b>
1.1 Optical lattices . . . . .	1
1.2 Ultracold atoms in optical lattices and the Bose-Hubbard Model .	8
1.3 Introducing disorder . . . . .	12
1.4 Large rare homogeneous patches in disordered systems . . . . .	14
1.5 Experiments on disordered bosons . . . . .	18
<b>2 The variational approach</b>	<b>27</b>
2.1 The Gutzwiller wave function for the Bose-Hubbard model . . . . .	28
2.2 The Jastrow wave function and the variational Monte Carlo . . . . .	30
2.3 The stochastic reconfiguration method . . . . .	36
2.4 The Green's function Monte Carlo method . . . . .	41
2.4.1 Importance Sampling . . . . .	43
2.4.2 Forward walking technique . . . . .	45
2.4.3 Many walkers formulation . . . . .	46
2.4.4 The superfluid stiffness . . . . .	48
<b>3 The Bose-glass phase in low-dimensional lattices</b>	<b>50</b>
3.1 The Bose-glass phase . . . . .	51
3.2 Model . . . . .	52
3.3 Results . . . . .	54
3.4 Disordered spinless fermions in a staggered ionic potential . . . . .	64
3.5 Conclusions . . . . .	68

<b>4</b>	<b>The onset of superfluidity of hardcore bosons in disordered ladders</b>	<b>70</b>
4.1	Hardcore bosons in presence of disorder in low dimensions . . . . .	71
4.2	Model and results . . . . .	73
4.2.1	The clean case . . . . .	75
4.2.2	Introduction of disorder . . . . .	76
4.3	Conclusions . . . . .	84
<b>5</b>	<b>Extracting the Mott gap from energy measurements in trapped atomic gases</b>	<b>85</b>
5.1	The formation of a Mott insulator in experiments with cold atoms	86
5.2	Model and Method . . . . .	88
5.3	Results . . . . .	90
5.4	Conclusion . . . . .	97
<b>6</b>	<b>Conclusions and perspectives</b>	<b>99</b>
	<b>References</b>	<b>112</b>

# Introduction

In 1958, P.W. Anderson conceived the revolutionary idea that the wave function of a particle in certain random lattices could become localized. [1] Even though the original idea of localization was introduced within the context of spin systems, the subsequent theoretical efforts were mainly concentrated on the localization properties of the electron wave function diffusing into a disordered lattice. In this context, Anderson's results meant that for sufficiently strong disorder the electron wave function at the chemical potential becomes localized, turning metals into insulators, after him called Anderson insulators. There are by now plenty of experimental evidences of Anderson's localization phenomenon in amorphous semiconductors, [2] in light-wave experiments, [3, 4] microwaves, [5] sound waves, [6] and electron gases. [7]

Although the initial Anderson's motivation was diffusion in spin systems, which are equivalent to hardcore bosons, [8] most of the interest was focused on electron localization. The bosonic counterpart had received much less attention until 1980's, when experiments revealed the importance of studying the competition between disorder and superfluidity, the so-called dirty boson problem. Perhaps the earliest relevant experiments were on superfluidity of thin helium films,  $^4\text{He}$  adsorbed in porous Vycor glass, granular thin film superconductors and disordered Josephson arrays. Such experiments motivated a lot of theoretical work. The phase diagram was conjectured in seminal papers by Fisher *et al.* and Giamarchi and Schulz, [9, 10] which, in turn, motivated further numerical as well as analytical works. The situation with bosons is particularly dramatic, since the non-interacting limit is pathological due to the statistics of bosons. Indeed, all bosons with no interaction get localized in the vicinity of a small portion of space corresponding to the deepest minimum of the random potential, leading to

---

a non-thermodynamic phase with infinite density in a finite region of space. This implies that there is no sensible non-interacting starting point about which to perturb. In fact, as soon as interaction is switched on, that state can not survive and the particles are redistributed in space leading to a stable thermodynamic phase. Therefore, interaction has to be introduced from the very beginning in order to get a sensible theoretical description of the system. In their original paper, Fisher *et al.* argued that bosons hopping on a lattice with short-range repulsive interaction subject to a random bounded potential have three possible ground states: 1) an incompressible Mott insulator with a density of bosons commensurate with the lattice and a gap for particle-hole excitations, 2) a superfluid state with off-diagonal long-range order (or quasi-long-range order in one dimension); and 3) a gapless Bose-glass phase, which is an insulator with exponentially decaying superfluid correlations but compressible. Furthermore, it was conjectured that the localized Bose-glass phase should always intervene between the superfluid and Mott insulator. However, subsequent numerical as well as analytical results were controversial and some supported the initial ideas by Fisher *et al.* while some others contradicted it. [11, 12, 13, 14, 15, 16, 17, 18]

Although the problem of disordered bosons has been now extensively studied during the last 20 years and important aspects of the problem are well clarified, some open issues remained, like a precise determination of the phase diagram and a proper characterization and understanding of the emerging phases. Even though there were some experimental realizations of interacting dirty bosons, the difficulties in obtaining bosons in a controlled disordered environment left aside some open issues. Much more recently, with the advent of cold atoms the discussion of the dirty boson problem have gained renewed interest and become lively. Unlike in realistic materials, experiments with cold Fermi and Bose atoms trapped in optical lattices provide a good opportunity to realize simple low-energy models that have been largely considered in condensed-matter physics with an almost perfect control of the Hamiltonian parameters by external fields. Therefore, experimental realizations of lattice models as the Bose and Fermi Hubbard models, which are believed to capture the essential physics underneath important phenomena, such as, for example, superfluidity or the Mott metal-insulator transition, have been experimentally realized with unprecedented control of the

---

environment. One of the first successes of these experiments has been the observation of a superfluid to Mott insulator transition in bosonic atoms trapped in optical lattices upon varying the relative strengths of interaction and interwell tunneling. [19] The possibility of introducing and tuning disorder was then exploited, through speckles or additional incommensurate lattices, and it also led to the observation of Anderson localization for weakly interacting Bose gases in optical lattices. [20, 21] These important achievements progressively opened the way towards the challenging issue of realizing and studying a Bose-Hubbard model in the presence of disorder and interaction. [22, 23].

This thesis focuses on the the Bose-Hubbard model in presence of disorder from a theoretical point of view using numerical simulations mainly based on quantum Monte Carlo. We consider variational Monte Carlo, [24, 25] using a variational wave function based on a translational invariant density-density Jastrow factor applied to a state where all bosons are condensed at  $q = 0$ , and on top of that we add a one-body local term which accounts for the effect of the on-site disorder. The flexibility of this variational state makes it possible to describe superfluid, Bose-glass, and Mott-insulating states. We also consider Green's function Monte Carlo, [26, 27] a zero-temperature algorithm that provides numerically exact results because of the absence of sign problem for this particular problem. In that method, one starts from a trial (e.g., variational wave function) and filters out high-energy components by iterative statistical applications of the imaginary-time evolution operator. By using these two methods, we investigate the properties of the Bose-glass phase and the superfluid to insulator transition in several low-dimensional geometries. Particularly, we show that a proper characterization of the phase diagram on finite disordered clusters requires the knowledge of probability distributions of physical quantities rather than their averages. This holds in particular for determining the stability region of the Bose-glass phase, where the finite compressibility arises due to exponentially rare regions which make its detection on finite clusters unlikely. However, by determining the distribution probability of the gap on finite sizes, we show that Bose glass intervenes between the superfluid and Mott insulator and it is characterized by a broad distribution of the gap that is peaked at finite energy but extends down to zero (hence compressible), a shape remarkably reminiscent of preformed

---

Hubbard sidebands with the Mott gap completely filled by Lifshitz's tails. This result suggests that a similar statistical analysis should be performed also to interpret experiments on cold gases trapped in disordered lattices, limited as they are to finite sizes. A similar approach is also used to study the ground-state properties of a system of hardcore bosons on a disordered two-leg ladder. However, measuring the distribution probability of the gap poses several challenges when quantitatively comparing experimental data and theoretical results. Particularly, one relevant experimental issue comes from the inevitable spatial inhomogeneities induced by the optical trap, which is necessary to confine particles. With that in mind, we devise a method which in principle should allow the possibility to extract the value of the Mott gap from energetic measurements of confined systems only. For the sake of simplicity, we test our idea using an insightful variational approach based upon the Gutzwiller wave function in one- and two-dimensional trapped bosonic systems. However, similar results must hold also in fermionic systems and bosons in any dimension because the superfluid to Mott-insulator transition occurs in any dimension accompanied by the opening of a gap in the spectrum, even at the mean-field level.

## Overview

This thesis is divided in 5 main chapters:

**Chapter 1** In this chapter, the problem of interacting atoms on optical lattices is introduced, emphasizing that these systems constitute an almost perfect realization of simple low-energy models extensively used in condensed matter physics. The main experimental realizations of the Bose-Hubbard model are discussed both in the clean and disordered case and we provide insight on the nature of the phase diagrams of such models based on simple arguments.

**Chapter 2** The variational approach is explained by introducing the Gutzwiller wave function. The Gutzwiller approach is extended in order to include spatial correlations by supplementing it with a long-range Jastrow wave function. We extend the variational approach to study disordered systems

---

and explain how to optimize the wave functions by mean of the stochastic reconfiguration technique. Finally, the Green's Function Monte Carlo technique is described.

**Chapter 3** In this chapter we discuss the emergence of the Bose-glass phase in low-dimensional lattices by means of the variational and Green's function Monte Carlo techniques. We show that a proper characterization of the phases on finite disordered clusters requires the knowledge of probability distributions of physical quantities rather than their averages.

**Chapter 4** In this chapter we discuss the effect of disorder on the zero-temperature phase diagram of a two-leg ladder of hardcore bosons using numerical simulations. We analyze the low-density regime of the phase diagram in presence of disorder and find an intervening Bose-glass phase between the frozen Mott insulator with one or zero particles per site and the superfluid phase. We also discussed the effect of disorder on the rung Mott insulator which is a gapped phase occurring exactly at half filling. We argue, based on numerical and single-particle arguments, that this gapped phase is always surrounded by the Bose glass.

**Chapter 5** In this chapter we show that the measurement of the so-called release energy makes it possible to assess the value of the Mott gap in the presence of the confinement potential in experiments with cold atoms. We analyze two types of confinement, the usual harmonic confinement and the recently introduced off-diagonal confinement in which the kinetic energy of the particles is varied across the lattice, being maximum at the center of the lattice and vanishing at its edges, which naturally induces a trapping of the particles.

# Chapter 1

## Ultracold atoms on optical lattices and the dirty boson problem

In this chapter, the problem of interacting atoms on optical lattices is introduced, emphasizing that these systems constitute an almost perfect realization of long-standing models extensively used in condensed matter and statistical physics. The way optical lattices are created and how the particles are loaded onto the lattices are briefly explained. The main experimental realizations of the Bose-Hubbard model using ultracold atoms are discussed, together with the description of some of the experimental techniques used to detect the emerging phases of the system. Furthermore, the way disorder is introduced on top of the clean optical lattice is described in detail, and its effect on the phase diagram of the Bose-Hubbard model is discussed from a theoretical perspective based on known arguments. Finally, we explain recent experimental realizations of bosonic systems in which disorder plays a crucial role and the physics of the system is captured by the disordered Bose-Hubbard model.

### 1.1 Optical lattices

Real solid state materials are incredibly complex. Their main constituents, the nuclei and electrons, are assembled in an intricate complex way and even though

we do know how they mutually interact, the behavior of the resulting assembly of particles cannot generally be anticipated. A complicated band structure of the underlying crystal, Coulomb interaction among electrons, lattice vibrations, disorder and impurities on the crystal are, in many cases, relevant for a comprehensive description of the physics of condensed matter systems. More the rule than the exception, taking into account all these effects in a theory at once is yet hardly possible. Not to mention how hard it is to single out which effects are relevant in a particular physical situation and which are not, especially when interpreting the outcome of experiments. As a particular example of the complexity of condensed matter systems, we have the high-temperature superconductors. After more than twenty years of intensive research the origin of high-temperature superconductivity is still not clear. The subtle interplay between Coulomb interaction, spin fluctuations, charge fluctuations, crystal and band structure give rise to the underlying cooper pairs which are responsible for superconductivity. In deep connection with the description of phenomena in real materials, several topics and questions are at the interface between condensed matter physics and the physics of ultracold atoms loaded on optical lattices. Indeed, recent remarkable advances in the area of ultracold atomic gases have given birth to a field in which condensed matter physics is studied with atoms and light. It has now opened a way towards the creation of an artificial crystal of quantum matter, with complete control over the periodic crystal potential. The shape of the periodic potential, its depth and the interactions among the particles that have been introduced on top of the lattices can be changed with a high degree of control and the particles could be moved around in a very controlled way. [28] An optical lattice provides precisely that possibility: it is a crystal formed by interfering laser beams, with a typical dimension about 1000 times larger than that of a conventional crystal but imperfection-free and no lattice vibrations. The particles in the lattice play the role of electrons in the solid; they tunnel across lattice sites just as single electrons tunnel through a real solid. All these things are possible because neutral atoms can be trapped in the periodic intensity pattern of light created by the coherent interference of laser beams. The light field of the interference pattern induces an electric dipole moment in the atoms of the ultracold gas, modifying their energy via the A.C. Stark shift, also known as the "light shift". [29] The induced dipole

moment of the atom, in turn, interacts at the same time with the electric field which creates a trapping potential  $V_{dip}(\mathbf{r})$ :

$$V_{dip}(\mathbf{r}) = -\mathbf{d} \cdot \mathbf{E}(\mathbf{r}) \propto \alpha(\omega) |\mathbf{E}(\mathbf{r})|^2 \quad (1.1)$$

Here  $\alpha(\omega)$  denotes the polarizability of an atom and  $I(\mathbf{r}) \propto |\mathbf{E}(\mathbf{r})|^2$  characterizes the intensity of the laser light field, with  $\mathbf{E}(\mathbf{r})$  its electric field amplitude at position  $\mathbf{r}$ . [29] The electric field will have a certain oscillatory spatial behavior such that the intensity mimics the periodic structure of a crystal. The laser light frequency  $\omega$  is usually tuned far away from an atomic resonance frequency, such that spontaneous emission effects from resonant excitations can be neglected and the resulting dipole potential is purely conservative in nature. It can be attractive for laser light with a frequency  $\omega$  smaller than the atomic resonance frequency  $\omega_0$ , or repulsive for a laser frequency larger than the atomic resonance frequency. Therefore, depending on the frequency of the light, atoms are pulled towards either the bright (red detuning) or the dark regions (blue detuning) and are consequently confined in space at the minima of the potential due to the interference pattern of the lasers. The strength of the confinement is proportional to the laser's intensity along its propagation. By using additional lasers from different directions, two- or even three-dimensional lattice structures can be constructed, as well as different geometries by varying the angle between the lasers as in Fig. 1.1 (taken from Ref. [28]). Rectangular, triangular, hexagonal and even Kagomé lattices have been explored using interfering lasers. [30, 31] Introducing the cold atoms onto the optical lattice is carried out by initially trapping the atoms in a magnetic trap that confines the system, followed by the lowering of the temperature by evaporative cooling technique. In this technique, the hottest atoms are selectively removed from the system and the remaining ones rethermalize via two-body collisions. After that, one slowly ramps up the lasers to create the periodic lattice potential, and the atoms reorder to adapt to their new environment. Similarly, the whole lattice can be removed from the atoms simply by ramping down the lasers, thus liberating the atoms into free space once more. [28] While in the trapped system without the lattice the cold gases are dilute and mean-field theory provides a useful framework to study the role of the interaction between particles, with the optical lattice switched on the

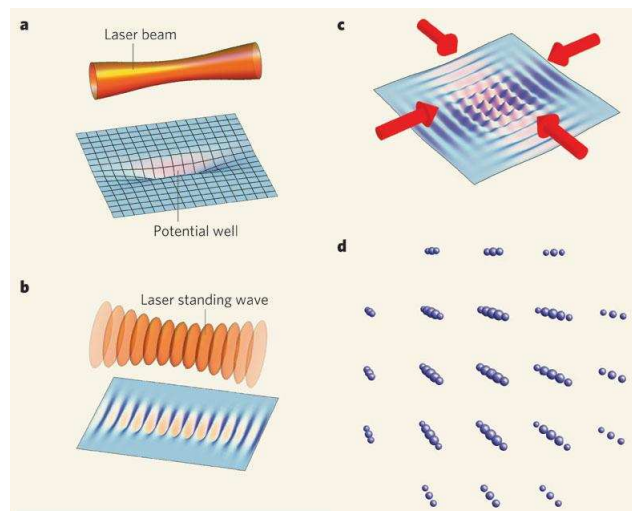


Figure 1.1: Potential landscapes of optical lattices. a) Laser light creates a repulsive or an attractive potential. b) By allowing two counter-propagating laser beams to interfere, a sinusoidal standing wave can be formed. c), d), Adding more laser beams at right angles to the first one creates a two-dimensional (c) and finally a three-dimensional cubic lattice (d).

kinetic energy is heavily quenched and the strongly correlated regime can be accessed where the effects of interaction are very much enhanced. Therefore, by combining the optical lattice with magnetically trapped atoms, it is possible to study a very broad class of many-body systems such as interacting bosons and fermions in several geometries and dimensions, avoiding difficulties encountered in real materials or introducing their complicated effects in a highly controlled way such that a better understanding of complex quantum-mechanical physical phenomena can be reached.

### **Feshbach resonance: Independent control of interactions in ultracold gases**

The most direct way of reaching strong interaction regime in dilute, ultracold gases are Feshbach resonances, which allow to increase the scattering length beyond the average interparticle spacing. [32] Quite generally, a Feshbach resonance in a two-particle collision appears whenever a bound state in a closed channel is coupled resonantly with the scattering continuum of an open channel. The two channels may correspond, for example, to different spin configurations for atoms. The scattered particles are then temporarily captured in the quasibound state, and the associated long-time delay gives rise to a resonance in the scattering cross section. [32] For instance, by the simple change of a magnetic field, the interactions between atoms can be controlled over an enormous range. This tunability arises from the coupling of free unbound atoms to a molecular state in which the atoms are tightly bound. The closer this molecular level lays with respect to the energy of two free atoms, the stronger the interaction between them. The magnetic tuning method is the common way to achieve resonant coupling and it has found numerous applications. [33] However, Feshbach resonances can be achieved by optical methods, leading to optical resonances which are similar to the magnetically tuned ones. A magnetically tuned Feshbach resonance can be described by a simple expression, introduced in Ref. [34] for the s-wave scattering length  $a$  as a function of the magnetic field  $B$ ,

$$a = a_{bg} \left( 1 - \frac{\Delta}{B - B_0} \right) \quad (1.2)$$

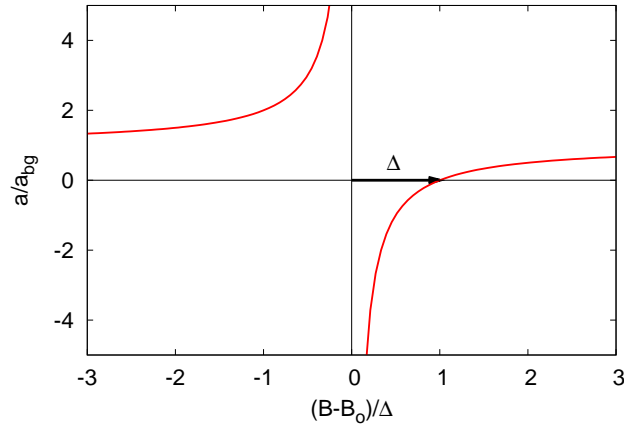


Figure 1.2: Scattering length as function of the magnetic field  $B$  in a magnetically tuned Feshbach resonance.

Figure 1.2 shows a plot of this resonance expression. The background scattering length  $a_{bg}$ , which is the scattering length associated with interaction potential of the open channel, represents the off-resonant value. The parameter  $B_0$  denotes the resonance position, where the scattering length diverges ( $a \rightarrow \pm\infty$ ), and the parameter  $\Delta$  is the resonance width. [33]. Note that both  $a_{bg}$  and  $a$  can be positive or negative such that a wide range of attractive and repulsive interactions between cold atoms can be considered. Among the most important experiments triggered by the possibility to tune the interaction by using Feshbach resonances, we have the realization of a Bose Einstein condensate in a sample of  $^{85}\text{Rb}$ , [35] investigations of the BEC-BCS crossover, [36] and evidence for the existence of Efimov States that was obtained in an experiment which could not have been performed without control over the scattering length. [37]

## Time of flight experiments

The possibility to image trapped atoms on optical lattices is heavily restricted because the lattice spacing is of the order of some nanometers, and therefore the optical resolution of the typical imaging systems is not sufficient to resolve individual lattice sites. Nevertheless, when all trapping potentials are switched

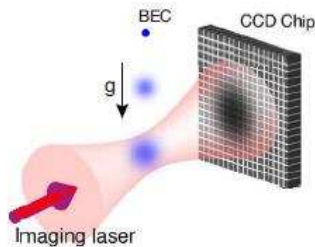


Figure 1.3: Time of flight experiment schematics. A laser images the condensate after a certain expansion time  $\tau$ . The registered image is used to determine whether the trapped system exhibits phase coherence or not.

off, the wave packets confined at each lattice site expand, start to overlap, and interfere with each other giving rise to an interference pattern of matter waves. After a certain time of expansion, the condensate has increased its size because of expansion and it is now large enough such that it can be imaged. If the effects of interaction between atoms during the expansion of the condensate can be neglected, the shape of the interference pattern will be proportional to the momentum distribution of the atoms before the expansion, such that it can provide crucial information on the quantum-mechanical state of the in-trap particles. Schematically, a standard time of flight experiment is performed by letting the atoms expand under the action of gravity. After a certain expansion time  $\tau$ , the cloud is shone with a further imaging laser. The “shadow” left by the condensate is imaged by a charge couple device (CCD), see Fig. 1.3. Perhaps the most important information from the time of flight experiments is that if the interference pattern recorded by the CCD exhibits sharp peaks, it implies that the matter waves feature phase coherence across the lattice in the sense that the phase fluctuations of the matter waves emerging across lattice are correlated. Instead, if the interference pattern is broad, the spatial correlations across the lattice vanish, implying the absence of long-range order in the quantum mechanical state of the atoms in the trap.

## 1.2 Ultracold atoms in optical lattices and the Bose-Hubbard Model

One of the most spectacular experiments with ultracold atoms has been the observation of a superfluid to Mott insulator transition in bosonic atoms trapped in optical lattices upon varying the relative strengths of interaction and interwell tunneling in a three-dimensional (3D) lattice. [19] A conceptually simple model that describes the physics of such systems is the Bose-Hubbard model, [9, 38] which describes interacting bosons on a lattice potential. The Hamiltonian in its second quantized form reads:

$$\mathcal{H} = -\frac{t}{2} \sum_{\langle i,j \rangle} b_i^\dagger b_j + h.c. + \sum_i \left( \frac{U}{2} n_i (n_i - 1) + (\epsilon_i - \mu) n_i \right), \quad (1.3)$$

where  $\langle \dots \rangle$  indicates nearest-neighbor sites,  $b_i^\dagger$  ( $b_i$ ) creates (destroys) a boson on site  $i$ , and  $n_i = b_i^\dagger b_i$  is the local density operator. The on-site interaction is parameterized by  $U$ . The strength of the tunneling term in the Hamiltonian is characterized by the hopping matrix element  $t$  between neighbors  $i, j$ , whereas the local  $\epsilon_i$  is an energy offset of the  $i$ th lattice site. This local energy offset is in principle a general on-site potential. It could represent the inhomogeneities due to an external magnetic confinement, a random variable due to disorder, a staggered potential, combinations of the above mentioned, among other possibilities.  $\mu$  is the chemical potential that fixes the total number of particles in the system  $M$ . In the limit of vanishing interactions, where the tunneling is dominating  $t \gg U$ , the ground state of the Hamiltonian is well described by single-particle wave functions of  $M$  bosons totally spread out over the entire lattice with  $L$  sites. Under these conditions, the many-body ground state for a homogeneous lattice  $\epsilon_i = 0$ , is given by,

$$|\Phi_{SF}\rangle_{U=0} = \left( \sum_i^L b_i^\dagger \right)^M |0\rangle. \quad (1.4)$$

Clearly, in this state all atoms occupy the identical extended Bloch state and it is prone to superfluidity. On the other hand, when the interactions are dominant  $U \gg t$ , all the the particles tend to localize due the strong repulsion between them, in such a way that it is not energetically favorable for the particles to

## 1.2 Ultracold atoms in optical lattices and the Bose-Hubbard Model

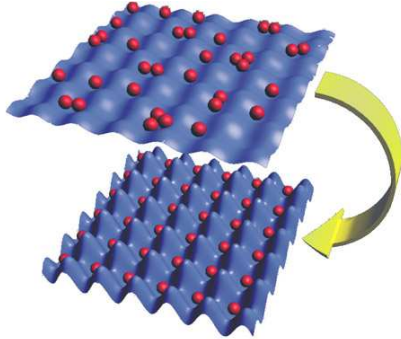


Figure 1.4: Pictorial representations of the superfluid (above) and Mott-insulating (below) phases of bosons on an optical lattice.

wander through the crystal, but stay fixed in space. The many-body ground state is a perfect Mott insulator, a product of local Fock states for each lattice site. In this limit, the ground state of the many-body system for a commensurate filling of  $n$  atoms per lattice site in the homogeneous case is given by

$$|\Phi_{Mott}\rangle_{t=0} = \prod_i^L (b_i^\dagger)^n |0\rangle. \quad (1.5)$$

In this state no phase coherence is prevalent in the system, but perfect correlations in the atom number exist between lattice sites. Furthermore, there is an energy gap to create a particle-hole excitation of  $U$  which makes the system incompressible. In Fig. 1.4 a pictorial representation of both the superfluid and the Mott insulating phases is presented, where in the superfluid phase (upper part) the particles are expected to move across the lattice with associated charge fluctuations, while in the Mott phase (lower part) the particles are pinned to the lattice sites with strongly reduced fluctuations. Now, suppose that in the Mott insulator a small  $t \ll U$  is turned on, such that the particles are allowed to hop between lattice sites. Then the kinetic energy ( $\sim t$ ) gained by allowing an extra particle-hole excitation to hop around the lattice is yet insufficient to overcome the potential energy cost due to interaction. Therefore, even at finite small  $t$  the Mott insulator survives in a range of values of tunneling, until the system reaches a certain critical value of the ratio  $(U/t)_c$  where the energy gained by the tunneling

## 1.2 Ultracold atoms in optical lattices and the Bose-Hubbard Model

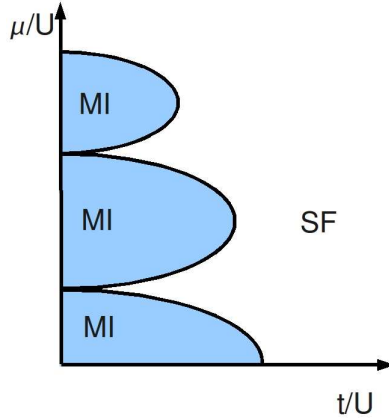


Figure 1.5: Schematic zero temperature phase diagram for the Hubbard Model.

is dominant for which the system will undergo a quantum phase transition from the Mott-insulating state to the superfluid. This transition is accompanied by a marked change in the excitation spectrum of the system, where in the superfluid regime the system becomes gapless. [9] If instead now, by increasing (decreasing) the chemical potential  $\mu$  at fixed  $U/t$  in the Mott-insulating phase, the system will eventually reach a point where the kinetic energy gained by adding (removing) an extra particle (hole) and letting it hop around the system will balance the associated potential energy cost. Since this extra nonzero density of particles (holes) is free to wander around the system, those particles (holes) will immediately Bose condense producing a superfluid state. [9] A sketch of the emerging phase diagram following the above arguments is presented in Fig. 1.5. The phase diagram consists of Mott-insulating lobes with integer average density  $n$ , and a finite gap to particle-hole excitations (blue regions) and gapless superfluid regions which can attain integer and non-integer fillings (white regions).

### Superfluid to Mott insulator in experiments

Before the introduction of the important experiments using ultracold atoms loaded in optical lattices, possible physical realizations of strongly interacting bosonic systems included short-correlation-length superconductors, granular superconductors, Josephson arrays, the dynamics of flux lattices in type-II superconduc-

## 1.2 Ultracold atoms in optical lattices and the Bose-Hubbard Model

tors, and critical behavior of  $^4\text{He}$  in porous media, magnetic systems in presence of external magnetic field which possesses interacting bosonic excitations, among others. [11] The generation of the first Bose-Einstein condensates in the mid-1990's boosted the first experiments using optical lattices, mainly used as mechanism to further cool down the atoms at first. However, experiments with complex many-body states reached with optical lattices, relevant for simulating condensed matter systems, started only around 2000, first with Bose-Einstein condensates in three-dimensional lattices, and later with ultracold Fermi gases. Following the proposal in Ref. [38], the superfluid to Mott insulator transition was observed by Greiner *et al.* [19] loading  $^{87}\text{Rb}$  atoms from a Bose-Einstein condensate into a three-dimensional optical lattice potential. The system they studied was characterized by a low atom occupancy per lattice site of around 1 to 3 atoms, providing a clear realization of the Bose-Hubbard model. As the lattice potential depth was increased, the hopping matrix element  $t$  decreased and the effect of the on-site interaction matrix element  $U$  increased, bringing the system across the critical ratio  $(U/t)_c$ , inducing the superfluid to Mott-insulator transition. In the experiment, absorption images were taken after suddenly releasing the atoms from the lattice potential and waited a fixed expansion time  $\tau = 15\text{ms}$ . The images corresponding to different values of lattice potential depth and are reproduced in Fig. 1.6. The experiment confirmed that whenever the strength of the potential is relatively small, such that the atoms have considerable kinetic energy, the system is in a superfluid state from which coherent matter waves emerge during the expansion, giving rise to sharp peaks in the interference pattern provided by the absorption images. After increasing the lattice depth, the sharp peaks in the absorption images disappear which implies that the phase of the wave function of system across the lattice is not stable, signaling the transition to the Mott-insulating regime of the system. Further measurements probing the excitation spectrum accompanied the time of flight experiments and they confirmed that superfluid to Mott insulator transition is accompanied by the opening of a gap to particle-hole excitation in the excitation spectrum. Remarkably, the critical ratio  $(U/t)_c$  obtained in the experiment is in very good agreement with theoretical calculations based on the Bose-Hubbard model, [9, 38] which further indicates that these experiments with ultracold atoms exceptionally realize the

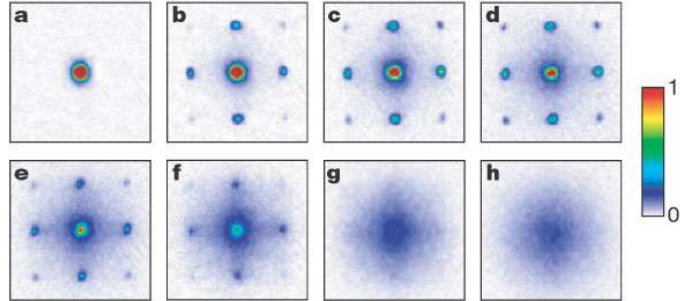


Figure 1.6: Absorption images of multiple matter wave interference patterns across the superfluid to Mott-insulator transition. From a. through h. the strength of the lattice potential is increased. The time of flight is fixed to  $\tau = 15ms$

Bose-Hubbard model. More recently, a similar scenario was observed also in one and two dimensions. [39, 40]

### 1.3 Introducing disorder

It is natural to consider whether the presence of disorder may affect the properties of ultracold atomic systems. Not to mention old known realizations of strongly correlated systems where disorder plays a major role, as in the earliest relevant experiments involving disordered interacting bosons on superfluidity of very thin  $^4\text{H}$  adsorbed in porous Vycor glass. [41] Motivated by those early experimental realizations of disordered bosons, attempts to give detailed theoretical explanations of the interplay between disorder and interaction in correlated Bose systems were successfully introduced by Giamarchi and Schulz and Fisher *et al.* [9, 10] In these two seminal works, they have precisely analyzed the effect of disorder introduced on top of the clean Hubbard model of Eq. (1.3). In this case the local on-site energy offset was chosen to be a disordered potential described by random variables  $\epsilon_i$  that are uniformly distributed in  $[-\Delta, \Delta]$  (see Fig. 1.7(a)), which we will use throughout the whole thesis. It was then conjectured that the phase diagram of a disordered Bose-Hubbard model is supposed to include three different phases: When the interaction is strong and the number of bosons is a

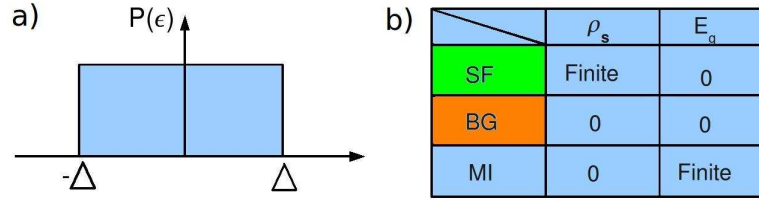


Figure 1.7: a. Distribution probability  $P(\epsilon)$  of the local energy offset. b. Summary of the properties of the phases of the disordered Bose-Hubbard model. ( $E_g$  denotes the charge gap, while  $\rho_s$  denotes the superfluid stiffness. They will be carefully defined later in the thesis) While both the Mott insulator and Bose glass are insulators with vanishing superfluid stiffness, the Bose glass differs from the Mott insulator because it is compressible and gapless, as opposed to the Mott insulator which is incompressible and gapped.

multiple of the number of sites, the model should describe a Mott insulator, with bosons strongly localized in the potential wells of the optical lattice. This phase is neither superfluid nor compressible. When both interaction and disorder are weak, a superfluid and compressible phase must exist. These two phases are also typical of clean systems as it was discussed before in this chapter. In the presence of disorder, a third phase arises, the so-called Bose glass, which is compressible and gapless but not superfluid. The properties of the three phases are summarized in Fig. 1.7(b). The appearance of the new Bose glass can be understood by considering what happens when a disordered Mott insulator is doped with particles or holes. In a clean system, those extra particles or holes propagating on top of the background Mott phase condense and form a superfluid flow. However, if disorder is introduced, those few particles, now encounter a disordered background potential. Those extra bosons occupy the lowest-lying single particle states of the random effective potential due to the on-site disorder and the (ideally) frozen Mott state. Since the particles or holes are very dilute, they are effectively non-interacting and the usual Anderson localization arguments show that the low-energy effective single-particle states must be localized in the deepest minima of the underlying potential, just as with fermions but in this case the effect of Pauli exclusion is played by the strong on-site interaction. The coherent

## 1.4 Large rare homogeneous patches in disordered systems

---

tunneling of a boson between these wells is suppressed just as in the usual Anderson localization, hence the absence of superfluidity, in spite of the fact that displacing a boson from one well to another one may cost no energy, hence a finite compressibility. Only after sufficient particles or holes have been introduced the residual random potential gets sufficiently smooth such that the transition to the superfluid phase takes place. It is harder to rule what happens, however, when the transition is not driven by number fluctuations but it is dominated by hopping, i.e., through the tip of the Mott lobe. Through the tip, both particles and holes are created simultaneously and the gap for producing particle-hole excitations vanishes. Assuming that those particle-hole pairs become immediately superfluid implies that they do not get localized by the random environment, which is unlikely to happen but possible, specially if disorder is weak. Even if the Bose glass is present, one expects a stronger tendency towards superfluidity because of the presence of particles and holes and smaller Bose glass region around the tip of the Mott lobe. Among the possible scenarios for the nature of the phase diagram of the Bose-Hubbard model with disorder, three of them were the most likely, as shown in Fig. 1.8. However, based on these single-particle description used for explaining Anderson localization, it was argued that disorder prevents a direct superfluid-to-Mott insulator transition, supporting the scenario in Fig. 1.8(a), a speculation that has been subject to several controversial numerical and analytical studies. [9, 13, 14, 42, 43, 44, 45, 46]

## 1.4 Large rare homogeneous patches in disordered systems

The question about whether the Bose glass phase must completely surround the Mott lobe, or whether, in fact, a direct Mott-superfluid transition might take place at larger tunneling  $t$ , close to the tip, or perhaps only through the tip has generated much controversy during recent years. Strong arguments have been presented in Ref. [9, 11, 42] that forbid such a direct transition, but a rigorous proof remained unclear, while many numerical calculations were performed, some supporting the idea of a direct transition and some other suggesting a transition

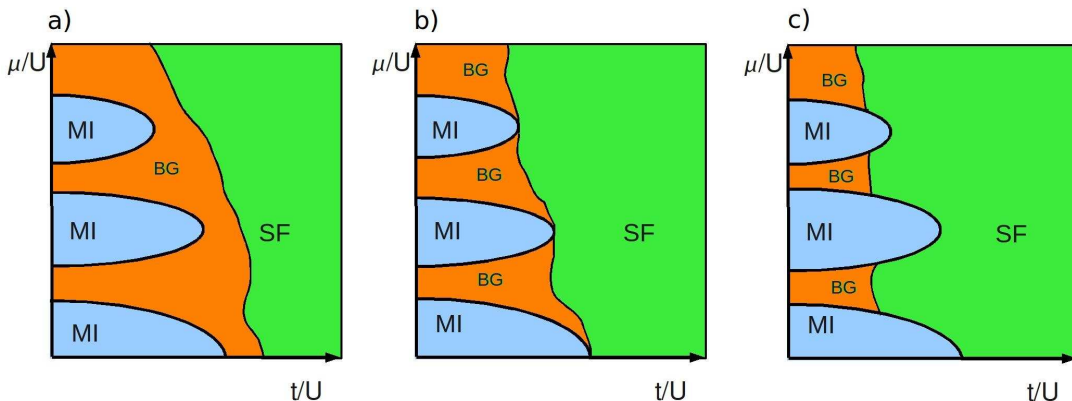


Figure 1.8: Possible scenarios for the phase diagram of disordered interacting bosons: a. The Bose glass always intervenes between the Mott and superfluid phases. b. The Bose glass always intervenes between the Mott and superfluid phases, except at the tip of the Mott lobe. c. Direct transition between the superfluid and the Mott phase is allowed.

always through the Bose glass. In a recent paper, Pollet *et al.* [17] gave strong arguments aimed at proving the absence of a direct quantum phase transition between a superfluid and a Mott insulator in a bosonic system with generic, bounded disorder. Their conclusions follow from a general argument which they named theorem of inclusions, it states that for any transition in a disordered system, one can always find rare regions of the competing phase on either side of the transition line. Furthermore, they formalized a theorem which was already introduced in Ref. [9, 11] (to be referred to as theorem 1) which we now explain.

### Theorem 1

Theorem 1<sup>1</sup> states that if the bound of the disorder  $\Delta$  is larger than half of the energy gap  $E_g/2$  necessary to dope the ideal clean Mott insulator with particles or holes, then the system is in a compressible state. This theorem immediately implies that whenever the critical disorder bound  $\Delta_c$  of the superfluid to the insulating transition is greater than  $E_g/2$ , then the transition is to a compressible,

<sup>1</sup>The name of theorem 1 for this argument has been introduced in Ref. [17]

## 1.4 Large rare homogeneous patches in disordered systems

---

gapless phase, i.e., to the Bose-glass phase. This theorem by itself does not fix the transition line, however its importance relies on the possibility to verify by numerical simulations that the transition between the superfluid to the insulating phase is to the Bose glass and not to the Mott insulator by computing only  $\Delta_c(U)$  and comparing it to  $E_g(U)/2$ , for instance through the calculation of the superfluid fraction  $\rho_s$  and the clean gap  $E_g$ , which are numerically accessible and do not suffer dramatic size effects. The proof of theorem 1 is based on the fact that in the infinite system at fixed  $U/t$ , one can always find arbitrarily large ‘‘Lifshitz’’ regions where the chemical potential is nearly homogeneously shifted downwards or upwards by  $\Delta$ , as sketched in Fig. 1.9. There is no energy gap<sup>1</sup> for particle transfer between such regions, and they can be doped with particles or holes [9, 11, 17, 42]. Furthermore, this argument implies that whenever the disorder potential is unbounded, the system will always be gapless, i.e., there is no longer room for the Mott-insulating state to survive. The appearance of arbitrarily large but exponentially rare regions can be illustrated, for example, with a sequence of flips of a fair coin. An infinite sequence of flips will have arbitrarily long subsequences (the analogous rare regions in which the chemical potential is nearly constant) that appear to be those of an unfair coin, in which for instance, the outcome is always heads or tails only. The probability  $P(k)$  to find a subsequence with  $k$  trials in which the outcome is always heads is  $P(k) = (1/2)^k$ , which is exponentially small. Similarly, with the disordered potential described by random variables  $\epsilon_i$  that are uniformly distributed in  $[-\Delta, \Delta]$ , the probability  $P(k, \delta\mu)$  to find a large subregion of  $k$  lattice sites in which the local disordered potential takes its values within a very small window  $\delta\mu$  around a generic constant value of  $\epsilon$  is

$$P(k, \delta\mu) = \left(\frac{\delta\mu}{2\Delta}\right)^k = e^{-\frac{k}{\xi}}, \quad (1.6)$$

which is exponentially small with the size of the subregion  $k$ , with the decay controlled by  $\xi = 1/\ln\left(\frac{2\Delta}{\delta\mu}\right)$ .

---

<sup>1</sup>There is still some debate about this point, since in Ref. [46] it has been derived an effective theory in which they argued that the gap does not couple linearly to the local disorder, which implies that comparing the disorder bound  $\Delta$  and the energy gap  $E_g$  makes no sense.

## 1.4 Large rare homogeneous patches in disordered systems

---

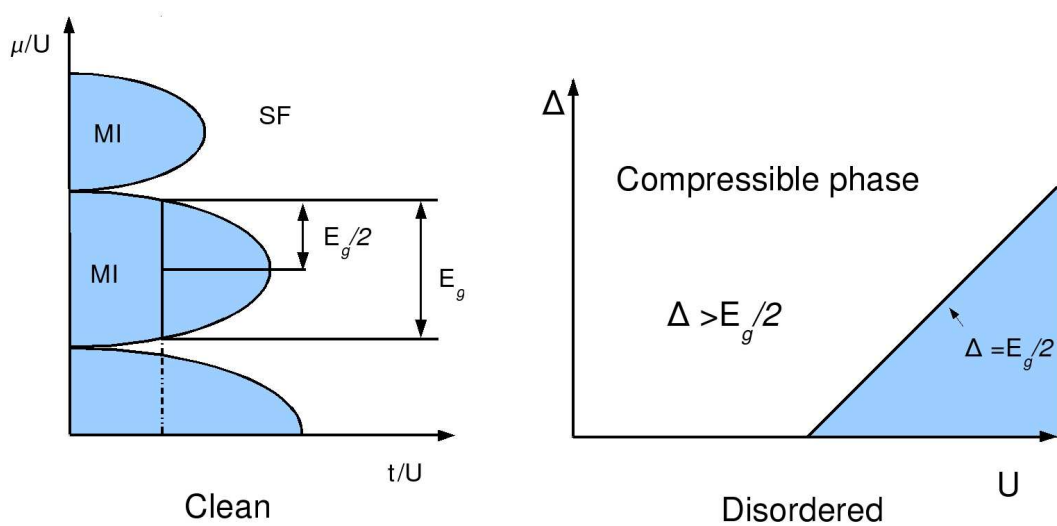


Figure 1.9: Illustrating the proof of theorem 1. Left: By shifting upwards or downwards the chemical potential by half of the energy gap  $E_g$ , the clean system becomes superfluid, just as it would happen in a hypothetical large rare region. Right: Sketch of the compressible regions in presence of bounded disorder in the  $\Delta - U$  plane.

### Theorem of inclusions

In Ref. [17] Pollet *et al.* introduced a stronger theorem, called theorem of inclusions which states that in presence of generic, bounded disorder, there exist rare but arbitrarily large regions of the competing phases across a (generic) transition line. The meaning of generic disorder is understood in the sense that any particular realization has a nonzero probability density to occur in a finite volume. By generic transition it is meant any first- or second-order phase transition with an onset that is sensitive to all disorder characteristics, like strength, correlations, standard deviation, higher-order momenta of the distribution of disorder, etc. For instance, in the superfluid to insulator transition, not only would the vanishing of the stiffness in a generic transition be sensitive to the disorder bound, but also to the correlations of the disordered potential, the variance of the distribution, etc. This theorem immediately implies the absence of a direct superfluid to Mott insulator quantum phase transition. The reason why this is the case is because if one of the possible competing phases is gapless (let us say that phase A), then the competing phase (say phase B) is automatically gapless because it will strictly include arbitrarily large rare regions which locally look exactly as phase A, which is gapless. The importance of this theorem relies on the fact that a direct transition from the superfluid to the Mott insulator is ruled out and consequently a Bose glass should always intervene between the superfluid and the Mott insulator<sup>1</sup>. A detailed sketch of the proof can be found in Ref. [18].

## 1.5 Experiments on disordered bosons

Due to the high degree of control of the parameters offered by the experiments on ultracold atoms loaded in optical lattices, the possibility to introduce disorder in a controlled way has been and it continues to be explored. Those experiments realize the Bose-Hubbard model in presence of disorder in several limits, ranging from the strongly correlated phases where interaction and disorder compete to

---

<sup>1</sup>Care should be taken when applying the theorem of inclusions to the transition from the Bose glass to the Mott insulator, where the transition is not generic in the sense described above. [18]

## 1.5 Experiments on disordered bosons

---

the limit of vanishing interactions in presence of disorder where the physics of Anderson localization is expected to take place. Apart from the experimental realizations of the disordered Hubbard model using cold atoms, the possibility to explore disorder and strong correlations in Bose systems has been investigated using magnetic systems in presence of a magnetic field. Although the phenomenon of Bose-Einstein condensation has been mainly observed with bosonic atoms in liquid Helium and cold gases, the concept is much more general. Analogous states, where excitations in magnetic insulators can be treated as bosonic particles, have been explored in presence of disorder. Their localization due to disorder has been already observed. [47]

### Anderson localization of matter waves

It is now recognized that Anderson localization is a phenomenon ubiquitous in wave physics, as it originates from the interference of waves between multiple-scattering paths, not only common in quantum mechanics but a very general wave phenomenon. Experimentally, localization has been reported in spectacular experiments for light waves, [3, 4] microwaves, [5] sound waves, [6] and electron gases. [7] Also very recently, experimental observation of localization of matter waves using ultracold atoms has been carried out by adding disorder to essentially non-interacting Bose condensates. [20, 21] The non-interacting Bose-Einstein condensate is prepared by cooling a cloud of interacting  $^{39}\text{K}$  atoms in an optical trap, and then tuning the  $s$ -wave scattering length almost to zero by means of a Feshbach resonance. In the experiment in Ref. [21], they have studied localization of non-interacting bosons in a one-dimensional lattice perturbed by a second, weak incommensurate lattice, which constitutes an experimental realization of the non-interacting Aubry-André model. [48] The Aubry-André model is a single-particle non-interacting model that exhibits a localization transition in one dimension and its defined by the Hamiltonian

$$\mathcal{H} = -t \sum_{\langle i,j \rangle} b_i^\dagger b_j + h.c. + \Delta \sum_i \cos(2\pi\beta i) n_i, \quad (1.7)$$

where  $\Delta$  controls the amplitude of the disordering weak incommensurate lattice (here  $\Delta$  plays the analogous role of the disorder bound in a fully disordered sys-

## 1.5 Experiments on disordered bosons

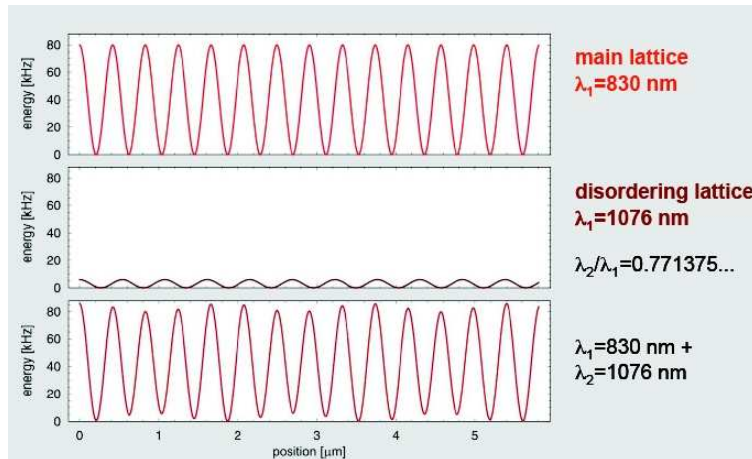


Figure 1.10: On top of the main optical lattice, a second incommensurate disordering lattice is added. The ratio of the wavelengths of the main lattice to the disordering one  $\lambda_2/\lambda_1$  should be as close as possible to an irrational number, which in turn makes the period of the lattice larger and larger resembling a fully disordered lattice.

tem), and  $\beta = \lambda_1/\lambda_2$  the ratio between the wavelengths of the main to the weak lattice. The generated bichromatic potential can display features of a perfectly ordered system, when the two wavelengths are commensurate, but also of quasidisorder when  $\beta$  is irrational. [48] In the latter case, a common choice in the study of the Aubry-André model is the inverse of the golden ratio,  $\beta = (\sqrt{5} - 1)/2$ , for which the model displays a “metal-insulator” phase transition from extended to localized states at  $\Delta/t = 2$ , as opposed to a fully disordered model, in which Anderson localization holds regardless of how small the strength of disorder is. In Fig. 1.10 the way of creating the bichromatic lattice is sketched, where the lattice is realized by perturbing a tight primary lattice with a weak secondary lattice with incommensurate wavelength with respect to the main lattice. It is important that the ratio of the wavelengths of the primary to the secondary lattice is close to an irrational number, such that the period of the lattice grows, hence resembling a fully disordered lattice. The clearest evidence of Anderson localization of the experiment has been obtained through the observation of transport across the lattice after having switched off the additional harmonic confinement neces-

## 1.5 Experiments on disordered bosons

---

sary to confine the non-interacting condensate. They have detected the spatial distribution of the atoms at increasing evolution times using absorption imaging, as reproduced in Fig. 1.11. In a regular ordered lattice the eigenstates of the potential are extended Bloch states, and the system expands ballistically as the time passes by. Instead, in the limit of large disorder<sup>1</sup> ( $\Delta/t > 7$ ) no diffusion is observed, because in this regime the condensate can be described as the superposition of several localized eigenstates whose individual extensions are less than the initial size of the condensate, therefore providing a clear experimental proof of Anderson localization. The transition occurs at a disorder strength larger than the expected value of  $\Delta/t = 2$  because in the experiment the ratio  $\beta$  is not exactly an irrational number. Nevertheless, it is expected that the closer the ratio  $\beta$  to an irrational number, the closer the transition point to the expected value of  $\Delta/t = 2$ . A second experiment, in which Anderson localization has been observed, was performed introducing disorder through a laser speckle potential. [49] A laser speckle is the random intensity pattern produced when coherent laser light is scattered from a rough surface resulting in spatially modulated phase and amplitude of the electric field. One example of a speckle pattern together with the schematics of its experimental realization is shown in Fig. 1.12 [50]. In a fully developed speckle pattern, the sum of the random scattered waves emerging from the ground glass diffuser results in random real and imaginary components of the electric field at the focal plane (at distance  $l$  from the ground glass) whose distributions are independent and Gaussian. Consequently the speckle intensity  $I$  follows an exponential law:

$$P(I) = \frac{1}{\langle I \rangle} e^{-\frac{I}{\langle I \rangle}} \quad (1.8)$$

where  $\langle I \rangle$  is the average value of the intensity. This distribution is unbounded with finite variance and it possesses spatial correlations that depend on the details of the optical setup used to generate the speckle pattern. Indeed, in Ref. [20] cold atoms have been loaded in a speckle pattern and another observation of Anderson localization has been detected. The atomic density profiles have been imaged as

---

<sup>1</sup>In this thesis I have used  $t$  for the hopping amplitude which is the most common usage in the condensed matter physics community, however in quantum optics and cold atoms it is often used the notation  $J$  as it has been used in Fig. 1.11 taken from Ref. [21]

## 1.5 Experiments on disordered bosons

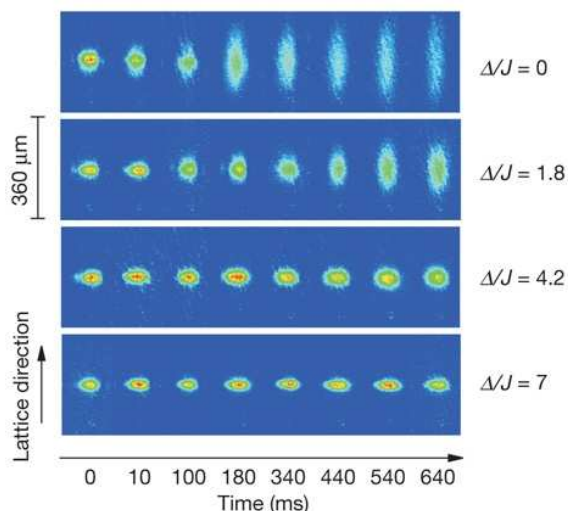


Figure 1.11: In situ absorption images of the Bose-Einstein condensate diffusing along the quasi-periodic lattice for different values of disorder. For  $\Delta/t > 7$  ( $\Delta/J > 7$  in their notation) the size of the condensate remains at its original value, reflecting the onset of localization.

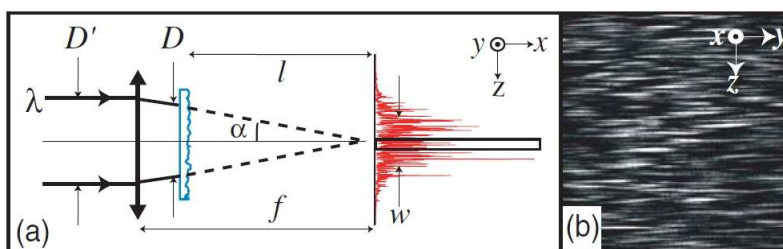


Figure 1.12: a) Experimental realization of the speckle pattern. A laser beam of diameter  $D'$  and wavelength  $\lambda$  is first focussed by a convex lens. The converging beam of width  $D$  is then scattered by a ground glass diffuser. The transverse speckle pattern is observed at the focal plane of the lens. b) Image of an anisotropic speckle pattern created using cylindrical optics to induce a  $1D$  random potential.

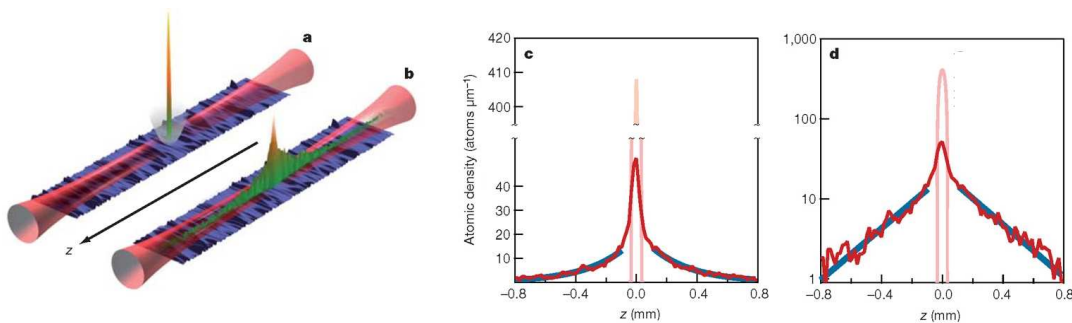


Figure 1.13: a. A small BEC is formed in a hybrid trap that is the combination of a horizontal optical waveguide and a loose magnetic longitudinal trap. b. When the longitudinal trap is switched off, the BEC starts expanding and then localizes, as observed by direct imaging of the fluorescence of the atoms irradiated by a resonant probe. c, d. Density profiles (red) of the localized BEC one second after release, in linear (c) and semi-log (d) coordinates.

a function of time, and found that weak disorder can stop the expansion which leads to the formation of a stationary, exponentially localized wave function, a direct signature of Anderson localization. [20] The density profiles are reproduced in Fig. 1.13, where the tails of the density distribution have been fitted and found to be indeed exponential, a clear signature of Anderson localization.

## The experiments on the role of interactions and the quest for a Bose glass

Even more interesting, preliminary experimental results on the interplay between disorder and interaction have been already carried out. As it has been mentioned already, apart from superfluid and Mott insulator from the clean system, the presence of disorder introduces a new phase to the system of interacting bosons, the so-called Bose glass. In 2007, Fallani and collaborators have provided experimental evidence on the presence of a Bose glass by loading and cooling a sample of interacting bosonic atoms onto a 1D optical lattice. [51] In their experiment they have used a bichromatic optical lattice to experimentally realize a disordered system of ultracold strongly interacting  $^{87}\text{Rb}$  bosons. The excitation spectrum

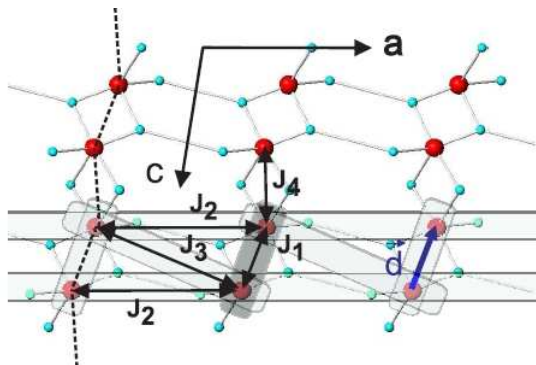


Figure 1.14: Layers of magnetic Cu<sup>2+</sup> (red) and the bridging Cl ions (cyan) in IPA-CuCl<sub>3</sub>. Actual asymmetric spin ladders (shaded) are parallel to the **a** direction. The ladder rungs are defined by the vector **d**.

of the system has been measured as function of disorder while keeping track of the phase coherence properties of the system by means of standard time-of-flight experiments. In an ordered Mott insulator the excitation energy spectrum is roughly made of discrete resonance peaks, which essentially represent the energy required to remove an atom from its well and place it into a neighboring well. Increasing disorder, it has been observed a broadening of the Mott-insulator resonances and the transition to a state with vanishing long-range phase coherence and a flat density of excitations, which was interpreted as the formation of a Bose-glass phase.

### Magnetic Bose glass

The elementary excitations in antiferromagnets are magnons, quasiparticles with integer spin and Bose statistics. [52] It is thus natural to wonder whether those particles undergo Bose Einstein condensation or not and the answer is yes, as it has been shown in numerous theoretical investigations of quantum antiferromagnets (see Ref. [53] and the references therein). The advantages of such bosonic systems are that they are homogeneous, as opposed to the experiments with cold atoms where the yet inevitable spatial inhomogeneities due to the magnetic trap are to be taken into account. Also, the density of bosons can be controlled by

## 1.5 Experiments on disordered bosons

---

the magnetic field, which plays the role of a chemical potential and the density of bosons can be directly measured by measuring the magnetization. Thus, the compressibility can be measured. The long-range superfluid order corresponds to an antiferromagnetic order in the  $XY$  plane. It can thus directly be measured by neutron scattering experiments. In a recent experiment a new realization of the Bose glass has been obtained in Ref. [47] and the results have been interpreted by just taking advantage of the above mentioned correspondence. The experiment is based on the antiferromagnetic spin parent compound, a two-leg spin ( $S = 1/2$ ) IPA-CuCl<sub>3</sub> ladder in a magnetic field. The structure of the disorder-free compound is shown in Fig. 1.14. The most prominent exchange interactions are  $J_1$  which is ferromagnetic and  $J_2$  which is antiferromagnetic. The ground state of the system was determined to be a singlet with a spin gap to triplet excitations and as the magnetic field is increased, bosonic excitations (magnons) are generated which in the clean case Bose condense. Quenched disorder was introduced by means of partial chemical substitution of the non-magnetic ions Br<sup>-</sup> for the likewise non-magnetic Cl<sup>-</sup>, with the advantage that this modification does not directly involve the spin-carrying Cu<sup>+2</sup>. Simultaneously they have measured the bulk magnetization and the magnetic Bragg spectroscopy response of the system. See Fig. 1.15. From their experiment it was observed that in the clean system, upon application of the magnetic field, the onset of magnetization was always accompanied by the formation of strong Bragg peaks which signaled long-range order, meaning that the underlying excitations exhibited Bose-Einstein condensation. After the introduction of disorder, the onset of magnetization was not immediately accompanied by the appearance of magnetic order which was interpreted as the appearance of the Bose-glass phase, i.e., a compressible but incoherent phase with absence of spin diffusion. After further increase of the magnetic field, phase coherence showed up signaling the transition from the Bose glass to the superfluid.

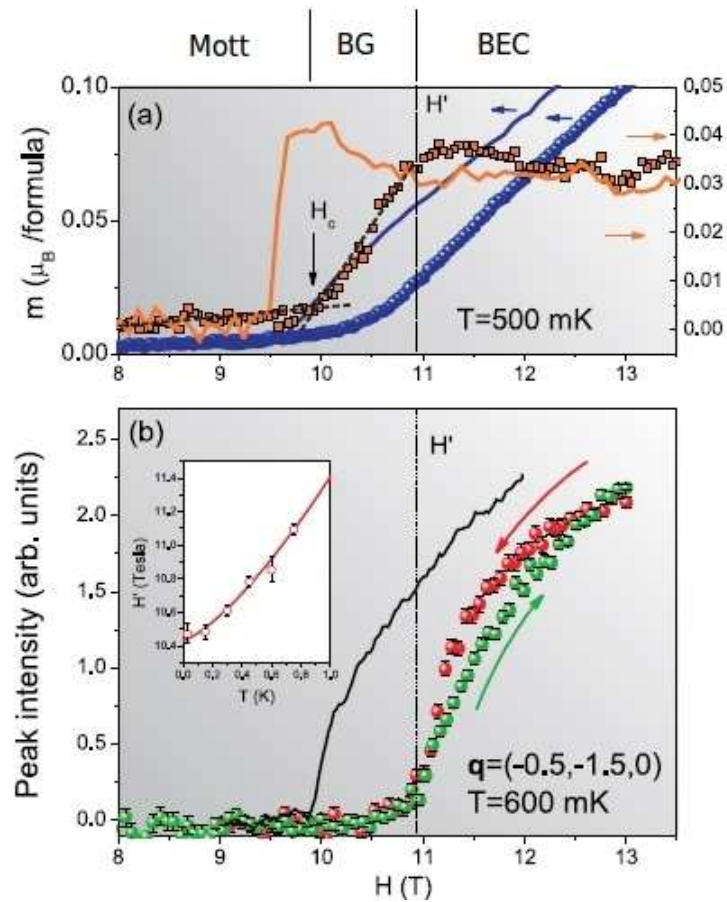


Figure 1.15: a. Measurement of the magnetization as function of the applied magnetic field. Both the clean (blue curve) and disordered (orange curve) are shown. b. Magnetic Bragg spectroscopy peak intensity. Both the clean (black curve) and disordered (green and red curves) are shown. In the disordered case there is a window of values of the magnetic field  $H$  for which the magnetic susceptibility is finite, though there is no signal of magnetic order, fact that is interpreted as the appearance of a magnetic Bose glass.

## Chapter 2

# The variational approach

We now introduce the variational approach, a powerful tool to study correlated systems. We start off by introducing one of the simplest variational wave functions, i.e., the Gutzwiller wave function. For bosons, this wave function can be easily treated without further approximations and a qualitatively correct description of the superfluid to insulator transition of the Bose-Hubbard model is obtained. This approach is flexible enough to treat inhomogeneous systems such as optically or magnetically trapped bosons, as well as disordered lattices. We then introduced an improved wave function, which generalizes the Gutzwiller one, based on a long-range Jastrow factor which provides a proper description of a Mott insulator. We describe how this wave function can be treated within the variational Monte Carlo scheme, together with its generalization to treat disordered bosons too. Furthermore, the way these wave functions are optimized by means of the stochastic reconfiguration technique is described. In this way, the best approximations to the real ground states of the systems are obtained, given a functional form of the wave function parameterized through a certain number of variational parameters. Finally, the Green's Function Monte Carlo technique, a zero-temperature algorithm that provides numerically exact results, is explained. In this method one starts from a trial, e.g., variational wave function, and filters out high-energy components by iterative applications of the imaginary-time evolution operator. The closer the wave function to the ground state of the system the more efficient the method would perform, hence the importance of finding accurate variational states describing the ground state.

## 2.1 The Gutzwiller wave function for the Bose-Hubbard model

In all this chapter we will be interested in obtaining approximate and exact solutions to the Bose-Hubbard Hamiltonian,

$$\hat{\mathcal{H}} = -\frac{1}{2} \sum_{\langle i,j \rangle} t_{i,j} \hat{b}_i^\dagger \hat{b}_j + h.c. + \frac{U}{2} \sum_i \hat{n}_i (\hat{n}_i - 1) + \sum_i \epsilon_i \hat{n}_i, \quad (2.1)$$

where  $\langle \dots \rangle$  indicates nearest-neighbor sites,  $\hat{b}_i^\dagger$  ( $\hat{b}_i$ ) creates (destroys) a boson on site  $i$ , and  $\hat{n}_i$  is the local density operator.  $U$  is the on-site interaction,  $t_{i,j}$  is the hopping amplitude, and  $\epsilon_i$  is a local energy offset due to either an external trapping potential, disorder or both. Within the Gutzwiller ansatz the ground-state wave function is approximated as

$$|\Psi_G\rangle = \prod_i \left( \sum_{m=0}^{\infty} f_m^i |m\rangle_i \right), \quad (2.2)$$

where  $|m\rangle_i$  is the Fock state with  $m$  particles at site  $i$  and  $f_m^i$  are variational parameters which are to be determined by minimizing the expectation value of the Hamiltonian in Eq. (2.1). The sum in Eq. (2.2) runs from states with zero particles up to infinity. However, from a numerical perspective, we have to consider a cutoff and take only states up to a maximum number of particles (per site)  $M_{max}^i \gg \langle \Psi_G | \hat{n}_i | \Psi_G \rangle$  such that the contribution of those states with higher density are negligible and observables are converged to a certain desired precision. A different approach to that of the Gutzwiller wave function can be used and it consists in solving the following mean-field decoupled Hamiltonian: [54, 55]

$$\begin{aligned} \hat{\mathcal{H}}_{mf} = & -\frac{1}{2} \sum_{\langle i,j \rangle} t_{i,j} \left( \hat{b}_i^\dagger \Psi_j + \Psi_i^* \hat{b}_j - \Psi_i^* \Psi_j \right) + h.c. \\ & + \frac{U}{2} \sum_i \hat{n}_i (\hat{n}_i - 1) + \sum_i (\epsilon_i - \mu) \hat{n}_i, \end{aligned} \quad (2.3)$$

where  $\Psi_i$  is the mean-field potential which is self-consistently defined as  $\Psi_i = \langle \Psi_G | \hat{b}_i | \Psi_G \rangle$ . The parameter  $\mu$  is the chemical potential that fixes the number of bosons and it has been introduced because after the mean-field decoupling the

## 2.1 The Gutzwiller wave function for the Bose-Hubbard model

---

Hamiltonian no longer conserves the number of particles. This Hamiltonian is obtained by a mean-field decoupling of the hopping terms as,

$$\hat{b}_i^\dagger \hat{b}_j \simeq \hat{b}_i^\dagger \Psi_j + \hat{b}_j \Psi_i^* - \Psi_i^* \Psi_j, \quad (2.4)$$

where we have neglected the fluctuations around the mean-field  $\Psi_i$ . Note that this Hamiltonian can now be written as the sum over single site Hamiltonians, coupled only through the constant terms  $\Psi_i$ . If the system possesses translational invariance, then all sites are equivalent and one is left with a single-site local Hamiltonian. The  $f_m^i$  are related to the ground-state eigenvector components of the converged solution of the local Hamiltonian in Eq. (2.3). [54] To see that, one just has to compute the expectation value of the energy of the Gutzwiller state on the mean-field Hamiltonian in Eq. (2.3) and insert the self consistency condition  $\Psi_i = \langle \Psi_G | \hat{b}_i | \Psi_G \rangle$ . The resulting expectation value is exactly the variational energy (the expectation value on Eq. (2.1)) of the Gutzwiller state. Therefore, solving self consistently the mean-field Hamiltonian or minimizing the expectation value of the many-body Hamiltonian on the Gutzwiller state with respect to the  $f_m^i$ 's is completely equivalent. In this thesis, we have mainly used the first approach based on solving self consistently the mean-field Hamiltonian, although we have verified that the results are consistent with the second approach in the simplest case of totally clean Bose-Hubbard model. The technical implementation of the self-consistent method is as follows:

1. First an initial set of nonzero  $\Psi_i$ 's is given arbitrarily.
2. A set of mean-field Hamiltonians (2.3) is constructed using a local basis  $|m\rangle_i$  for each lattice site  $i$  based on the initial guess of  $\Psi_i$ . The basis set is truncated and only states with a maximum number of bosons of  $M_{max}^i$  are considered.
3. The set of local Hamiltonians is diagonalized. The diagonalization provides the ground-state of the Hamiltonian with which a new set  $\Psi_i^{new}$  can be computed.

## 2.2 The Jastrow wave function and the variational Monte Carlo

---

4. It is now checked if the  $\Psi_i^{new}$  are equal to the previous  $\Psi_i$ . If they are equal within a given small precision  $\epsilon$  then the self consistency has been reached and the algorithm stops and the ground-state is the optimal.
5. If the new set of  $\Psi_i^{new}$  is not equal to the previous one  $\Psi_i$ , then  $\Psi_i = \Psi_i^{new}$  and the set is taken to step 2 and the process is iteratively repeated until condition 4 is satisfied.

Once the iterative process has stopped, then the ground state of the mean-field Hamiltonian (or the optimized variational wave function) is used to compute all sort of correlation functions like average local density, condensate fraction, energy, local density fluctuation, etc. In Fig. 2.1 it is presented the evolution of the energy as function of the iteration step  $k$  of self-consistency procedure, as well as the convergence of the  $\Psi$  for a single site mean-field Hamiltonian. The input of the calculation is  $U/t = 7.0$  with chemical potential  $\mu = 2.0$  and an initial guess for  $\Psi = 1.0$ . A large basis cutoff is set to  $M_{max} = 40$  in order to obtain well converged results. Results are also presented for  $U/t = 7.0$  with initial guess of  $\Psi = 0.1$  and chemical potential fixed to  $\mu = 1.0$ . For the case of  $U/t = 7.0$  and  $\mu = 2.0$  the system is in the Mott-insulating phase with vanishing  $\Psi = 0.0$  and for the  $\mu = 1.0$  the system is in the superfluid state with finite value of  $\Psi$ .

## 2.2 The Jastrow wave function and the variational Monte Carlo

Even though the Gutzwiller wave function introduced in the preceding section describes well, at least qualitatively, the superfluid to Mott-insulator transition, the description of the Mott insulator is rather poor. This wave function completely removes charge fluctuations which are natural to real Mott insulators, removing completely on-site occupancies different from the average one. A step forward has been recently accomplished, where it has been shown that a Gutzwiller wave function supplemented by a long-range Jastrow factor offers a very accurate description of a Mott insulator. [56] In the clean bosonic case, a good description of

## 2.2 The Jastrow wave function and the variational Monte Carlo

---

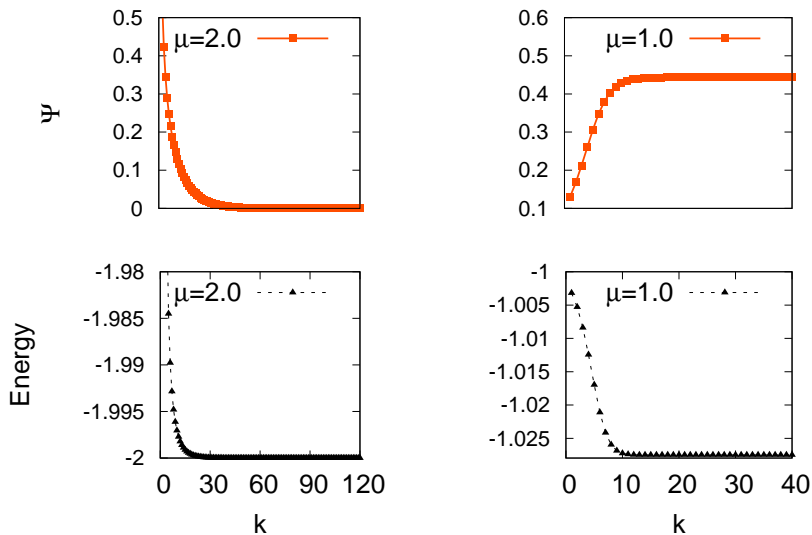


Figure 2.1: Convergence of the iterative procedure. Left:  $\mu = 2.0$  which converges to a Mott insulator. Right:  $\mu = 1.0$  which converges to the superfluid regime.

the physics behind the Mott transition is obtained by applying a density-density Jastrow factor to a state where all bosons are condensed at  $q = 0$ , i.e.,

$$|\Psi_{clean}\rangle = \exp\left(\sum_{i,j} v_{i,j} \hat{n}_i \hat{n}_j\right) |SF\rangle \quad (2.5)$$

where  $|SF\rangle = \left(\sum_i \hat{b}_i^\dagger\right)^M |0\rangle$  is the non-interacting Bose condensate of  $M$  particles,  $\hat{n}_i$  is the on-site density operator, and  $v_{i,j}$  are translationally invariant parameters that are determined by minimizing the variational energy. This wave function contains both ingredients, a superfluid part that dominates when the kinetic energy of the particles is large and a term which introduces correlation effects due to interaction, while keeping the charge fluctuations. It has been shown that the introduction of the long-range Jastrow term properly describes the superfluid and the Mott insulating phases in one, two and three dimensions. [56] In the presence of disorder, we just add to Eq. (2.5) a site-dependent one-body Jastrow

## 2.2 The Jastrow wave function and the variational Monte Carlo

---

factor

$$|\Psi\rangle = \exp\left(\sum_i g_i \hat{n}_i\right) |\Psi_{clean}\rangle \quad (2.6)$$

where  $g_i$ 's are  $L$  additional variational parameters. This wave function becomes the exact ground state for  $U = 0$  and finite  $\Delta$  if  $v_{i,j} = 0$  and  $g_i = \ln \alpha_i$  with  $\alpha_i$  being the amplitude at site  $i$  of the lowest-energy single-particle eigenstate of the non-interacting Hamiltonian. A similar wave function has been recently used to describe the fermionic Hubbard model in the presence of disorder. [57] The flexibility of this variational state makes it possible to describe equally well superfluid, Bose-glass, and Mott-insulating states. We have chosen the two-body Jastrow factor to be translational invariant, even in the disordered case, where the translational invariance is lost. In principle, the two-body Jastrow could be defined for each pair of sites, which would lead to a number of Jastrow parameters  $v_{i,j}$  of the order of  $L^2$ , as opposed to a translational invariant one, where the number grows linearly with  $L$ . However, the reason why the Jastrow factor is important relies on the fact that it correctly describes the natural charge fluctuations of the Mott-insulating phase. Therefore, even though the Hamiltonian of the system in presence of disorder is not translational invariant, in the Mott phase the inhomogeneities are heavily suppressed due to the strong repulsion between particles and the ground state translational invariance is almost recovered, specially for large values of interaction.

Although the definition of the long-range Jastrow is quite simple, its treatment is rather involved because, contrary to what happens with the Gutzwiller wave function, this correlated wave function cannot be factorized into on-site independent terms. Evaluating correlation functions involves the calculation of multi-dimensional integrals that cannot be handled analytically or in numerically exact way. One has to rely on approximate methods; particularly we concentrate on the variational Monte Carlo method that allows us to evaluate, by means of a stochastic sampling, integrals over a multidimensional space.

## The variational Monte Carlo

The key ingredient of the variational Monte Carlo (VMC) approach is the property of any quantum system, that the expectation value of an Hamiltonian  $\mathcal{H}$  over any trial wave function  $|\Psi\rangle$ , gives an upper bound to the exact ground-state energy  $E_0$ ,

$$E = \frac{\langle \Psi | \mathcal{H} | \Psi \rangle}{\langle \Psi | \Psi \rangle} \geq E_0 \quad (2.7)$$

This can be easily seen by inserting the complete set of eigenfunctions  $|\Phi_i\rangle$  of  $\mathcal{H}$  with energies  $E_i$ ,

$$\frac{\langle \Psi | \mathcal{H} | \Psi \rangle}{\langle \Psi | \Psi \rangle} = \sum_i E_i \frac{|\langle \Phi_i | \Psi \rangle|^2}{\langle \Psi | \Psi \rangle} = E_0 + \sum_i (E_i - E_0) \frac{|\langle \Phi_i | \Psi \rangle|^2}{\langle \Psi | \Psi \rangle} \geq E_0 \quad (2.8)$$

Therefore, this important property allows us to define a route to obtain the best wave function by finding the one with the smallest energy. Perhaps the greatest difficulty with this approach is that the evaluation of the energy in Eq. (2.7) is that when dealing with many-body systems, the Hilbert space of the system grows exponentially with the spatial size. Since we are mainly interested in the thermodynamic limit of the system, the Hilbert space is enormous, and a direct calculation, although straightforward, becomes prohibitively expensive. Therefore, on larger sizes the most efficient way to compute observables, depending on a large number of variables, is to use the Monte Carlo approach. In order to show how a statistical approach can be used to calculate expectation values like Eq. (2.7), we introduce a complete set of states  $|x\rangle$  on which correlated wave functions can be easily calculated:

$$\frac{\langle \Psi | \mathcal{H} | \Psi \rangle}{\langle \Psi | \Psi \rangle} = \frac{\sum_{x,x'} \Psi^*(x) \mathcal{H}_{x,x'} \Psi(x')}{\sum_x |\Psi(x)|^2} \quad (2.9)$$

where  $\Psi(x) = \langle x | \Psi \rangle$  and  $\mathcal{H}_{x,x'} = \langle x | \mathcal{H} | x' \rangle$ . As the basis set we choose  $|x\rangle$  to be real space bosonic configurations. Given the total number of bosons  $M$ , a configuration will be a list of  $L$  sites with its corresponding occupation of bosons  $n_i$ . A site  $i$  can contain a number of particles  $n_i$  in the interval  $[0, M]$ . The configuration will therefore be  $|x\rangle = |n_1, n_2, \dots, n_{L-1}, n_L\rangle$ , such that  $\sum_i n_i = M$ ,

## 2.2 The Jastrow wave function and the variational Monte Carlo

---

i.e, the total number of bosons remains fixed. Let us now introduce the so called *local energy*  $E_x$  as

$$E_x = \sum_{x'} \mathcal{H}_{x,x'} \frac{\Psi(x')}{\Psi(x)} \quad (2.10)$$

Eq. (2.9) can then be written in terms of the local energy as,

$$E = \frac{\langle \Psi | \mathcal{H} | \Psi \rangle}{\langle \Psi | \Psi \rangle} = \frac{\sum_x |\Psi(x)|^2 E_x}{\sum_{x'} |\Psi(x')|^2} \quad (2.11)$$

Since most realistic Hamiltonians are very sparse, the number of configurations  $|x'\rangle$  connected to  $|x\rangle$  is relatively small and it does not grow exponentially with the size of the system. Therefore the local energy in Eq. (2.10) can be computed quite efficiently. Moreover, the local energy  $E_x$  depends crucially on the choice of the wave function  $|\Psi\rangle$ . In particular, if  $|\Psi\rangle$  is the exact ground state of  $\mathcal{H}$  with eigenvalue  $E_0$ , the local energy does not depend on  $|x\rangle$ , namely  $E_x = E_0$  with no fluctuations, this is the so-called zero variance property. The evaluation of the total energy  $E$  can be done by generating a sample  $X$  of  $\mathcal{N}$  configurations, according to the probability distribution

$$p(x) = \frac{|\Psi(x)|^2}{\sum_{x'} |\Psi(x')|^2} \quad (2.12)$$

By taking the average over such sample  $X$ , we can estimate the value of the energy by averaging the local energy,

$$\bar{E} \simeq \frac{1}{\mathcal{N}} \sum_{x \in X} E_x \quad (2.13)$$

The simplest method to generate a set of configurations according to the probability distribution  $p(x)$  is the Metropolis algorithm, [58] which tells us that starting from a configuration  $|x\rangle$ , a new configuration  $|x'\rangle$  is accepted if a random number  $\eta$ , between 0 and 1, satisfies the condition

$$\eta < \frac{p(x')}{p(x)} = \left| \frac{\Psi(x')}{\Psi(x)} \right|^2 \quad (2.14)$$

otherwise the new configuration is kept equal to the old one  $|x'\rangle = |x\rangle$ . The central limit theorem ensures that,

$$\lim_{\mathcal{N} \rightarrow \infty} \bar{E} = E \quad (2.15)$$

## 2.2 The Jastrow wave function and the variational Monte Carlo

---

Since the true expectation value is reached exactly only if we take an infinitely large sample  $X$ , there will always be an error associated to the estimation given by  $\bar{E}$  which is due to the finite sampling. This error can be estimated from the variance of  $\bar{E}$ . First, the variance of the random variable  $E_x$  is exactly equal to the quantum variance of the Hamiltonian on the variational state,

$$\sigma^2(E) = \frac{\langle \Psi | (\mathcal{H} - E)^2 | \Psi \rangle}{\langle \Psi | \Psi \rangle} = \text{var}(E_x) \quad (2.16)$$

One can show that the statistical error scales as the square root of the inverse length  $\mathcal{N}$  of the Markov chain, namely that the variance of  $\bar{E}$

$$\sigma^2(\bar{E}) \simeq \frac{\tau}{\mathcal{N}} \sigma^2(E) \quad (2.17)$$

where  $\tau$  is the autocorrelation time, i.e., the number of steps of the Markov chain which separate two statistically independent configurations. The autocorrelation time arises because in practice, given a configuration  $|x\rangle$ , a new configuration is proposed by moving a single boson from site  $j$  to site  $i$  among all possible  $M$  bosons. Therefore the new configuration  $|x'\rangle$  will be very similar to the previous one, and hence the measurements of the local observables at configuration  $|x'\rangle$  will be correlated with respect to the ones measured at  $|x\rangle$ . This leads to an subestimation of the error bars on the observables we will be interested in. In order to decorrelate the measurements we have used two strategies. First, measurements are only taken after a certain number  $w$  of moves have been tried.  $w$  should be of the order of the size of the system  $L$  for the configuration  $|x'\rangle$  to look different to the one of the previous measurement  $|x\rangle$ . Second, we have used the so-called bin technique. In this technique we divide up a long Markov chain with  $\mathcal{N}$  steps into several  $K$  segments (bins), each of length  $M = \mathcal{N}/K$ . The average is then taken on each bin, and the error is estimated using the  $M$  averaged measurements.  $M$  should be large enough compared to the autocorrelation time, i.e.,  $M \gg \tau$ , such that the measurements performed on each bin are completely uncorrelated. A detailed description of the bin technique can be found in Ref. [59]. Therefore, for large enough samplings, the average quantities calculated with the Metropolis algorithm give reliable estimates of the true expectation values of the system, as the error goes to zero when increasing the sampling. By the Variational Monte

---

## 2.3 The stochastic reconfiguration method

Carlo, other static correlation functions can be computed in a similar way to the energy

$$\langle O \rangle = \frac{\langle \Psi | \hat{O} | \Psi \rangle}{\langle \Psi | \Psi \rangle} = \frac{\sum_x |\Psi(x)|^2 O_x}{\sum_{x'} |\Psi(x')|^2}. \quad (2.18)$$

The local value of the operator is  $O_x$  given by

$$O_x = \sum_{x'} \hat{O}_{x,x'} \frac{\Psi(x')}{\Psi(x)} \quad (2.19)$$

with  $\hat{O}_{x,x'} = \langle x | \hat{O} | x' \rangle$ . Finally, just as with the energy, the expectation value  $\langle O \rangle$  of any operator  $\hat{O}$  reduces to average over the values assumed by  $O_x$  along the  $\mathcal{N}$  steps of the Markov chain:

$$\bar{O} \simeq \frac{1}{\mathcal{N}} \sum_{x \in X} O_x \quad (2.20)$$

## 2.3 The stochastic reconfiguration method

In the previous section, a variational wave function aimed at describing the properties of the disordered Hubbard model has been introduced. This wave function is parameterized through a set of variational parameters  $\alpha = \{\alpha_k\}$ ,  $k = 1, \dots, p$  appearing in the two-body Jastrow factor and the one-body local on-site term. These set of parameters have to be optimized in such a way that the trial state is as close as possible to the real ground state, using the variational principle previously introduced, i.e., by minimizing the expectation value of the Hamiltonian on the trial state as function of the set of parameters  $\alpha$ . In the following we show how to optimize the variational wave function minimizing the energy through the stochastic reconfiguration algorithm, introduced in Ref. [60]. First of all let us introduce the notation  $|\Psi(\alpha)\rangle$  for a generic variational wave function parameterized through a set  $\alpha$  of  $p$  variational parameters. Let  $|\Psi(\alpha^0)\rangle$  be the initial wave function depending on the initial set of parameters  $\alpha^0$ . We now consider a small variation of the parameters  $\alpha_k = \alpha_k^0 + \delta\alpha_k$ . Then we can Taylor expand the wave function around  $\alpha_k^0$ , keeping only the linear terms on  $\delta\alpha_k$ ,

$$|\Psi(\alpha)\rangle = |\Psi(\alpha^0)\rangle + \sum_{k=1}^p \delta\alpha_k \frac{\partial}{\partial\alpha_k} |\Psi(\alpha^0)\rangle + \mathcal{O}(\delta\alpha_k^2) \quad (2.21)$$

### 2.3 The stochastic reconfiguration method

---

We define a diagonal operator  $\hat{\mathcal{O}}_k$ , such that

$$\hat{\mathcal{O}}_k |\Psi(\alpha)\rangle = \frac{\partial}{\partial \alpha_k} |\Psi(\alpha)\rangle. \quad (2.22)$$

It follows from its definition that,

$$\hat{\mathcal{O}}_k(x) = \frac{\partial \ln \langle x | \Psi(\alpha) \rangle}{\partial \alpha_k}. \quad (2.23)$$

We can now write  $|\Psi(\alpha)\rangle$  as

$$|\Psi(\alpha)\rangle = \sum_{k=0}^p \delta \alpha_k \hat{\mathcal{O}}_k |\Psi(\alpha^0)\rangle + \mathcal{O}(\delta \alpha_k^2), \quad (2.24)$$

where we have defined  $\hat{\mathcal{O}}_0 = 1$  to be the identity operator and  $\delta \alpha_0 = 1$ . However, the normalization of  $|\Psi(\alpha)\rangle$  will naturally lead to  $\delta \alpha_0 \neq 1$ . In this case, the variation of the parameters will be rescaled as,

$$\delta \alpha_k \rightarrow \delta \alpha_k / \delta \alpha_0. \quad (2.25)$$

It is important to notice that Eq. (2.24) can be read as the expansion of  $|\Psi(\alpha)\rangle$  on the subspace spanned by the vectors  $\{|\Psi(\alpha^0)\rangle, \hat{\mathcal{O}}_k |\Psi(\alpha^0)\rangle\}$  with  $k = 1, \dots, p$ , namely the subspace defined by the variational parameters. Now the key point is to determine the new parameters so to have a lower variational energy. The stochastic reconfiguration algorithm is based on the projection method idea: the exact ground state can be filtered out by iteratively applying the Hamiltonian to the trial wave function. In particular, we can apply one step of the power method starting from  $|\Psi(\alpha^0)\rangle$

$$|\Psi'(\alpha)\rangle = (\Lambda - \mathcal{H}) |\Psi(\alpha^0)\rangle, \quad (2.26)$$

where  $\Lambda$  is a large positive constant which ensures convergence to the ground state. The equations for determining the new parameters can be found by imposing that  $|\Psi'(\alpha)\rangle$  coincides with  $|\Psi(\alpha^0)\rangle$  within the subspace spanned by the vectors  $\{\hat{\mathcal{O}}_k |\Psi(\alpha^0)\rangle\}$  with  $k = 1, \dots, p$ . Then by combining Eq. (2.26) and (2.24) and projecting the results on the  $k^{\text{th}}$  component of that subspace, we obtain

$$\langle \Psi(\alpha^0) | \hat{\mathcal{O}}_k (\Lambda - \mathcal{H}) |\Psi(\alpha^0)\rangle = \sum_{k'=0}^p \delta \alpha_{k'} \langle \Psi(\alpha^0) | \hat{\mathcal{O}}_k \hat{\mathcal{O}}_{k'} |\Psi(\alpha^0)\rangle \quad (2.27)$$

### 2.3 The stochastic reconfiguration method

---

Thus we found a system of  $(p+1)$  linear equations that can be solved to calculate the parameters  $\delta\alpha_k$ . From the  $k = 0$  term of Eq. (2.27), a relation for  $\delta\alpha_0$  is obtained

$$\delta\alpha_0 = \Lambda - E - \sum_{k=1}^p \delta\alpha_k \langle \Psi(\alpha^0) | \hat{O}_k | \Psi(\alpha^0) \rangle \quad (2.28)$$

that inserted in Eq. (2.27) for  $k \neq 0$  returns

$$\langle \mathcal{H} \rangle \langle \hat{O}_k \rangle - \langle \mathcal{H} \hat{O}_k \rangle = \sum_{k'} \left( \langle \hat{O}_{k'} \hat{O}_k \rangle - \langle \hat{O}_{k'} \rangle \langle \hat{O}_k \rangle \right) \delta\alpha_{k'} \quad (2.29)$$

where  $\langle \dots \rangle$  indicates the average over  $|\Psi(\alpha^0)\rangle$ . We recognize the first part of Eq. (2.29) to be the generalized forces

$$f^k = -\frac{1}{2} \frac{\partial E}{\partial \alpha_k} = \langle \mathcal{H} \rangle \langle \hat{O}_k \rangle - \langle \mathcal{H} \hat{O}_k \rangle \quad (2.30)$$

and we define the positive definite  $p \times p$  matrix

$$s_{l,k} = \langle \hat{O}_l \hat{O}_k \rangle - \langle \hat{O}_l \rangle \langle \hat{O}_k \rangle \quad (2.31)$$

By using these new definitions, Eq. (2.29) can be written in a compact form

$$\sum_l \delta\alpha_l s_{l,k} = f^k \quad (2.32)$$

Finally, the parameters variations  $\delta\alpha_k$  obtained through Eq. (2.32) can be rescaled by an acceleration constant  $\delta t$ , i.e.,  $\delta\alpha_k \rightarrow \delta\alpha_k / \delta t$ . Thus, the change on the variational parameters within the stochastic reconfiguration algorithm becomes

$$\delta\alpha_k = \delta t \sum_l s_{k,l}^{-1} f^l. \quad (2.33)$$

From this relation we observe that the role of the acceleration  $\delta t$  is to control the extension of the optimization steps. The positive definiteness of the matrix  $s_{k,l}$  ensures that the algorithm converges. In fact the energy variation corresponding to a small change in the parameters is:

$$\Delta E = -\delta t \sum_{k=1}^p \sum_{l=1}^p s_{k,l}^{-1} f^k f^l + \mathcal{O}(\delta t^2) \quad (2.34)$$

## 2.3 The stochastic reconfiguration method

---

which is always negative for small enough  $\delta t$ , unless the minimum condition of  $f^k = 0$  is reached. It is important to notice that the stochastic reconfiguration method is very similar to the simpler steepest descent method. In fact substituting  $s_{k,l}$  with the identity  $\delta_{k,l}$  in Eq. (2.33) defines the steepest descent algorithm

$$\delta\alpha_k = f^k \delta t \quad (2.35)$$

The fundamental difference between the stochastic reconfiguration minimization and the steepest descent method is the definition of the distance  $\Delta_\alpha$  between a new set of parameters  $\{\alpha_k\}$  and the previous one. The distance  $\Delta_\alpha$  is crucial for the stability of the optimization method: in fact in these iterative methods the new parameters have to be chosen close enough to the old ones in terms of the prescribed distance. Within the stochastic reconfiguration scheme  $\Delta_\alpha$  is chosen to be the square distance between the wave functions before and after the change of parameters within the physics Hilbert space, yielding

$$\Delta_\alpha = \sum_{l,k} s_{l,j} (\alpha'_k - \alpha_k) (\alpha'_l - \alpha_l), \quad (2.36)$$

while in the steepest descent algorithm the distance is defined by the Cartesian metric in the parameter space

$$\Delta_\alpha = \sum_k |\alpha'_k - \alpha_k|^2. \quad (2.37)$$

The advantage of the stochastic reconfiguration method compared with the steepest descent is then clear because sometimes a small change of the variational parameters corresponds to a large change of the wave function, and the stochastic reconfiguration takes into account this effect as it is clear from the definition of the distance  $\Delta_\alpha$ . We now briefly describe how all these things are put together in order to optimize a general wave function with any number of parameters.

### Optimization algorithm

The idea of the optimization algorithm proceeds as follows.

1. Provided a functional form of the wave function, an initial set of variational parameters  $\alpha_k^0$  is inserted.

## 2.3 The stochastic reconfiguration method

---

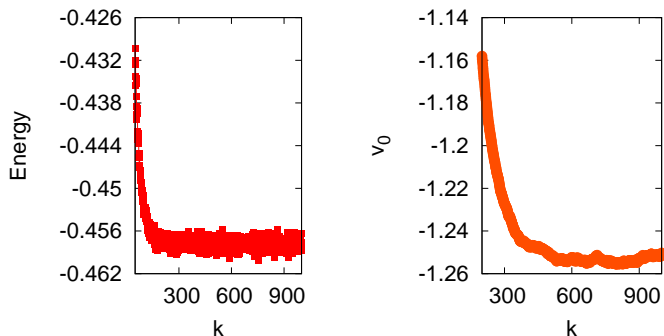


Figure 2.2: Convergence of the iterative application of the stochastic reconfiguration procedure. Left: Convergence of the energy as function of the iteration step  $k$ . Right: Convergence of the on-site Gutzwiller variational parameter  $v_0$ .

2. By means of the variational Monte Carlo, the forces  $f^k$  as well as the overlap matrix  $s_{l,k}$  are computed.
3. With those quantities at hand, the change  $\delta\alpha_k$  is computed and the parameters are updated as  $\alpha'_k = \alpha_k + \delta t \delta\alpha_k$ .
4. The convergence of the parameters is verified by checking that both the energy and the parameters themselves are no longer changed within the natural fluctuations of the Monte Carlo procedure, i.e., the parameters fluctuate around their converged mean value.
5. If the convergence has been reached the algorithm stops. If not, then the new parameters  $\alpha'_k$  are inserted in step 2 iteratively until convergence is reached.

After the algorithm has reached convergence, we perform several iterations in that regime; in this way, the variational parameters can be determined more accurately by averaging them over all these iterations and by evaluating also the corresponding statistical error bars. In Fig. 2.2 it is shown how the convergence

---

## 2.4 The Green's function Monte Carlo method

of the energy and one of the variational parameters corresponding to the on-site Gutzwiller parameter  $v_0$  is reached. The stochastic reconfiguration method is applied to the Bose Hubbard model in a one-dimensional lattice with  $L = 10$  and  $U/t = 2.0$ , with a translationally invariant Jastrow wave function with 5 parameters. In the figure we have plotted only one variational parameter, but all parameters are likewise converged.

## 2.4 The Green's function Monte Carlo method

The Green's Function Monte Carlo approach [61, 62] is based on a stochastic implementation of the power method technique that allows, in principle, to extract the actual ground state  $|\Psi_{GS}\rangle$  of a given Hamiltonian  $\mathcal{H}$ , from any starting wave function  $|\Psi_0\rangle$ , provided that  $\langle\Psi_0|\Psi_{GS}\rangle \neq 0$ :

$$|\Psi_{GS}\rangle = \lim_{n \rightarrow \infty} (\Lambda - \mathcal{H})^n |\Psi\rangle. \quad (2.38)$$

On large sizes it is not possible to evaluate exactly this recursive equation, because, after few steps, the application of  $(\Lambda - \mathcal{H})$  generates transitions to a very large number of different states, implying a huge amount of memory occupation. Therefore, we define a stochastic approach, in the sense that the wave function

$$\langle x | (\Lambda - \mathcal{H})^n | \Psi \rangle \quad (2.39)$$

is evaluated in a stochastic way. To this purpose, we define the so-called walker, which corresponds, at each iteration  $n$  of the Markov chain, to a configuration  $|x_n\rangle$  with an associated weight  $\omega_n$  associated to the amplitude of the wave function at configuration  $|x_n\rangle$ . The goal of the Green's function Monte Carlo approach is to define a Markov process, yielding, after a large number  $n$  of iterations, a probability distribution  $P_n(x_n, \omega_n)$  for the walker<sup>1</sup>, which determines the ground-state wave function  $|\Psi_{GS}\rangle$ . To be specific, in the most simple formulation we would require:

$$\int d\omega \omega P_n(x_n, \omega) = \langle x | \Psi_n \rangle, \quad (2.40)$$

---

<sup>1</sup>From now on, we will indicate the configuration  $|x\rangle$  simply as  $x$

## 2.4 The Green's function Monte Carlo method

---

i.e., the amplitude of the wave function  $|\Psi_n\rangle$  at  $x_n$  is obtained by integrating, over all the weights  $\omega_n$ , the probability  $P_n(x_n, \omega_n)$ . In order to construct a Markov chain for solving the ground state of the Hamiltonian  $\mathcal{H}$ , it is necessary to assume that all the matrix elements of the so-called Green's function

$$G_{x',x} = \langle x' | \Lambda - \mathcal{H} | x \rangle, \quad (2.41)$$

are positive definite, so that they may have a meaning of probability. For the diagonal element  $G_{x',x}$  there is no problem: we can always satisfy this assumption by taking a sufficiently large shift  $\Lambda$ . However, the requirement of positiveness is indeed important, and not trivial, for the non-diagonal elements of  $G$ , and is fulfilled only by particular Hamiltonians, like the Bose-Hubbard model, and generally for bosonic Hamiltonians without frustration. If it is not fulfilled, i.e., if  $G_{x',x} < 0$  for some pairs  $(x', x)$ , we say that we are in presence of the so-called sign problem. Once positiveness is assumed to hold, we can divide up the Green's function into the product of two factors: a stochastic matrix  $p_{x',x}$  (by definition, a matrix with all positive elements and with the normalization condition  $\sum_{x'} p_{x',x} = 1$ ) times a scale factor  $b_x$ . Indeed, if we define  $b_x = \sum_{x'} G_{x',x}$  to be such a scale factor, then  $p_{x',x} = G_{x',x}/b_x$  is trivially positive and column normalized, and is therefore the stochastic matrix we are looking for. Now we are able to define a Markov process that leads to the condition in Eq. (2.40) after a large enough number of iterations. Indeed, given  $(x_n, \omega_n)$  we can generate  $x_{n+1}$  with probability  $p_{x_{n+1},x_n}$ , and update the weight according to  $\omega_{n+1} = \omega_n b_{x_n}$ . This Markov process can be very easily implemented for generic correlated Hamiltonians on a lattice, since the number of non-zero entries in the stochastic matrix  $p_{x_{n+1},x_n}$ , for given  $x_n$ , is small, and typically growing only as the number of lattice sites  $L$ . Now, it is immediate to verify that the conditional probability  $K$  of the new walker  $(x_{n+1}, \omega_{n+1})$ , given the old one at  $(x_n, \omega_n)$ , is simply:

$$K(x_{n+1}, \omega_{n+1} | x_n, \omega_n) = p_{x_{n+1},x_n} \delta(\omega_{n+1} - b_{x_n} \omega_n) \quad (2.42)$$

Thus, the Master equation corresponding to the probability density  $P_n(x_n, \omega_n)$  is given by

$$P_{n+1}(x_{n+1}, \omega_{n+1}) = \sum_x \int d\omega K(x_{n+1}, \omega_{n+1} | x, \omega) P_n(x, \omega) \quad (2.43)$$

---

## 2.4 The Green's function Monte Carlo method

Finally, given Eq. (2.43), it can be proved, by means of the induction principle, that the following relation holds:

$$\Psi_{GS}(x) = \lim_{n \rightarrow \infty} \langle \omega_n \delta_{x,x_n} \rangle = \lim_{n \rightarrow \infty} \int d\omega \omega_n P_n(x_n, \omega_n) \quad (2.44)$$

Now, within this formalism, we can compute the ground-state energy, by averaging the random variable  $e(x) = \sum_{x'} \mathcal{H}_{x',x} = \Lambda - b_x$ . In fact:

$$\frac{\langle \omega_n e(x_n) \rangle}{\langle \omega_n \rangle} = \frac{\sum_{x_n} \int d\omega_n \omega_n e(x_n) P_n(x_n, \omega_n)}{\sum_{x_n} \int d\omega_n \omega_n P_n(x_n, \omega_n)} = \frac{\sum_{x_n} e(x_n) \Psi_n(x_n)}{\sum_{x_n} \Psi_n(x_n)} \quad (2.45)$$

which, in the limit  $n \rightarrow \infty$  tends to the ground state energy. However, in Eq. (2.45), the calculation of the energy, with the above described Green's function technique, will not satisfy the zero variance property, which holds instead for the variational Monte Carlo we introduced before. [59] In fact, the random quantity  $e(x)$ , defined above, does not depend on any variational guess  $|\Psi_g\rangle$  and, therefore, its statistical fluctuations cannot be reduced by a better wave function  $|\Psi_g\rangle$ , as it is possible in the variational Monte Carlo case.

### 2.4.1 Importance Sampling

It is possible to recover this important property of the variational Monte Carlo, by a slight modification of the iteration technique. To this purpose, it is enough to consider the so-called importance sampling Green's function:

$$\bar{G}_{x',x} = \Psi_g(x') G_{x',x} / \Psi_g(x). \quad (2.46)$$

The spectrum of the new operators  $\bar{H}$  ( $\bar{G}$ ) is unchanged, however the eigenvector is transformed. To see this, let us just write the matrix product of the Hamiltonian  $H_{x,x'}$  and one generic eigenstate  $\Psi_k(x)$  with eigenvalue  $E_k$ ,

$$\Psi_k(x) E_k = \sum_{x'} H_{x,x'} \Psi_k(x') \quad (2.47)$$

The important sampled problem will have eigenvectors which are different from the ones of the initial problem, the transformed problem now looks like

$$\Psi_g(x) \Psi_k(x) E_k = \sum_{x'} \bar{H}_{x,x'} \Psi_g(x') \Psi_k(x'). \quad (2.48)$$

## 2.4 The Green's function Monte Carlo method

---

Nevertheless, it is clear that the eigenvalues remain unchanged. Whenever  $\bar{G}_{x',x} \geq 0$  for every  $(x', x)$  we can decompose it in the following manner, to define a Markov chain similar to the one we already introduced:

$$p_{x',x} = \bar{G}_{x',x}/b_x \quad (2.49)$$

$$b_x = \sum_{x'} \bar{G}_{x',x} = \Lambda - \frac{\sum_{x'} \Psi_g(x') \mathcal{H}_{x',x}}{\Psi_g(x)} = \Lambda - E_x \quad (2.50)$$

where  $E_x$  is the local energy, already defined in Eq. (2.10). Now, if the trial wave function  $|\Psi_g\rangle$  used in the importance sampling procedure coincides with the correct ground-state wave function, i.e.,  $|\Psi_g\rangle = |\Psi_{GS}\rangle$ , consequently  $E_x = E_{GS}$  is a constant for every  $x$ , and statistical fluctuations vanish exactly. All the previous derivations can be repeated also in this case with importance sampling, the difference being only appropriate factors depending on  $|\Psi_g\rangle$ . We thus obtain for instance

$$\langle \omega_n \delta_{x,x_n} \rangle = \Psi_g(x) \Psi_n(x) \quad (2.51)$$

$$E_{GS} = \lim_{n \rightarrow \infty} \frac{\langle \omega_n E_x \rangle}{\langle \omega_n \rangle} = \lim_{n \rightarrow \infty} \frac{\langle \Psi_g | \mathcal{H} (\Lambda - \mathcal{H}) | \Psi_0 \rangle}{\langle \Psi_g | (\Lambda - \mathcal{H}) | \Psi_0 \rangle} \quad (2.52)$$

Since the convergence of the above limit is exponentially fast in  $n$  (at least for any finite size lattice, where a finite gap to the first excitation exists), it is enough to stop the iteration to a reasonably small finite  $n = l$ . Then, instead of repeating the Markov chain several times up to  $n = l$ , to accumulate statistics, it is clearly more convenient to average over a long Markov chain with  $N \gg l$ , where  $N$  is the total number of iterations, and considering the corresponding estimates in Eq. (2.52):

$$E_{GS} \simeq \frac{\sum_{n>n_0}^N Q_n^l E_{xn}}{\sum_{n>n_0}^N Q_n^l} \quad (2.53)$$

where  $n_0$  is the number of iterations required for the statistical equilibration of the Markov process and the weighting factors  $Q_n^l$  are given by:

$$Q_n^l = \prod_{i=1}^l b_{x_{n-i}}. \quad (2.54)$$

So, at each discrete time  $n - l$  we can take an equilibrated configuration, and consider  $l$  iterations of the Markov process with initial condition  $\omega_{n-l} = 1$ , leading, after  $l$  iterations, to a final weight  $\omega_l = Q_n^l$ , at time  $n$ .

### 2.4.2 Forward walking technique

Besides energy, Green's function Monte Carlo can be also used efficiently to compute expectation values of local operators  $\hat{O}$ , i.e., operators which are diagonal on all the elements of the configuration basis  $|x\rangle$ ,

$$\hat{O}|x\rangle = O(x)|x\rangle \quad (2.55)$$

where  $O(x)$  is the eigenvalue corresponding to the configuration  $|x\rangle$ , which coincides with its local value  $O_x$  just because the operator is diagonal. By using the Green's function Monte Carlo, the configurations of the walkers are distributed according to  $\Psi_g(x)\Psi_{GS}(x)$ , however, in order to compute

$$\langle \hat{O} \rangle = \frac{\langle \Psi_{GS} | \hat{O} | \Psi_{GS} \rangle}{\langle \Psi_{GS} | \Psi_{GS} \rangle} \quad (2.56)$$

further work is required. In contrast with what happens for energy, we cannot write the equality

$$\langle \hat{O} \rangle = \lim_{b \rightarrow \infty} \frac{\langle \omega_n O_{x_n} \rangle}{\langle \omega_n \rangle} = \frac{\langle \Psi_g | \hat{O} | \Psi_{GS} \rangle}{\langle \Psi_g | \Psi_{GS} \rangle} \quad (2.57)$$

because the ground state is not an eigenstate of the operator  $\hat{O}$ . In fact, the quantity  $\langle \hat{O} \rangle_{MA} = \frac{\langle \Psi_g | \hat{O} | \Psi_{GS} \rangle}{\langle \Psi_g | \Psi_{GS} \rangle}$ , called mixed average, is equal to  $\langle \hat{O} \rangle$  only if the ground state is an eigenstate of  $\hat{O}$ , as it happens with the energy. In order to compute the mean value of a generic local operator  $\hat{O}$  over the ground state, we introduce the so-called forward walking technique, for which we filter the ground state on both sides of the operator as follows,

$$\langle \hat{O} \rangle = \lim_{l, m \rightarrow \infty} \frac{\langle \Psi_g | (\Lambda - \mathcal{H})^m \hat{O} (\Lambda - \mathcal{H})^l | \Psi_0 \rangle}{\langle \Psi_g | (\Lambda - \mathcal{H})^{m+l} | \Psi_0 \rangle} \quad (2.58)$$

From a statistical point of view, Eq. (2.58) amounts to sample a configuration  $x$  after  $l$  steps, then measure the quantity  $O_x$ , and finally let the walker propagate forward for further  $m$  steps. In order to evaluate the stochastic average, an approach similar to that done for the energy is possible. In this case we have:

$$\langle \hat{O} \rangle = \frac{\sum_{n > n_0} O_{x_{n-m}} Q_n^{l,m}}{\sum_{n > n_0} Q_n^{l,m}} \quad (2.59)$$

## 2.4 The Green's function Monte Carlo method

---

where the new weight  $Q_n^{l,m}$  is given by

$$Q_n^{l,m} = \prod_{i=1}^{l+m} b_{x_{n-i}}. \quad (2.60)$$

The  $n_0$  is the number of iterations required for the statistical equilibration of the Markov process and also we have assumed that the weight  $\omega_{n-(m+l)-1} = 1$ . The exponents  $l$  and  $m$  should be large enough in order to filter out the high energy components on both sides of the operator  $\hat{O}$  in Eq. (2.58).

### 2.4.3 Many walkers formulation

All the previously described procedures are, in principle, free from any approximation and they give exact results within the statistical errors (so long as the condition  $\bar{G}_{x',x} \geq 0$  holds). Unfortunately, the weight  $Q_n^{l,m}$  grows exponentially with the increment of  $l + m$ , implying a divergent variance in the energy average. Indeed,  $Q_n^{l,m}$  is a product of  $l + m$  different factors and it can assume very large or very small values. This problem has a simple solution by considering the Green's Function Monte Carlo technique with many walkers and by introducing a reconfiguration scheme, which enables to drop out the irrelevant walkers with small weights. Calandra and Sorella [61] have introduced a reconfiguration scheme working at fixed number of walkers, in a way that allows us to control the bias due to the finite walker population. We consider  $M$  walkers and label the corresponding configurations and weights with a couple of vectors  $(\mathbf{x}, \boldsymbol{\omega})$ , with each component  $(x_i, \omega_i)$ ,  $i = 1, \dots, M$  corresponding to the  $i$ -th walker. It is then easy to generalize the Master equation of Eq. (2.43) to many independent walkers. If the evolution of the distribution probability  $P$  is done without further restrictions, each walker is uncorrelated from any other one, and we have:

$$P_n(x_1, \dots, x_M, \omega_1, \dots, \omega_M) = P_n(x_1, \omega_1) \dots P_n(x_M, \omega_M) \quad (2.61)$$

Similarly to the previous case (2.52), we can define the state evolved at iteration  $n$  with the Green's function  $\bar{G}$ :

$$\Psi_n(x) \Psi_g(x) = \left\langle \frac{1}{M} \sum_{i=1}^M \omega_i \delta_{x,x_i} \right\rangle = \int [d\boldsymbol{\omega}] \sum_{\mathbf{x}} \frac{\sum_i \omega_i \delta_{x,x_i}}{M} P_n(\mathbf{x}, \boldsymbol{\omega}) \quad (2.62)$$

## 2.4 The Green's function Monte Carlo method

---

where the symbol  $[d\boldsymbol{\omega}]$  indicates the  $M$  dimensional integral over the  $\omega_i$  variables. Since we are interested in the state  $|\Psi_n\rangle$ , we can define a reconfiguration process (that is the process of removing the most irrelevant walkers) that changes the probability distribution  $P_n$  without changing the statistical average  $\langle \frac{1}{M} \sum_{i=1}^M \omega_i \delta_{x,x_i} \rangle$ , that is relevant in the calculation of  $|\Psi_n\rangle$ . This can be obtained by a particular Markov process applied to the configuration  $(\mathbf{x}, \boldsymbol{\omega})$ , which leads to a new set of walkers  $(\mathbf{x}', \boldsymbol{\omega}')$ . Each new walker  $(x'_j, \omega'_j)$ , with  $j = 1, \dots, M$ , will have the same weight  $\omega'_j = \bar{\omega} = \frac{1}{M} \sum_j^M \omega_j$  and an arbitrary configuration  $x'_j$ , among the  $M$  possible old configurations  $x_k$ ,  $k = 1, \dots, M$ , chosen with a probability  $p_k$  proportional to the weight of that configuration,  $p_k = \frac{\omega_k}{\sum_j \omega_j}$ . It is clear that, after this reconfiguration, the new set of  $M$  walkers have by definition the same weights  $\bar{\omega}$ , and most of the irrelevant walkers with small weights have dropped out. It is also easy to derive the Master equation corresponding to this reconfiguration Markov process:

$$P'_n(\mathbf{x}', \boldsymbol{\omega}') = \sum_{\mathbf{x}} \int [d\boldsymbol{\omega}] K(\mathbf{x}', \boldsymbol{\omega}' | \mathbf{x}, \boldsymbol{\omega}) P_n(\mathbf{x}, \boldsymbol{\omega}), \quad (2.63)$$

where the kernel  $K$  is given by

$$K(\mathbf{x}', \boldsymbol{\omega}' | \mathbf{x}, \boldsymbol{\omega}) = \prod_{j=1}^M \left( \frac{\sum_i \omega_i \delta_{x'_j, x_i}}{\sum_i \omega_i} \right) \delta \left( \omega'_j - \frac{1}{M} \sum_i^M \omega_i \right) \quad (2.64)$$

Let us note that  $K$  is simple, in this case, because all the new walkers are independent from each other, and  $K$  factorizes for each of them. By iterating this process the weights of all the walkers are kept approximately equal during the simulation. This property yields a considerable reduction of the statistical errors, as the variance of the average weight is reduced by a factor of  $\sqrt{M}$ . This allows therefore a more stable propagation even for large  $l$ .

### Forward walking technique with many walkers

Similarly to what happens in the forward walking technique for a single walker, this technique amounts to sample a set of configurations  $x_j$ , with  $j = 1, \dots, M$  after having propagated them  $l$  steps. Then we measure  $O_x^j$  for each walker and

## 2.4 The Green's function Monte Carlo method

---

finally let them propagate forward for further  $m$  steps. In order to evaluate the stochastic average, we have:

$$\langle \hat{O} \rangle = \frac{\sum_{n>n_0} \hat{O}_{x_{n-m}} \hat{Q}_n^{l,m}}{\sum_{n>n_0} Q_n^{l,m}} \quad (2.65)$$

The value of the quantity  $\hat{O}_{x_{n-m}}$  has to be carefully explained. In practice, the local value of the operator at step  $m - n$ ,  $O_{x_{n-m}}^j$  is measured for all walkers  $j = 1, \dots, M$ .  $m$  steps further (now at step  $n$ ), due to the reconfiguration to keep the walker population stable, some walkers have disappeared and some others have survived. In the average quantity  $\hat{O}_{x_{n-m}}$  we have to take into account only the value of those walkers that survived after the  $m$  reconfiguration steps. Therefore, we have to bookkeep only the values that survive. To do that, we simply replace recursively for  $m$  steps and for each walker  $j$ ,  $O_{x_{k+1}}^j = O_{x_k}^{F_k(j)}$ , for  $k = n - m, n - m + 1, \dots, n$ . The function  $F_k(j)$  describes the reconfiguration scheme at each step  $k$  in the Markov chain: The walker with index  $j$  after the reconfiguration will assume the configuration with index  $F_k(j)$  before it. This function has to be stored for each step in the Markov chain. The average is then computed, after the  $m$  steps reconfiguration as

$$\hat{O}_{x_{n-m}} = \frac{\sum_{j=1}^M O_{x_{n-m}}^j b_{x_n}^j}{\sum_{j=1}^M b_{x_n}^j}, \quad (2.66)$$

taking into account only those values of  $O_{x_{n-m}}^j$  that survived the reconfiguration with their corresponding weights at step  $n$ . Finally we specify the weight in Eq. (2.65)

$$\hat{Q}_n^{l,m} = \prod_{i=1}^{l+m} \hat{b}_{x_{n-i}}, \quad (2.67)$$

where  $\hat{b}_{x_{n-i}} = \frac{1}{M} \sum_{j=1}^M b_{x_{n-i}}^j$ .

### 2.4.4 The superfluid stiffness

We now consider the measurement of the superfluid stiffness. In analogy to what has been done by Pollock and Ceperley at finite temperature, [63] this quantity

## 2.4 The Green's function Monte Carlo method

---

can be also calculated directly at zero temperature by using the Green's function Monte Carlo and the winding numbers:

$$\rho_s = \lim_{\tau \rightarrow \infty} \frac{\langle \Psi_{GS} | |\vec{W}(\tau)|^2 | \Psi_{GS} \rangle}{dL\tau} \quad (2.68)$$

where  $d$  is the dimension,  $L$  is the volume of the system,  $\tau$  is the imaginary diffusion time.  $\vec{W}(\tau) = \sum_i [\vec{r}_i(\tau) - \vec{r}_i(0)]$ . The vector  $\vec{r}_i(\tau)$  is the position of the  $i$ -th particle after evolving it for a imaginary diffusion time  $\tau$  from the initial position  $\vec{r}_i(0)$ . The diffusion process must be done without considering periodic boundary conditions, namely, by increasing or decreasing the values of the coordinates of a particle that crosses the boundaries of the cluster. By doing that, the operator  $\vec{W}(\tau)$  describes the net number of times the paths of the total number of particles have wound around the periodic cell of the simulations by tracing the path of the particles from time 0 to  $\tau$ . Pictorially, the superfluid stiffness measures how the particles diffuse in imaginary time. If the superfluid stiffness is finite, the particles flow and the ground state is extended, if it is zero it means that they do not spread over the whole lattice and localize in a certain volume.

## Chapter 3

# The Bose-glass phase in low-dimensional lattices

In this Chapter we discuss the emergence of the Bose-glass phase in low-dimensional lattices by means of the variational and Green's function Monte Carlo techniques. We show that a proper characterization of the phase diagram on finite disordered clusters requires the knowledge of probability distributions of physical quantities rather than their averages. This holds in particular for determining the stability region of the Bose-glass phase, the compressible but not superfluid phase that exists whenever disorder is present. The analysis of the distribution of the gap is carried out in detail for several lattices which we use to study the evolution of Bose-glass phase by going from one dimension to two dimensions. This evolution is tracked by performing numerical simulations in one dimension, two-leg ladder, three-leg ladder and finally in a true two-dimensional lattice. These results suggest that a similar statistical analysis could be performed also to interpret experiments on cold gases trapped in disordered lattices, limited as they are to finite sizes. Finally, we study a simple system of non-interacting spinless fermions with a staggered potential immersed in a disordered on-site potential for which large size systems can be reached. The results suggest that the expected critical points of phase transitions which are driven by exponentially rare regions are expected to be visible on very large scales. Nevertheless, the competing phases are numerically observed and they are, therefore, expected to be observed in experiments on finite lattices as for instance with ultracold atoms.

### 3.1 The Bose-glass phase

As it was discussed in chapter 1, the phase diagram of a disordered Bose-Hubbard model is supposed to include three different phases. [9, 10] When the interaction is strong and the number of bosons is a multiple of the number of sites, the model should describe a Mott insulator, with bosons localized in the potential wells of the optical lattice. This phase is not superfluid nor compressible. When both interaction and disorder are weak, a superfluid and compressible phase must exist. In the presence of disorder a third phase arises: the Bose glass, which is compressible but not superfluid. [9] Indeed, when disorder is very strong, bosons localize in the deepest potential wells, which are randomly distributed. The coherent tunneling of a boson between these wells is suppressed just as in the usual Anderson localization, hence the absence of superfluidity, in spite of the fact that displacing a boson from one well to another one may cost no energy, hence a finite compressibility. Based on the same single-particle description used for explaining Anderson localization, it was argued that disorder prevents a direct superfluid to Mott insulator transition, [9] a speculation that has been subject to several theoretical studies. [11, 12, 13, 14, 15, 16, 17, 18]

A simple way to justify the validity of the single-particle arguments is to imagine that the few carriers, which are released upon doping a Mott insulator, effectively behave as bosons at low density. In this case the single-particle Anderson localization scenario is likely to be applicable since the few interacting bosons occupy strongly localized states in the Lifshitz's tails. The implicit assumption is that the Mott-Hubbard side bands survive in the presence of disorder and develop Lifshitz's tails that fill the Mott-Hubbard gap. This scenario is quite appealing hence worth to be investigated theoretically. However, a direct comparison of theory with experiments has to face the problem that experiments on cold gases are unavoidably limited to finite systems with hundreds of sites and finite number of disorder realizations. Therefore, objects like Lifshitz's tails, which arise from rare disorder configurations, might not be easily accessible. This fact demands an effort to identify salient features of the Bose glass that may distinguish the latter from a superfluid or a Mott insulator already on finite systems. This is actually the scope of this chapter. Specifically, we are going to show that the

statistical distribution of the energy gaps extracted by a numerical simulation of finite size systems is a significant property that can discriminate among different phases. [64] The numerical simulations have been carried out for a single chain, a two- and three-leg ladder system and finally for a genuine two-dimensional lattice. The ladder systems are of interest because they can be experimentally realized, not only in optical lattices but also in magnetic materials, as mentioned in chapter 1 where a very recent neutron scattering data reported the evidence of the spin-analogous of a Bose-glass phase in a spin-ladder compound in which disorder was induced by random chemical substitution. [47] Finally, in this chapter we shall also briefly discuss how the probability distribution of the energy gaps could be experimentally accessed.

## 3.2 Model

As it was discussed in the introductory chapter, the simplest Hamiltonian that contains the basic ingredients of strong correlations and disorder is

$$\mathcal{H} = -\frac{t}{2} \sum_{\langle i,j \rangle} b_i^\dagger b_j + h.c. + \sum_i \left( \frac{U}{2} n_i (n_i - 1) + \epsilon_i n_i \right), \quad (3.1)$$

where  $\langle \dots \rangle$  indicates nearest-neighbor sites,  $b_i^\dagger$  ( $b_i$ ) creates (destroys) a boson on site  $i$ , and  $n_i = b_i^\dagger b_i$  is the local density operator. The on-site interaction is parameterized by  $U$ , whereas the local disordered potential is described by random variables  $\epsilon_i$  that are uniformly distributed in  $[-\Delta, \Delta]$ . Here, we consider bosons on a one-dimensional (1D) chain,  $N$ -leg ladders, and a two-dimensional (2D) square lattice, and study model of Eq. (3.1) by Green's function Monte Carlo with a fixed number  $M$  of bosons on  $L$  sites,  $n = M/L$  being the average density. Here the chemical potential  $\mu$  has not been considered since the algorithm works in the canonical ensemble, such that it does not play any role in our simulations. We recall that the Green's function Monte Carlo is a zero-temperature algorithm that provides numerically exact results because the off-diagonal elements of the Hamiltonian in Eq. (3.1) are all negative, implying the absence of sign problem. One starts from a trial, e.g., variational wave function and filters out high-energy components by iterative applications of the imaginary-time evolution operator. In

order to improve the numerical efficiency, it is important to consider an accurate starting wave function. In the clean case, it has been recently shown [56] that good accuracy can be achieved by applying a density-density Jastrow factor to a state where all bosons are condensed at  $q = 0$ , i.e.,

$$|\Psi_{clean}\rangle = \exp\left(\sum_{i,j} v_{i,j} n_i n_j\right) |SF\rangle \quad (3.2)$$

where  $|SF\rangle = \left(\sum_i b_i^\dagger\right)^M |0\rangle$  is the non-interacting Bose condensate of  $M$  particles,  $n_i$  is the on-site density operator, and  $v_{i,j}$  are translationally invariant parameters that are determined by minimizing the variational energy. In the presence of disorder, we just add to Eq. (3.2) a site-dependent one-body Jastrow factor

$$|\Psi\rangle = \exp\left(\sum_i g_i n_i\right) |\Psi_{clean}\rangle \quad (3.3)$$

where  $g_i$ 's are  $L$  additional variational parameters. This wave function becomes the exact ground state for  $U = 0$  and for any  $\Delta$  taking  $v_{i,j} = 0$  and  $g_i = \ln \alpha_i$  with  $\alpha_i$  being the amplitude at site  $i$  of the lowest-energy single-particle eigenstate of the non-interacting Hamiltonian. In order to find the wave function in this limit it is enough to diagonalize the single-particle Hamiltonian written in the real basis set,

$$\mathcal{H} = -\frac{t}{2} \sum_{\langle i,j \rangle} b_i^\dagger b_j + h.c. + \sum_i \epsilon_i n_i. \quad (3.4)$$

The single-particle ground state is given by  $\alpha_i$  and the many-body state is constructed by a condensate of  $M$  particles on that state,

$$|\Psi\rangle = \left(\sum_{i=1}^L \alpha_i b_i^\dagger\right)^M |0\rangle, \quad (3.5)$$

which in turn can be written by expanding the sum as

$$|\Psi\rangle = \sum_{k_1+k_2+\dots+k_L=M} \binom{M}{k_1, k_2, \dots, k_L} \alpha_1^{k_1} \alpha_2^{k_2} \dots \alpha_L^{k_L} \sqrt{k_1!} \sqrt{k_2!} \dots \sqrt{k_L!} |k_1, k_2, \dots, k_L\rangle, \quad (3.6)$$

where  $\binom{M}{k_1, k_2, \dots, k_L} = \frac{M!}{k_1! k_2! \dots k_L!}$  are the multinomial coefficients and the summation is taken over all sequences of nonnegative integer indices  $k_1$  through  $k_L$  such the

sum of all  $k_i$ 's is  $M$ . It is now clear that if we apply the operator  $e^{\sum_i^L g_i n_i}$  to the perfect superfluid state, we recover the wave function in Eq. (3.6) with  $g_i = \ln \alpha_i$ . A similar wave function to the one described in Eq. (3.3) has been recently used to describe the fermionic Hubbard model in the presence of disorder.[57] The flexibility of this variational state makes it possible to describe equally well superfluid, Bose glass, and Mott-insulating states.

### 3.3 Results

Let us start by analyzing the case of finite on-site interactions  $U/t$  and consider the case with  $n = 1$ . The Bose-Hubbard model has been extensively studied in recent years, [11, 12, 13, 14, 15, 16, 17, 18] with special focus on the question whether a direct superfluid to Mott insulator transition does exist or not. This issue has been finally solved only recently. The solution is based on the observation that, if the disorder strength  $\Delta$  is larger than half of the energy gap of the clean Mott insulator  $E_g^{\text{clean}}$ , then the ground state must be compressible, otherwise is incompressible. [17, 18, 42] Therefore, the independent measurements of the superfluid stiffness  $\rho_s$  at finite  $\Delta$  and of the clean Mott gap  $E_g^{\text{clean}}$  allow a precise determination of the phase boundaries between different phases and demonstrate unambiguously the existence of a Bose glass in between the superfluid and Mott phases as it was assumed in the introductory part of this thesis. [17, 18] The above prescription is very effective in a numerical simulation since both  $\rho_s$  with disorder and  $E_g^{\text{clean}}$  without disorder can be determined quite accurately. On the other hand, it would be desirable to have simple instruments to establish directly the nature of the phase of a given system in a realistic finite-size experimental setup. In a clean system, this program can be accomplished by measuring the gap, conventionally defined by  $E_g = \mu^+ - \mu^-$ , where  $\mu^+ = E_{M+1} - E_M$  and  $\mu^- = E_M - E_{M-1}$  ( $E_M$  being the ground-state energy with  $M$  particles). In disordered systems, the Mott gap can be overcome by transferring particles between two regions with almost flat disorder shifting the local chemical potential upward and downward, respectively. These regions may be far apart in space and represent rare fluctuations (Lifshitz's tail regions). Therefore, it is quite likely that the

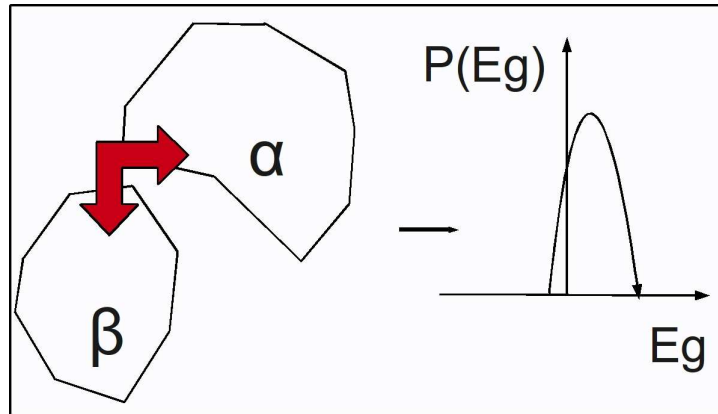


Figure 3.1: Sketch of the construction of the distribution of the gap  $P(E_g)$  by considering the energy cost of the transfer of particles between different realizations of disorder of clusters  $\alpha$  and  $\beta$ .

conventional definition of the gap,

$$\bar{E}_g = 1/\mathcal{N} \sum_{\alpha=1,\dots,\mathcal{N}} (\mu_{\alpha}^{+} - \mu_{\alpha}^{-}), \quad (3.7)$$

where  $\alpha$  denote the disorder realizations, will miss the Lifshitz's tails for any accessible number of disorder realizations  $\mathcal{N}$ . This fact gives rise to a finite gap, even when the actual infinite system would be compressible. To circumvent such a difficulty, it is useful to imagine that a large system is made by several subsystems, each represented by the  $L$ -site cluster under investigation, and construct the gap by using  $\mu^{+}$  and  $\mu^{-}$  from *different* disorder realizations, as depicted in Fig. 3.1, where the gap is analyzed by considering the processes of taking one particle from region  $\alpha$  to region  $\beta$  and vice versa, for all pair of the realizations among the total set of  $\mathcal{N}$ . In other words, one could define an alternative estimate of the gap as

$$E_g^{\min} = \min_{\alpha,\beta} |\mu_{\alpha}^{+} - \mu_{\beta}^{-}|, \quad (3.8)$$

with all the disorder realizations  $\alpha$  and  $\beta$ . In the limit of very large systems where boundary effects become negligible,  $E_g^{\min}$  must eventually coincide with  $\bar{E}_g$ . This is because as the size of the system gets larger and larger, the values of  $\mu_{\alpha}^{+}$  and  $\mu_{\beta}^{-}$  start to become more and more similar and independent of the choice

of the realizations, which implies that the distributions of the gap slowly shrink to the value of the gap in the infinite system. In finite systems the two estimates differ, nevertheless we believe that  $E_g^{\min}$  is more representative since it aims at capturing the phenomenon underneath the Lifshitz's tails, as we are going to show numerically. Besides  $E_g^{\min}$ , one can determine the full gap distribution,

$$P(E_g) = \sum_{\alpha\beta} \delta(E_g - \mu_\alpha^+ + \mu_\beta^-), \quad (3.9)$$

which we will show has remarkable properties. We mention that, by our definition,  $P(E_g < 0)$  could well be finite on finite systems, although it must vanish in the thermodynamic limit where  $P(E_g)$  becomes peaked at a single positive (or vanishing) value, i.e., the actual gap. Experimental estimates for the gap have been so far obtained in ultra-cold atomic systems mainly in two ways: one consists in applying a gradient potential that compensates the Mott energy gap and allows tunneling between neighboring sites; [19] the other method exploits a sinusoidal modulation of the main lattice height for stimulating resonant production of excitations. [39, 51] Further theoretical suggestions aimed at detecting the presence of a Mott gap include trap squeezing, in which the strength of the trap is varied after which measurements of the effect of the change of the chemical potential due to the change of the trapping are quantified. [65] Also, the energetics of the formation of Mott domains has been investigated in connection with time-of-flight experiments. [66] From our perspective, in experiments with ultra-cold atoms, both  $E_g^{\min}$  and  $P(E_g)$  could be accessed by measuring *separately*  $\mu^+$  and  $\mu^-$  for different disorder realizations. For instance, one could measure the energy releases  $E_M^{\text{rel}}$  of falling atoms when the trap is turned off with the reference number of particles  $M$  and with numbers  $M \pm M'$ . For  $M' \ll M$ , indeed  $E_{M+M'}^{\text{rel}} - E_M^{\text{rel}} \simeq M'\mu^+$  and  $E_M^{\text{rel}} - E_{M-M'}^{\text{rel}} \simeq M'\mu^-$ . In chapter 5 we will discuss how to obtain measurements of the gap in an experimental situation by considering the presence of inhomogeneities due to the confinement, natural to most experiments using cold atoms.

Let us start from the 1D case, whose zero-temperature phase diagram has been worked out by Density-Matrix Renormalization Group (DMRG). [67] Their main results on the phase diagram of the disordered Bose-Hubbard model are

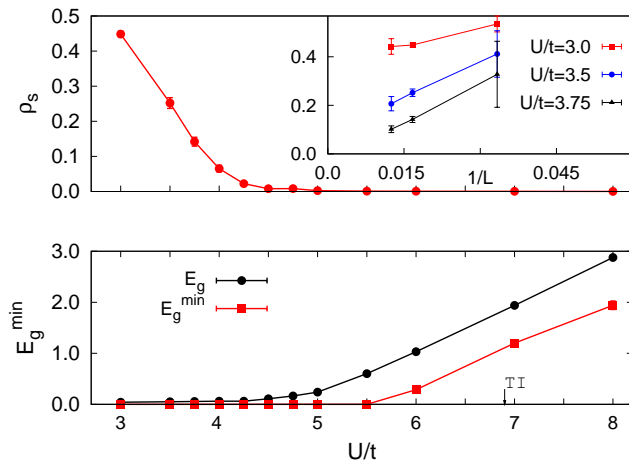


Figure 3.2: Superfluid stiffness  $\rho_s$  of the 1D Bose-Hubbard model as a function of  $U/t$ , the number of sites is  $L = 60$ ; in the inset, the size scaling of  $\rho_s$  is reported. Lower panel: the average and the minimum gap are shown as a function of  $U/t$ . The result obtained from theorem I is also presented with a black arrow around  $U/t \sim 6.9$

shown in Fig. 3.3. At finite values of  $\Delta$ , the on-site interaction  $U$  turns the Bose glass into a superfluid, which remains stable up to  $U = U_{c1}$ , where  $\rho_s$  vanishes. However, the system remains gapless for  $U_{c1} < U < U_{c2}$ , indicating the presence of a Bose-glass phase. At  $U = U_{c2}$  the system turns into an incompressible Mott insulator. For  $\Delta/t = 2$ , we have that  $U_{c1}/t \simeq 3.7$  as reported in Fig. 3.2. If we use  $\bar{E}_g$  as estimator of the actual gap, we find that the Bose glass survives up to  $U_{c2}/t \simeq 5$ , not far from the DMRG estimate, [67] but smaller than the value predicted by the condition  $\Delta = E_g^{\text{clean}}/2$ , which would lead to  $U_{c2}/t \simeq 6.9$ . As discussed before, this discrepancy arises by the inability to catch rare disorder configurations, which could be overcome by analyzing the minimum gap  $E_g^{\min}$  and the full distribution probability  $P(E_g)$ . Indeed, when using  $E_g^{\min}$  as a detector of gapless excitations, we obtain an estimate of  $U_{c2}/t \simeq 6.2$  (see Fig. 3.4), much closer to the value  $U_{c2}/t \simeq 6.9$ . As far as  $P(E_g)$  is concerned, we note that it behaves quite differently in the three different phase, see Fig. 3.5. As long as the phase is superfluid,  $P(E_g)$  is peaked at  $E_g = 0$ . In the Bose glass,  $P(E_g)$  is instead peaked at a finite  $E_g > 0$ , yet  $P(0)$  stays finite. In the Mott insulator,

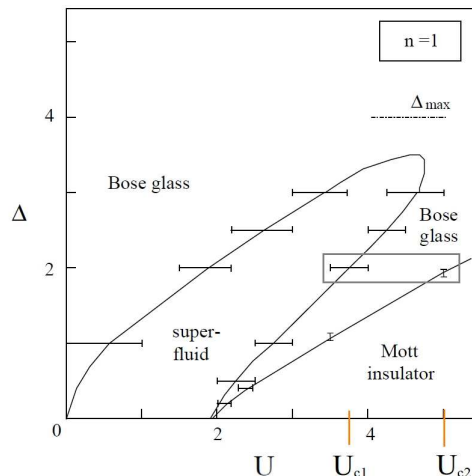


Figure 3.3: Phase diagram obtained by DMRG. Our results for  $\Delta = 2$  (orange sticks) for  $U_{c1}$  and  $U_{c2}$  obtained through the evaluation of  $\bar{E}_g$  are shown for comparison and they are in good agreement with those of the DMRG. The region highlighted inside the box corresponds to the Bose-glass phase

$P(E_g)$  remains peaked at a positive  $E_g$  but  $P(0) = 0$ . This suggests that  $P(E_g)$  could be an efficient tool for discriminating between the different phases.

It is also important to investigate the evolution of the distribution probability  $P(E_g)$  as function of the size of the system. It was already stated that in the limit of very large systems where boundary effects become negligible,  $E_g^{\min}$  must eventually coincide with  $\bar{E}_g$ . Indeed, what we observe is that as the size of the system is increased, the width of the distribution is decreased confirming this scenario, as it is shown in Fig. 3.6. Eventually, the distribution should become sharply peaked and centered at the value of the gap in the infinite system, such that both  $\bar{E}_g$  and  $E_g^{\min}$  will tend to the same value. It is also clear that the average gap obtained from the distribution decreases as the size of the system is increased. In turn it means that the system has more chance to find regions for which the transfer of a particle from a place to the other cost less and less energy, hence decreasing the value of the gap that the system can attain and thus enlarging the stability of the Bose-glass phase. These observations are particularly clear in Fig. 3.6 for  $U/t = 4.25$ , which corresponds to a Bose glass in which for  $L = 30$

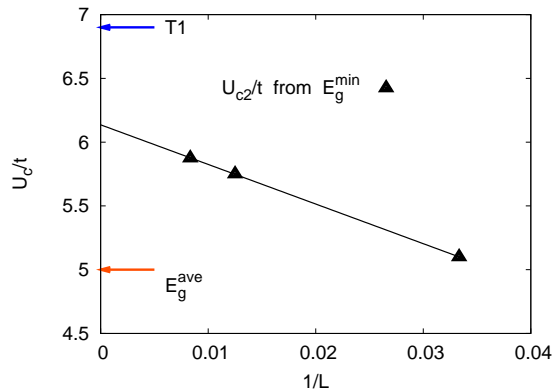


Figure 3.4: Size scaling of the critical  $U_{c2}/t$  obtained from  $E_g^{\min}$  for the 1D case. The results by theorem 1 and by the average gap are also presented for comparison.

the average gap is finite but  $P(0)$  is also finite. Instead as the system is enlarged to  $L = 60$  the distribution shrinks and it is shifted, such that the mean value of the gap now approaches zero, as it should be in the Bose glass. Similarly, in the case of  $U/t = 8$  and  $U/t = 3$ , the distribution is shifted and shrunk. The fact that the distributions are always shifted such that the gap is always smaller with the increase of the size is important to interpret the results. This means that, even though the simulations are carried in small lattices and the critical points expected from the rare region physics are hardly seen, the stability of the Bose glass is always increased with the increase of the size.

Let us now analyze the evolution of the phase diagram when the 2D limit is approached by increasing the number of legs. Moving from  $D = 1$  to  $D = 2$ , the stability region of the Bose glass is expected to shrink, [9] making its observation in experiments more and more difficult. In Fig. 3.7, we report our results for two- and three-leg ladders, and for comparison, also the 2D limit (evaluated for a rather small  $12 \times 12$  cluster). In this case, we take  $\Delta/t = 5$ , in order to have a larger Bose-glass region in between the superfluid and the Mott phases. In 1D, for such large disorder strength no superfluidity is found at all. By increasing the number of legs, we rapidly converge to the 2D results: this fact is particularly clear from the data on the gap. Both the results on the minimum gap and the ones

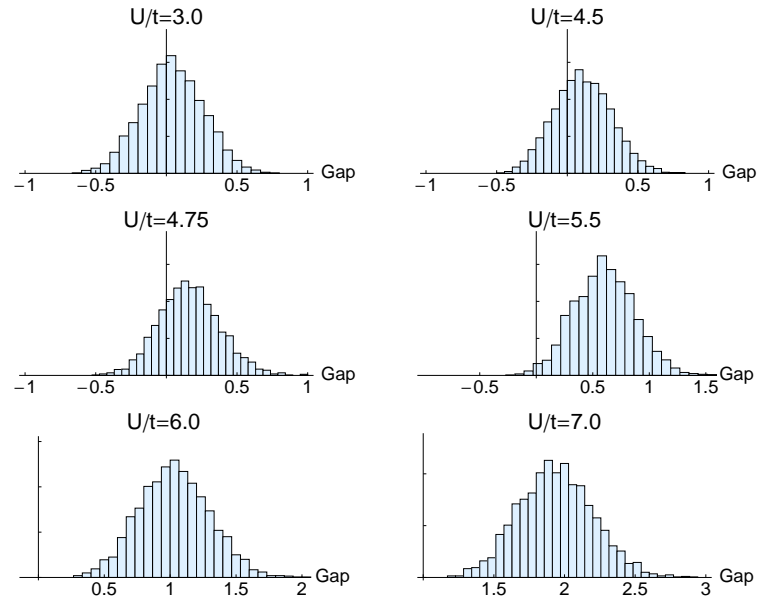


Figure 3.5: Distribution  $P(E_g)$  of the gap in the 1D Bose-Hubbard model for different values of  $U/t$  and  $L = 60$  sites.

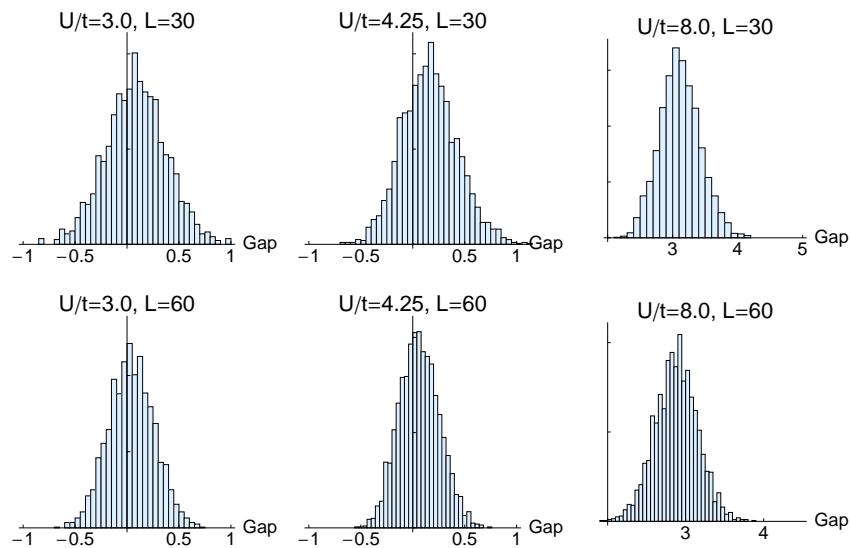


Figure 3.6: Distribution  $P(E_g)$  of the gap in the 1D Bose-Hubbard model for different values of  $U/t$  and  $L = 60$  and  $L = 30$  sites.

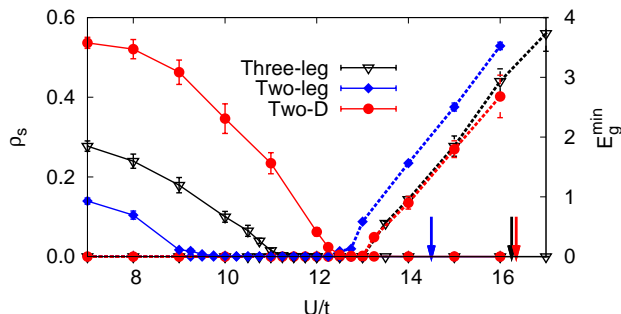


Figure 3.7: Superfluid stiffness  $\rho_s$  (solid lines on the left) and  $E_g^{\min}$  (dashed lines on the right) for different clusters. Two-leg (with  $2 \times 40$  sites) and three-leg (with  $3 \times 50$ ) ladders are shown; the 2D case with a  $12 \times 12$  cluster is also reported for comparison. In all cases the disorder strength is  $\Delta/t = 5$ .

that come from  $\Delta = E_g^{\text{clean}}/2$  shows that the critical  $U$  for the Mott transition is almost the same for three legs and 2D. Also the superfluid stiffness  $\rho_s$  seems to rapidly converge from below to the 2D limit. We also find that the behavior of  $P(E_g)$  is qualitatively similar to what found in 1D, confirming that it can actually discriminate among the different phases (see Fig. 3.8). We mention that, should we use as estimator of the gap  $\bar{E}_g$ , we would have concluded that the Bose glass never exists in 2D and that a direct superfluid to Mott insulator transition occurs. The use of  $E_g^{\min}$  instead demonstrates that the Bose glass does exist also in 2D and always intrudes between the superfluid and the Mott insulator, although its size is strongly reduced. One could argue that the stability of the Bose glass in 2D is not yet clear since the region we found is small, however this region can only get larger with the increase of the system, as the stiffness would get reduced with the enlargement of the cluster. Furthermore, the Bose glass would also be enlarged as it was demonstrated in 1D, because the gap also tends to be smaller as the system gets larger. In realistic experimental setups, a two-leg ladder can be realized through a double well potential along a direction (say,  $x$ ), [68] a potential creating a cigar geometry in the  $z$ -axis, and finally a periodic potential along  $z$ . Similar values of inter- and intra-chain hopping parameter may be achieved by an appropriate tuning of the lattice spacings and height of barriers. Similarly, a

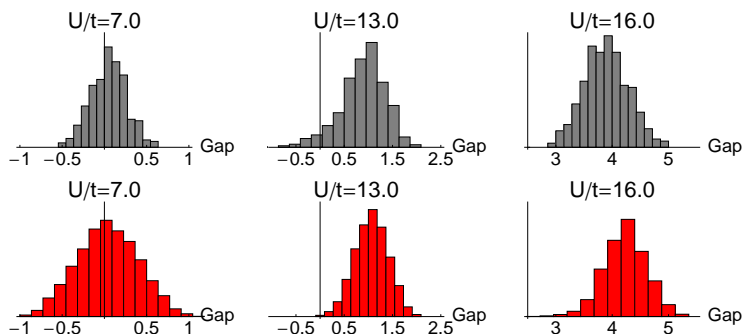


Figure 3.8: Distribution of the gap for the three-leg ladder  $3 \times 50$  (upper row) and 2D  $12 \times 12$  (lower row) for different values of  $U/t$ . In all cases, the disorder strength is  $\Delta/t = 5$

three-leg ladder could also be constructed by considering a three well potential plus a cigar geometry along  $z$ -axis.

We now study concentrate our attention to other quantities which are relevant for experiments. Let us start with the local density which has been recently gained attention from experimentalists. Several related experiments have attempted to perform in-situ imaging of ultracold atomic gases in which they have reported single-atom resolution images of the atomic cloud. Among the most remarkable experiments we have in-situ observation of the Mott-insulating domains, [69] probe of the superfluid-to-Mott-Insulator transition at the single-atom level, [70] and also single-atom-resolved fluorescence imaging of the Mott insulator. [71] Those experiments share one characteristic and it is the fact that they all attempt to directly observe the local density and local charge fluctuations. We now explore what happens to the density profile in disordered systems. In Fig. 3.9, we report the density profile for a given disorder configuration on the  $2 \times 40$  ladder. As soon as the on-site interaction is finite, particles become rather delocalized and many sites of the lattice acquire a finite boson density. There are large fluctuations in the local density with  $n_i$  ranging from  $\simeq 0$  to  $n_i^{max} \simeq 4$ . Although there is a number of sites with very small density, the superfluid stiffness is finite (e.g.,  $\rho_s = 0.015(2)$  for  $U/t = 1$ ). We notice that, although the disorder is uncorrelated from site to site, there is a strong density correlation between

the two legs. By increasing further  $U/t$ , the density becomes more and more homogeneous (for  $U/t = 5$ ,  $n_i^{max} \simeq 2$ , still with rather large fluctuations).  $\rho_s$  has a maximum  $U/t \simeq 5$  and then is suppressed (e.g.,  $\rho_s = 0.0015(5)$  at  $U/t = 11$ ). However, as far as the local density is concerned, we do not observe a drastic modification between the superfluid (e.g.,  $U/t \lesssim 9$ ) and the Bose glass (e.g.,  $U/t \gtrsim 9$ ), even though fluctuations look considerably suppressed for  $U/t = 11$ , see Fig. 3.9. Eventually, for  $U/t \gtrsim 12$  the incompressible Mott phase is reached, with very small density fluctuations ( $n_i \simeq 1$ ), which are not very different from the ones observed in the Bose glass close to the transition. From the analysis of the local density, we get no sharp features for which to distinguish between phase, except for the Mott insulator in which the density distribution is quite homogeneous. A remarkable result is that it is possible to attain superfluidity in a rather disordered density landscape. This means that the notion of localization can not be quantified using estimators related to the local density fluctuations of the ground state of a system. The fact that a rather inhomogeneous phase can attain superfluidity, implies that one has to go beyond local density measurements in order to discriminate between a localized state and a delocalized one.

We now discuss the results for the momentum distribution  $n_k = \langle b_k^\dagger b_k \rangle$ , obtained by a variational technique outlined in Ref. [56]. This measurement is relevant for experiments, as it is the main tool used to determine whether phase coherence is prevalent along the lattice or not. The momentum distribution serves as a detector of the superfluid state, as the presence of phase coherence is generally associated with superfluidity. This quantity can be accessed by measuring the density distribution of the expanded cloud after having switched off all confining potentials as it was explained in chapter 1. In Fig. 3.10, we show the results for a  $2 \times 40$  ladder and different values of  $U/t$  (we also report the results for the variational gap). Since, this is an almost 1D system, no condensation fraction is expected (i.e.,  $n_0/L \rightarrow 0$  in the thermodynamic limit). However, the superfluid phase is characterized by quasi-long-range order with a cusp in  $n_k$  and a logarithmic divergent  $n_0$ , i.e, a large contrast in the interference pattern produced by the interfering cloud. On the other hand, both the Bose-glass and the Mott phases have a smooth momentum distribution, with  $n_0 \rightarrow \text{const}$  in the thermodynamic

### 3.4 Disordered spinless fermions in a staggered ionic potential

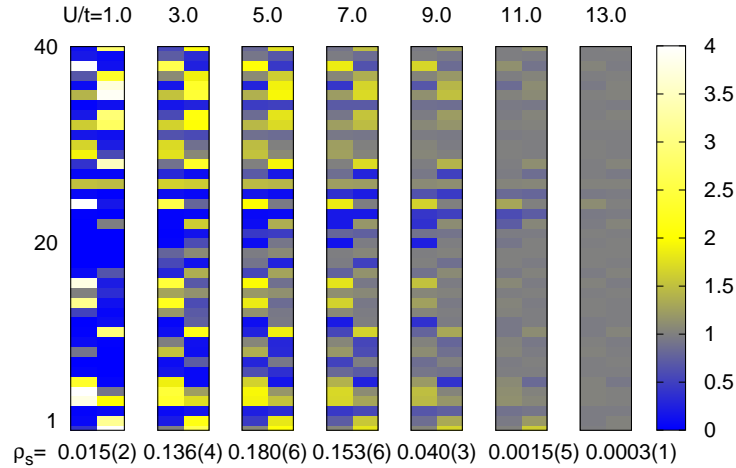


Figure 3.9: Local density for one disorder realization of the  $2 \times 40$  ladder. Darker (brighter) spots indicate lower (higher) densities. The values of the stiffness  $\rho_s$  for the same disorder realization are also reported.

limit, i.e, a low contrasted interference pattern. See also Fig. 3.11 for a detailed profile of the momentum distribution along the  $k_x$  axis. The difference between the Bose glass and the Mott insulator comes from the measurement of the minimum gap, where in the Bose glass vanishes, whereas in the Mott insulator it is finite. Remarkably, the superfluid, the Bose glass and the Mott insulator are correctly described with our simple variational ansatz in Eq. (3.3).

### 3.4 Disordered spinless fermions in a staggered ionic potential

Let us briefly turn our attention to a very simple but illustrative system that can be treated exactly using numerical exact diagonalization, reaching fairly large system sizes. The system under consideration is that of non-interacting one-dimensional spinless fermions in a staggered ionic potential to which an additional

### 3.4 Disordered spinless fermions in a staggered ionic potential

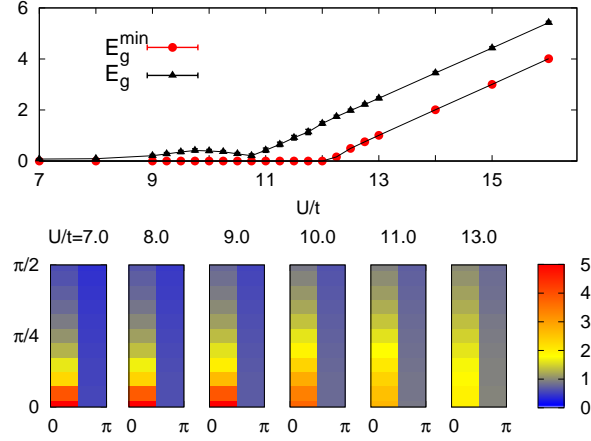


Figure 3.10: Upper panel: variational results for the excitation gap  $\bar{E}_g$  and  $E_g^{\min}$ , for a  $2 \times 40$  ladder. Lower panels: momentum distribution  $n_k$  for the same cluster.

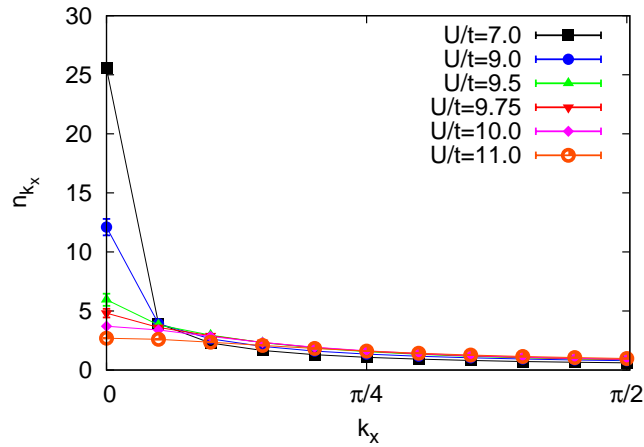


Figure 3.11: Profiles of the momentum distribution  $n_{k_x}$  for the same  $2 \times 40$  ladder

### 3.4 Disordered spinless fermions in a staggered ionic potential

---

disorder term has been added. The Hamiltonian of the system is,

$$\mathcal{H} = -t \sum_{\langle i,j \rangle} (c_i^\dagger c_j + h.c.) + \frac{m}{2} \sum_i n_i (-1)^i + \sum_i (\epsilon_i - \mu) n_i \quad (3.10)$$

where  $\langle \dots \rangle$  indicates nearest-neighbor sites,  $c_i^\dagger$  ( $c_i$ ) creates (destroys) a spinless fermion on site  $i$ , and  $n_i = c_i^\dagger c_i$  is the local density operator. The strength of the on-site staggered potential is parameterized by  $m$ , whereas the local disordered potential is described by random variables  $\epsilon_i$  that are uniformly distributed in  $[-\Delta, \Delta]$ . The chemical potential  $\mu$  fixes the total number of particles  $M$ . Exactly at half filling, the ground state of the clean case  $\Delta/t = 0$  and finite  $m$  corresponds to an incompressible band insulator with an energy gap of exactly equal to  $m$ , whereas at arbitrary filling the system is metallic. The clean Hamiltonian can be diagonalized by a Fourier transform and the emerging spectrum is shown in Fig. 3.12 for  $m = 2$ . Similarly to what happens to a gapped Mott insulator in presence of disorder, one could wonder what is the effect of disorder on the band gap of this simple system. For small disorder  $\Delta \ll m$ , we expect the system to be again a band insulator, whereas for  $\Delta \gg m$  the disorder dominates and the usual Anderson localization takes place. For the situation in which  $\Delta$  and  $m$  are of the same order of magnitude, a phase transition from the band insulator to the Anderson localized phase is expected. Indeed, the situation is very similar to the case of disordered interacting bosons and arguments like theorem 1 should also hold in this case. In the infinite system of spinless fermions one can find exponentially rare regions in which the local disorder is homogeneously shifted upwards or downwards by  $\Delta$ . Suppose there is a large rare region of  $l$  sites where the disorder potential is roughly the same on all sites and equal to  $\Delta$ . In this region both lower and upper bands are rigidly shifted upwards. Similarly, one could find a region of size  $l'$  in which the disorder potential is equal to  $-\Delta$  on all sites, i.e., both lower and upper bands are rigidly shifted downwards. If the disorder bound is as large as half of the band gap  $m$ , then the top of the lower band in the  $l$ -site region is higher than the bottom of the upper band in the  $l'$ -site region, and the gap will be zero. This means that one electron can be moved from one region to the other at no energy cost, exactly like in the argument for interacting bosons. Even though the expected size effects will be enormous,

### 3.4 Disordered spinless fermions in a staggered ionic potential

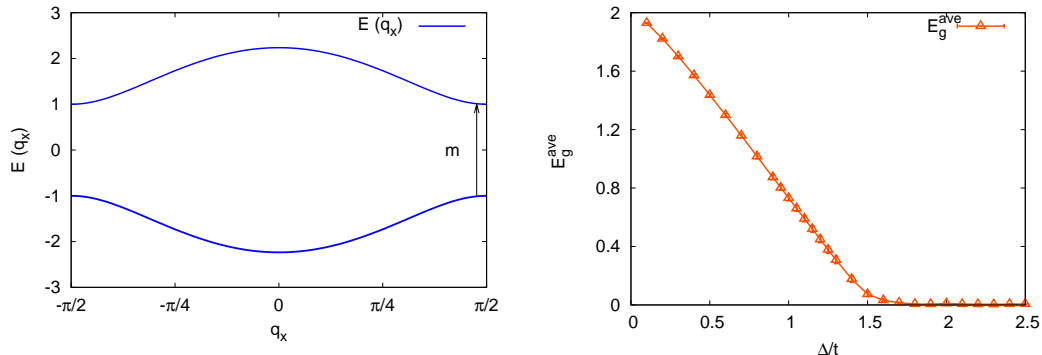


Figure 3.12: Left: Spectrum of the system of non-interacting spinless fermions for the clean case  $\Delta/t = 0$  and  $m = 2.0$ . The system possess an energy gap of  $m$  at  $q_x = \pi/2$ . Right: The average excitation gap  $\bar{E}_g$  at half filling in presence of disorder as function of  $\Delta/t$ . The size of the system has been set to  $L = 1200$  sites.

performing direct exact calculations on finite clusters of this system of spinless fermions is important because it could provide an idea of the experimental length scales at which the physics of rare regions would emerge. In fact, in Fig. 3.12 we report the average excitation gap  $\bar{E}_g$  at half filling in presence of disorder as function of  $\Delta/t$  for a lattice of  $L = 1200$  sites. We emphasize that experiments with ultracold atoms loaded on optical lattices can be realized with number of sites and particles of the order of  $10^2 \sim 10^5$  in arrays of decoupled 1D tubes. Our finite size calculations could then be used as benchmark to analyze the outcome of experiments, either with free fermions or bosons in the limit of very large values of interaction  $U/t \rightarrow \infty$  where spinless fermions are equivalent to hardcore bosons. [72] The transition to the Anderson-localized phase is observed around  $\Delta_c/t \simeq 1.7$  in contrast to what is expected from theorem 1,  $\Delta_c/t = 1$ , i.e., half of the gap  $m/2$  of the clean system. In Fig. 3.13 we also present the results of the distribution of the gap  $P(E_g)$  under the similar conditions  $\Delta/t = 1$  and  $m = 2$ , sampled from a calculation using  $10^6$  realizations of disorder in a small lattice  $L = 100$ . Again, the system is expected to be gapless, however the tails of the distribution are always very far from vanishing values such that the gap remains always finite. For the  $L = 1200$  cluster, the value of the gap at  $\Delta/t = 1$  is about

$\bar{E}_g \simeq 0.731$  while for  $L = 5000$ ,  $\bar{E}_g \simeq 0.593$ , thus decreasing very slowly with the increase of the size. Additionally, the results on the density of states (DOS) of the system are depicted in Fig. 3.13. With respect to the density of states of the clean system, the energy gap around zero energy in presence of disorder is clearly reduced and it is filled with states coming from particles that are strongly localized in the Lifshitz's tails that arise from the rare regions, just as in the usual Anderson localization where the density of states gets enlarged by the presence of such tails. [73] However, finding to which extent those tails are filling the density of states by numerical calculations is hard, as those exponentially rare regions are not captured by our simulations limited to a finite size and finite number of realizations which in principle should be exponentially large to be able to detect their effect. In summary, what all these results on spinless fermions together with our previous simulations on disordered bosons suggests, is that the criticality arising from the physics of rare regions is expected on very large scales, such that its observation is severely restricted to astronomically large systems that can perhaps only be reached in real materials. Nevertheless, the observation and characterization of the emerging phases is possible and it should in principle be experimentally accessible with ultracold atoms.

## 3.5 Conclusions

In this part of the thesis it has been presented a detailed study of the ground-state properties of the disordered Bose-Hubbard model in low-dimensional lattices, relevant for on-going experiments with cold atomic gases trapped in optical lattices. We have determined the distribution probability of the gap on finite sizes and shown that it contains useful information. In particular, we have found that the Bose-glass is characterized by a broad distribution of the gap that is peaked at finite energy but extends down to zero, a shape remarkably reminiscent of pre-formed Hubbard sidebands with the Mott gap completely filled by Lifshitz's tails. The Mott transition occurs when these tails terminate at finite energy. On the contrary, the gap distribution in the superfluid phase turns out to be strongly peaked at zero energy. These results suggest a simple and efficient way to discriminate between different phases in experiments, which, being performed on

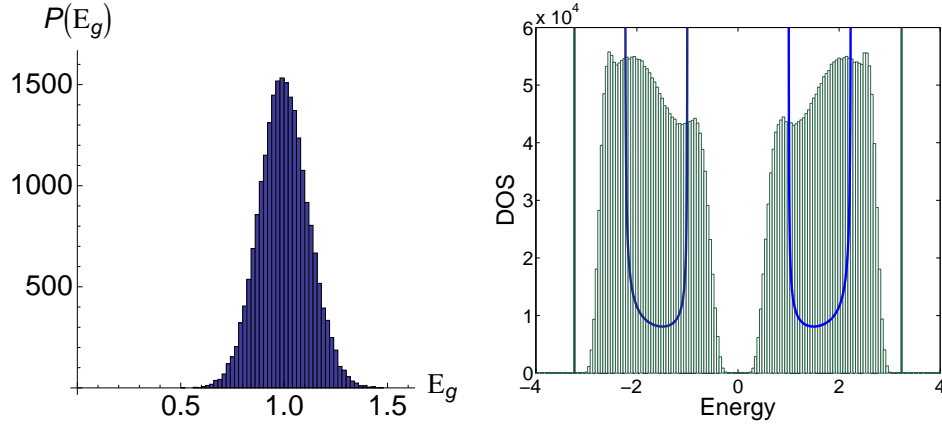


Figure 3.13: Left panel: Distribution probability  $P(E_g)$  for a system of spinless fermions at half filling with  $\Delta/t = 1.0$  and  $m = 2.0$ . Right panel: Density of states for the clean (solid lines) and disordered system (green bars). Both figures are constructed from  $10^6$  configurations of disorder on a cluster  $L = 100$  sites

finite systems, suffer from the same size limitations as our simulations. We have also investigated the disordered Bose-Hubbard model on  $N$ -leg ladder systems, emphasizing that these geometries could be quite useful to study the evolution from one to two spatial dimensions. Experiments with both cold atomic gases and magnetic systems are becoming now possible on ladders and our calculations represent an important benchmark in this direction.

## Chapter 4

# The onset of superfluidity of hardcore bosons in disordered ladders

In this chapter we discuss the effect of disorder on the zero-temperature phase diagram of a two-leg ladder of hardcore bosons using numerical simulations based on the Green's function Monte Carlo. We first review some important aspects of the clean system which are relevant for the understanding of the disordered case. Then the effect of the interchain hopping is analyzed followed by the study of the low-density regime of the phase diagram in presence of disorder. We find an intervening Bose-glass phase between the frozen Mott insulator with zero (or one) bosons per site and the superfluid phase. This superfluid phase is stabilized by the hopping between the otherwise insulating bosonic chains. We also investigate the effect of disorder exactly at half filling, where for small values of disorder, there is a commensurate phase with a gap to all excitations, which is eventually destroyed for larger values of disorder. We argue that this phase is always surrounded by the so-called Bose glass and a direct transition from the superfluid is found only in the clean system. Finally, a phase diagram based on our numerical evidence is suggested.

## 4.1 Hardcore bosons in presence of disorder in low dimensions

Low temperature one-dimensional interacting Bose systems are fascinating and fundamentally different from their higher dimensional counterparts. This is not a purely abstract problem since there are remarkable realizations of low-dimensional Bose systems. In fact, among the first experimental realizations of one-dimensional Bose systems we have Josephson junction arrays [74] and, more recently, ultracold bosons loaded in one-dimensional traps where the transition from the superfluid to Mott insulator has been already observed. [39] Other remarkable examples are the case of strongly correlated hardcore bosons with [75] and without [76] the optical lattice along one-dimensional tubes. In such examples, the repulsive interactions between bosonic particles confined to one dimension dominate the physics of the system. The bosons are prevented from occupying the same position in space due to the strong interaction between the particles. The strong interaction resembles the Pauli exclusion principle of fermions, which in one dimension causes the system to have some analogous properties which are fermionic in nature. In fact, using the Jordan-Wigner transformation, [72] hardcore bosons in one-dimensional lattices can be mapped onto one-dimensional spinless fermions, which in many cases makes it possible to obtain exact solutions for the ground state and dynamics of strongly interacting Bose systems. [77] After the Jordan-Wigner transformation, some observables have the same expectation values irrespective of whether working with spinless fermions or hardcore bosons. This is the case for the energy and the density, for instance. For other quantities like the density matrix and the momentum distribution, this correspondence is not valid and phase factors have to be taken into account. It was realized that these remarkable features of one-dimensional hardcore bosons get drastically modified when these bosonic chains are coupled together leading to the so-called ladder systems. [78, 79] Bosonic ladders are interesting because they allow the possibility to track the evolution of properties of the system as the dimensionality is changed from one to two dimensions. Ladders possess essentially a one-dimensional character, thus no long-range order is allowed, while sharing two-dimensional properties because that system contains tunneling between the chains, making it possi-

## 4.1 Hardcore bosons in presence of disorder in low dimensions

---

ble to study phenomena usually found in higher-dimensional systems. This fact is particularly evident in presence of disorder. In a one-dimensional chain with only nearest neighbor hopping, Anderson localization is expected for a system of hardcore bosons (or spinless fermions) for any value of the disorder and densities. Instead if we consider hardcore bosons in a two-leg ladder a superfluid phase is expected to be stabilized by the interchain hopping. [78] In addition, the study of ladder systems of hardcore bosons is expected to be relevant for experiments as they can be realized with optical lattices. [80, 81] In realistic experimental setup, to design, e.g., a two-leg ladder one can realize a double-well potential along a direction (say,  $x$ ) like in Ref. [82], and a potential creating a cigar geometry in the  $z$ -axis. Therefore, by superimposing a further periodic potential along  $z$ , one realizes a two-leg Bose-Hubbard model. By carefully playing with the distance between tubes the height of the barrier between the two legs, one could tune the hopping rate between the legs. Likewise, the intrachain hopping rate can be tuned by appropriately setting the strength of the periodic potential along the  $z$  direction. Superimposing a disordering lattice or introducing a speckle potential on top of the above mentioned ladder in order to consider disorder ladders is then straightforward. Additionally, bosonic ladder systems are of interest because they are experimentally realized also in magnetic materials. [53] For instance, the disorder-free compound IPA-CuCl<sub>3</sub> has been found to be a prototypical  $S = 1/2$  antiferromagnetic spin ladder material which can thought as a system of interacting hardcore bosons. [47] Furthermore, the disordered counterpart was created by means of random chemical substitution of the clean parent compound IPA-CuCl<sub>3</sub> and by using neutron scattering experiments, the evidence of the spin-analogous of a Bose-glass phase was found. [47]

In this chapter we concentrate our attention precisely to the system of hardcore bosons loaded on a two-leg ladder in presence of bounded on-site disorder. We attempt to draw a phase diagram based on simple arguments supported with numerical simulations using the Green's function Monte Carlo. Particularly, the effect of disorder in presence of a variable interchain hopping is addressed for several densities, where apart from the localized Bose-glass phase, we expect a stable superfluid phase not present in single chains. We are going to show that the gapped phase occurring at half filling in the clean system is destroyed by a large

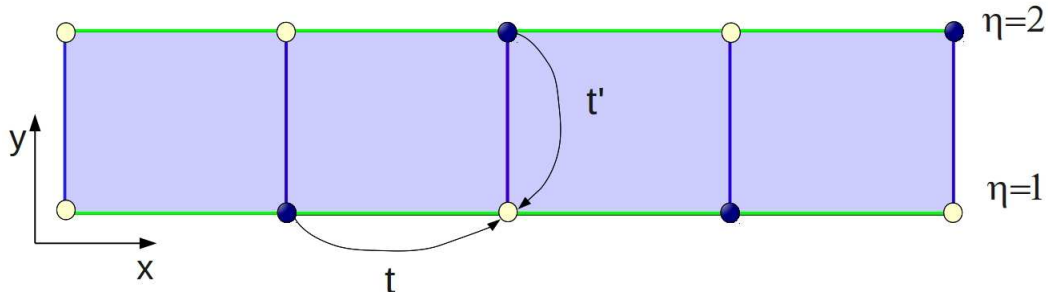


Figure 4.1: Two-leg ladder geometry. The label  $\eta = 1, 2$  denotes the leg label and the matrix elements  $t$  and  $t'$  are the hopping amplitudes along and between the chains, respectively.

enough disorder amplitude and present numerical simulations to test arguments supporting the existence of a Bose glass that completely surrounds the gapped phase. [83]

## 4.2 Model and results

We will consider a system of hardcore bosons on a  $L = 2 \times L_x$  lattice. The Hamiltonian is given by

$$\mathcal{H} = -t \sum_{i,\eta=1,2} \left( b_{i,\eta}^\dagger b_{i+1,\eta} + h.c. \right) - t' \sum_i \left( b_{i,1}^\dagger b_{i,2} + h.c. \right) + \sum_{i,\eta} \epsilon_{i,\eta} n_{i,\eta}, \quad (4.1)$$

where  $b_{i,\eta}^\dagger$  creates a hardcore boson at rung  $i$  on the chain  $\eta = 1, 2$ . The matrix elements  $t$  and  $t'$  are the hopping amplitudes along and between the chains respectively. The local disordered potential is described by random variables  $\epsilon_{i,\eta}$  that are uniformly distributed in  $[-\Delta, \Delta]$ . The lattice geometry is depicted in Fig. 4.1. We study the Hamiltonian of Eq. (4.1) by Green's function Monte Carlo with a fixed number  $M$  of bosons on  $L$  sites,  $n = M/L$  being the average density.

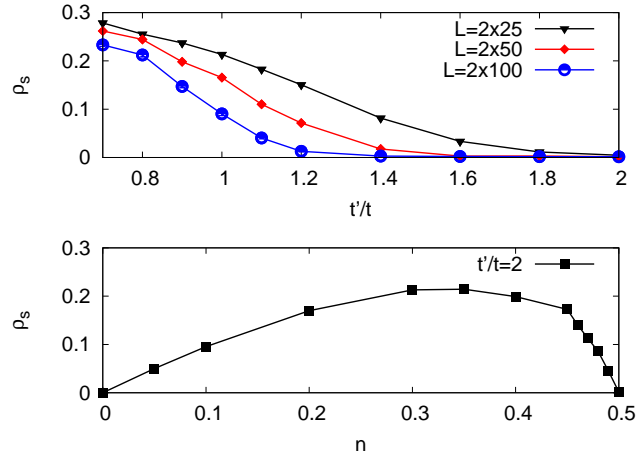


Figure 4.2: Upper panel: Superfluid stiffness as function of  $t'/t$  and different lattice sizes and fixed  $n = 0.5$ . Lower panel: Superfluid stiffness as function of the density  $n$  at fixed  $t'/t = 2$  on a lattice with  $L_x = 50$

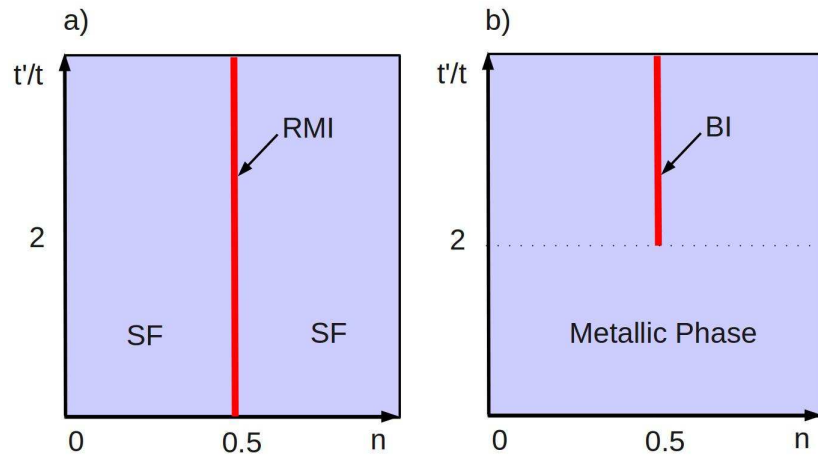


Figure 4.3: a. Phase diagram of hardcore bosons on a two-leg ladder as function of  $t'/t$  and density  $n$ . b. Same as in a. but for non-interacting spinless fermions. The rung Mott insulator is denoted as (RMI), superfluid as (SF) and a band insulator as (BI).

### 4.2.1 The clean case

Let us discuss the clean case, where  $\epsilon_{i,\eta} = 0$ , in two extreme limits. First, we consider the limit  $t' = 0$ , i.e., two uncoupled one-dimensional chains. In this situation the ground state is a superfluid with quasi-long-range order for any density  $0 < n < 1$ . [84] At densities  $n = 0, 1$  there will always be a totally frozen Mott insulator due to the infinite repulsion which completely suppresses the charge fluctuations. Instead, when  $t'/t \gg 1$  we expect differences depending on the filling. Exactly at half filling  $n = 1/2$ , i.e., one hardcore boson per rung, each boson goes into a zero y-momentum state. This means that the ground state can be approximately written as a independent product of single-particle rung states as

$$|\Psi_0\rangle \simeq \prod_i^{L_x} |\Psi_i\rangle \quad (4.2)$$

where  $|\Psi_i\rangle = 1/\sqrt{2}(b_{i,1}^\dagger + b_{i,2}^\dagger)|0\rangle$ . This situation is expected because it is energetically favorable to have an independent boson per rung delocalized along the y-axis gaining an amount of energy  $t'$  by hopping along the rungs back and forth. The system is in the so-called rung Mott insulator with a unique ground state and a gap to all excitations. [85] From these observations, at half filling there will be a phase transition between the superfluid and rung-Mott phase as function of the ratio  $t'/t$ . The critical value of the interchain hopping for this phase transition is argued to be  $(t'/t)_c = 0$ , namely that any small interchain hopping is relevant and opens up a gap in the spectrum. Moreover, this transition is of the Kosterlitz-Thouless type and thus the gap opens up very slowly, such that its observation with numerical simulations on finite size clusters is restricted to rather large systems. In Fig. 4.2 the values of the superfluid stiffness obtained by the Green's function Monte Carlo for hardcore bosons as function of  $t'/t$  for several sizes  $L_x = 25, 50$ , and  $100$  is presented. Our data on finite clusters suffer the difficulties inherent to a Kosterlitz-Thouless transition: Although a sizeable reduction is seen as  $t'/t$  is increased, the stiffness remains quite large even for systems as large as  $L_x = 100$ . We expect that, as the size of the system is increased, the stiffness will not saturate for any value of  $t'/t$  and it will eventually vanish. The correlation length, although huge, is finite and the system insulating. Now,

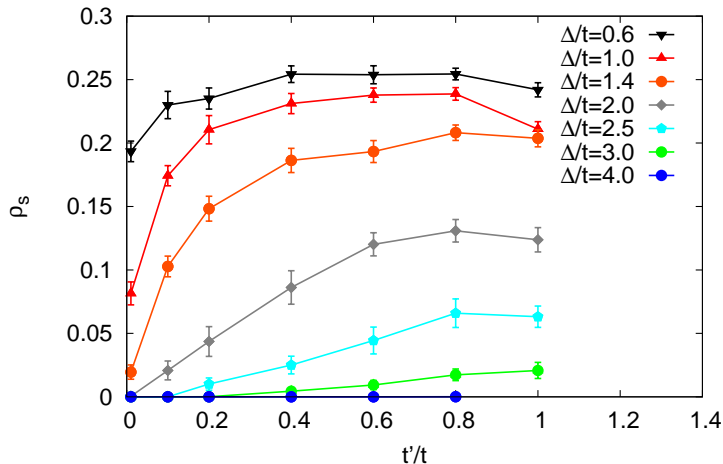


Figure 4.4: Superfluid stiffness  $\rho_s$  as a function of  $t'/t$  for different  $\Delta/t$  on a two-leg ladder with  $L = 2 \times 50$  sites. The density has been fixed to  $n = 0.4$

if we add or remove to that state a few carriers they will form a superfluid on top of the frozen state with one hardcore boson per rung. Thus, at any other filling  $0 < n < 1/2$  and  $1/2 < n < 1$  the system will always be superfluid as can be seen in Fig. 4.2 where the superfluid stiffness as function of the density  $n$  is shown for fixed  $t'/t = 2$ . The superfluid stiffness starts to grow at low density, then it reaches a maximum to finally go down until it exactly vanishes at  $n = 0.5$  at the rung Mott insulator. On the other hand, for non-interacting spinless fermions at half filling on the same ladder geometry, a correspondent phase transition is expected at a finite  $(t'/t)_c = 2$  where a gap opens up. In this case the transition is from the metallic phase to a band insulator. The clean phase diagrams for hardcore bosons and spinless fermions on a two-leg ladder are sketched in Fig. 4.3 for comparison.

### 4.2.2 Introduction of disorder

Now we turn our attention to the disordered system. First of all, the effect of varying the coupling  $t'$  on the otherwise insulating disordered decoupled chains in Fig. 4.4 is investigated. For any value of disorder, an arbitrarily small  $t'/t$  does not drive the system superfluid and the system remains in the Bose-glass

phase. A further increase of the ratio  $t'/t$  drives the system from the Bose glass to the superfluid. However, for small disorder, the correlation length of the tiny Bose glass at small  $t'/t$  and high density is expected to be very large, such that our finite size simulations fail to see the small Bose glass region. This effect is also observed in Fig. 4.4. Rapidly as a small  $t'$  is introduced a large superfluid response is obtained for small disorder. We see from our simulations that, by a further increase of the interchain hopping the superfluid stiffness reaches a maximum and then it decays. This means that, given a fixed disorder strength, there is an optimal value of  $t'$  for which the system attains the highest superfluid response. If  $t'$  is increased further, the effect of localization is enhanced and the superfluidity is reduced. Finally, as the disorder is increased, the superfluid stiffness is decreased, until a large value of disorder is reached for which the system cannot attain superfluidity anymore and remains localized for any value of  $t'$ .

### Low-density phase diagram

Let us consider the low-density regime of the phase diagram at fixed interchain hopping as function of the density and disorder. Fig. 4.5 shows the low-density phase diagram and as well as numerical calculations of the superfluid stiffness as function of disorder for several values of density and fixed  $t'/t = 1$ . We also present the transition line corresponding to a larger interchain hopping  $t'/t = 2$  which lies slightly below the line corresponding to  $t'/t = 1$ . It is found that for any finite disorder  $\Delta/t$ , the low-density phase is a Bose glass that turns superfluid above a critical density. The trivial Mott insulator with zero (or one) bosons per site is therefore separated from the superfluid phase by a Bose glass. We emphasize that the existence of a superfluid phase for hardcore bosons in a two-leg ladder is *per se* remarkable. Indeed, in a single chain with nearest-neighbor hopping, hardcore bosons are equivalent to spinless fermions, which Anderson localize for any density and in any dimension  $D \leq 2$ . Already in a two-leg ladder, hardcore bosons start to behave differently from spinless fermions. While the latter ones remain always localized, the former ones show a superfluid phase stabilized by the interchain hopping. The idea is that in a strictly one-dimensional

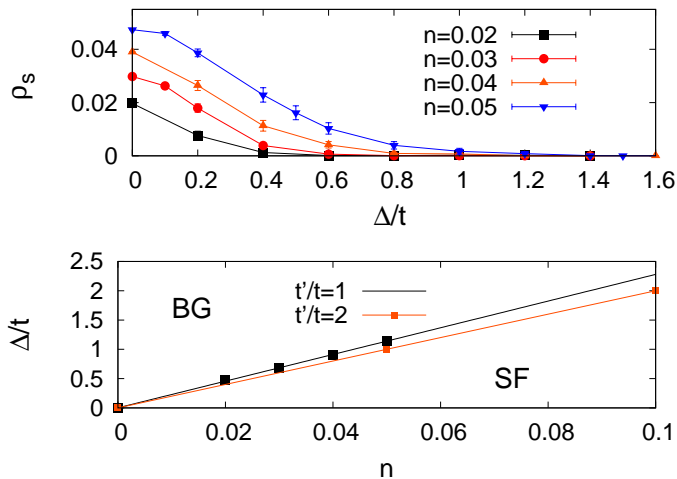


Figure 4.5: Upper panel: superfluid stiffness  $\rho_s$  as a function of the disorder strength  $\Delta/t$  for different  $n$  and  $t' = 1$ . Lower panel: low-density phase diagram of the hard-core bosonic model for  $t'/t = 1$  and  $t'/t = 2$ . Calculations have been done on a  $2 \times 50$  ladder system.

geometry with only nearest neighbor hopping, the statistics of the particles does not matter and hardcore bosons are equivalent to fermions. However, whenever a non-strictly one-dimensional path is allowed by the Hamiltonian dynamics, as in the two-leg ladder, bosons can form a superfluid, even in presence of disorder. We just mention that the same behavior holds also on a single chain with longer-range hopping. Superfluidity on a system of coupled disordered chains of strongly interacting bosons have been predicted using bosonization and renormalization-group techniques. [78] This scenario can be understood in very simple terms as follows. In a disordered lattice in any dimension  $D \leq 2$ , at very low fillings, the statistics of the particles does not matter so much and hardcore bosons, as free fermions, localize due to disorder giving rise to the Bose glass. This is because the length over which the single-particle wave function extends is short enough in such a way that the wave functions of two single particles never overlap. As soon as the filling is increased, the particles get closer to each other and the single-particle wave functions begin to overlap and the statistics of the particles starts to play a role. If the particles are fermions they will still be localized, whereas

bosons may stabilize a superfluid, as confirmed by our numerical simulations. In the regime of values of interchain hopping we have studied, the effect of a larger  $t'/t = 2$  in the low-density phase diagram is to slightly reduce the superfluid response of the system, as can be also seen in Fig. 4.5. We mention that the linear character of the transition line from the Bose glass to the superfluid is not altered.

Furthermore, we examine the same low-density transition from the Bose glass to the superfluid driven by density at fixed  $\Delta/t = 2$ . In Fig. 4.6 we present the results of the superfluid stiffness  $\rho_s$  as a function of the density  $n$ . As before, we found that superfluidity takes place for large enough density. We point out that our simulations have been performed on finite clusters and finite size effects are naturally expected, implying that the superfluid regions in the actual infinite size phase diagram could be slightly reduced. For comparison we have studied the case of spinless fermions for which we have calculated the Drude weight  $D$  on exactly the same lattice geometry, disorder strength and densities. In the case of spinless fermions no transition is found and the ground state is localized as confirmed in Fig. 4.6.

### Half-filled case

Concerning the phase diagram at higher densities, we now consider the half-filled case  $n = 0.5$ , where in absence of disorder the system is gapped. The expectation is that the presence of disorder tends to reduce the gap until a certain critical value of  $\Delta/t$  will completely make it vanish, as we show in Fig. 4.7 where we have calculated the distribution probability of the gap  $P(E_g)$  for several values of  $\Delta/t$ . Already for  $\Delta/t = 2$  the probability to find zero gap is finite, such that the gap of the infinite system is zero and the system is in the Bose glass. Similar arguments were carefully explained in chapter 3 in relation to the distribution probability of the gap and the presence of compressible regions in an infinite system. Furthermore, we can make use of the so-called theorem 1 in this case and related the gap of the clean system to that of the disordered one. In the clean case at half filling, for  $t'/t \gg 1$  the gap  $E_g \sim 2t'$ . If we apply disorder and use the theorem 1 in this situation, we expect the rung Mott gap to vanish

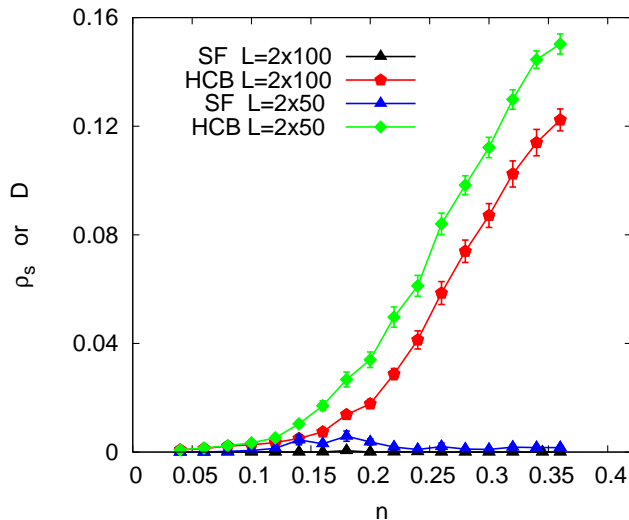


Figure 4.6: Upper panel: Superfluid stiffness  $\rho_s$  and Drude weight or charge stiffness  $D$  as a function of density  $n$  and  $\Delta/t = 2$  on a two-leg ladder with  $L = 2 \times 100$  sites. Lower panel: Size scaling of both  $\rho_s$  (left) and  $D$  (right).

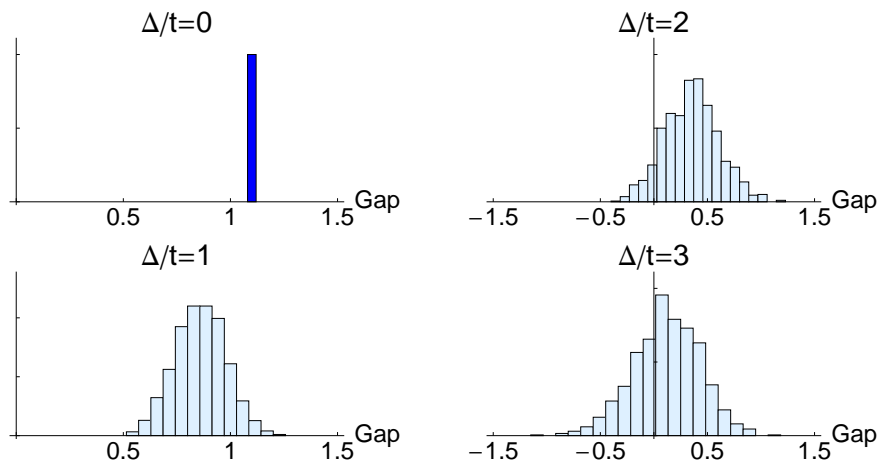


Figure 4.7: Distribution  $P(E_g)$  of the gap as function of disorder strength and fixed density  $n = 0.5$  and  $t'/t = 2$  on a two-leg ladder with  $L_x = 50$  sites. The clean gap is shown for comparison in the upper-left box as a blue bar.

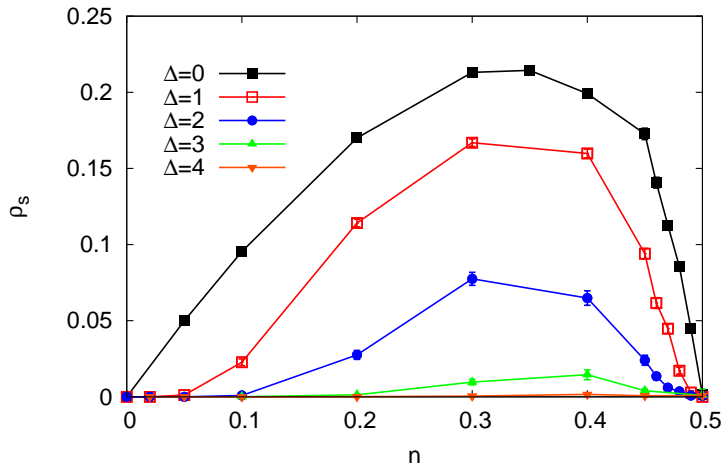


Figure 4.8: Superfluid stiffness  $\rho_s$  as a function of the density and several values of  $\Delta/t$  and fixed  $t'/t = 2$ . The clean stiffness is also shown for comparison.

around a critical value of disorder  $\Delta_c \sim t'$ . The theorem should hold exactly only in the infinite system and large size effects are expected, such that the transition from the gapped to the compressible phase in a finite system will take place for a larger  $\Delta_c$ , as it was the case in our finite size simulations of  $P(E_g)$ . This fact sets a lower bound for the observation of transition given by the critical  $\Delta_c \sim t'$  predicted by theorem 1.

### Transition from the superfluid to the gapped phase

Related to the gapped phase at half filling, we address the question of whether transition to the rung Mott insulator as the density approaches  $n \rightarrow 0.5$  is through the Bose glass or directly from the superfluid. If we dope the gapped state with particles or holes in presence of disorder, those few carriers on top of the rung-Mott phase will see a disordered background. Therefore, standard Anderson localization arguments apply and the system remains insulating by localizing those few carriers on the Lifshitz's tails that fill the rung-Mott gap. By further increase of the density, a superfluid is eventually formed. This simple single-particle argument implies the presence of an intervening Bose glass between the rung-Mott phase and the superfluid. We proceed to test this simple argument

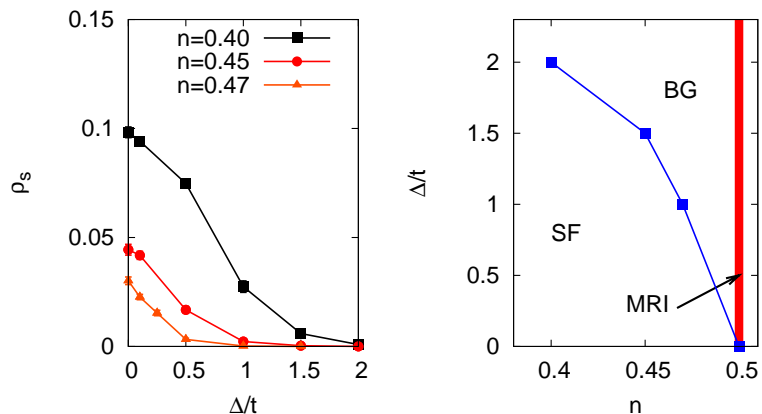


Figure 4.9: Left panel: The superfluid stiffness  $\rho_s$  as function of the disorder bound for several densities close to half filling and fixed  $L_x = 50$  and  $t'/t = 10$ . Right panel: The corresponding phase diagram in the vicinity of the rung-Mott phase.

quantitatively in two cases,  $t'/t = 2$  and  $t'/t = 10$ . Let us examine the behavior of the superfluid stiffness for densities close to  $n = 0.5$  and  $t'/t = 2$  as shown in Fig. 4.8. Our data is consistent with a transition driven by density from the superfluid phase through the Bose glass to finally end up with the rung Mott insulator. For instance, from the data for  $\Delta/t = 1$ , the superfluid stiffness appears to vanish just before  $n = 0.5$ , however the region in which the Bose glass takes place is very small. For  $\Delta/t = 2$  the rung Mott insulator has already been wiped out by the effect of disorder as it was previously shown in Fig. 4.7.

If a larger  $t'/t$  is considered, the localization due to disorder is expected to be greatly enhanced, thus, enlarging the Bose glass regions. This fact enables us to provide further evidence in favor of an intervening Bose glass in between the rung Mott and the superfluid as follows. We have performed simulations with a rather large  $t'/t = 10$  which are presented in Fig. 4.9 where we show the superfluid stiffness as function of the disorder bound for several densities close to half filling. From these simulations we can see that as the density approaches

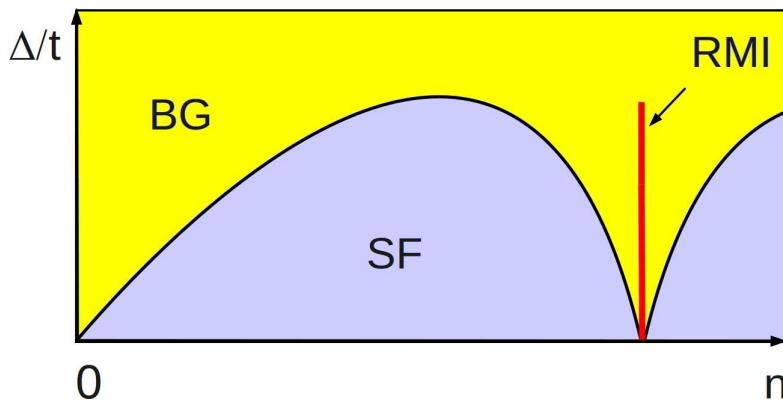


Figure 4.10: Generic phase diagram in the  $\Delta/t - n$  plane in presence of disorder. The red lines denotes the rung Mott insulator.

$n = 0.5$ , the critical disorder  $\Delta_c/t$  for the transition to the Bose glass gets smaller which leaves room for a large Bose glass in between the superfluid and the rung Mott insulator. We observe that the exact value of the clean gap computed numerically on a finite  $L_x = 50$  lattice with  $t'/t = 10$  is equal to  $E_g \simeq 17.31$ , such that according to theorem 1 we expect the transition from the gapped to the compressible phase to occur at least for value of disorder  $\Delta_c = 8.65$ . Therefore, we are confident that the system is gapped for disorder amplitudes  $\Delta \lesssim 8.65$ . From this last observation about the disordered gap  $E_g$  and from the calculations of the superfluid stiffness we can draw the phase diagram for densities close to the rung-Mott phase as presented in the right panel of Fig. 4.9.

By putting all our numerical evidence together we now attempt to draw a generic phase diagram for the two-leg ladder system of hardcore bosons in presence of bounded disorder which we depict in Fig. 4.10. Generally speaking, a large enough  $t'$  tends to reduce the superfluid response of the system while enhancing the rung Mott phase against disorder such that for larger  $t'$  the rung Mott insulator survives up to a larger value of disorder.

## 4.3 Conclusions

We have studied the effect of bounded disorder on the phase diagram of a two-leg ladder of hardcore bosons as function of density and interchain hopping. We found that at low filling the frozen Mott insulator with zero (or one) boson per site is separated from the superfluid phase by a compressible localized insulator, i.e., the Bose glass. This is in clear agreement with the arguments presented in Ref. [9] which suggested, based on single-particle arguments, that a direct transition from the superfluid to the Mott insulator in presence of disorder is unlikely to happen and that a Bose glass should intervene between them. We have also verified numerically that disorder tends to destroy the gap present on the clean version of the rung Mott insulator, which is a sort of Mott insulator happening exactly at half filling  $n = 1/2$ , i.e., one hardcore boson per rung, for which each boson goes into a zero  $y$ -momentum state with a gap to all excitations. We have also argued that this phase is always surrounded by the Bose glass, such that a direct transition from the superfluid is forbidden in presence of disorder. This result is also in agreement with the theorem of inclusions introduced in Ref. [17, 18] and explained in chapter 1. This theorem states that in presence of generic, bounded disorder, there exist rare but arbitrarily large regions of the competing phases across a (generic) transition line which, in turn, implies that a transition from the superfluid to gapped phase is not possible.

## Chapter 5

# Extracting the Mott gap from energy measurements in trapped atomic gases

In this chapter we show that the measurement of the so-called release energy, which can be addressed experimentally, makes it possible to assess the value of the Mott gap in the presence of the confinement potential that is unavoidable in real experiments with ultracold atomic gases. Indeed, the curve of the release energy as a function of the total number of particles shows kinks that are directly related to the existence of excitation gaps associated to the formation of Mott-insulating regions within the trapped system. This observation is introduced and discussed in analogy to what happens to a uniform system where the total energy curve as function of the density of particles exhibits kinks whenever the interaction strength is large enough and the density is fixed to an integer value. Calculations are presented within the Gutzwiller approach, but the final results go beyond this simple approximation and represent a genuine feature of the real system. We analyze two types of confinement, the usual harmonic confinement and the recently introduced off-diagonal confinement in which the kinetic energy of the particles is varied across the lattice, being maximum at the center of the trap and zero at the borders. In the case of harmonic confinement, the Mott gaps may be renormalized with respect to the uniform case. On the other hand, in the

## 5.1 The formation of a Mott insulator in experiments with cold atoms

case of the off-diagonal confinement, our results show good agreement with the homogeneous case.

### **5.1 The formation of a Mott insulator in experiments with cold atoms**

As it was mentioned in the introduction of this thesis, it has been established that ultra-cold Bose and Fermi gases trapped in optical lattices provide experimental realizations of long-standing lattice models widely considered in condensed matter physics and statistical mechanics, such as the Bose and Fermi Hubbard models. [28, 86] Experimental realizations of those models have been already explored successfully, both for bosons and fermions. Although certain experimental realizations of the Hubbard model have been successfully realized, several challenges arise when quantitatively comparing experimental data and theoretical results. One of the most important problems is due to inevitable spatial inhomogeneities induced by the optical trap, which is necessary to confine particles. [38, 87, 88] Further complications are connected to determine temperature effects present in experiments, [89] and also to the limited available tools for the experimental characterization of the phases. Here, we would like to focus our attention on the possibility to make quantitative estimations of the Mott gap  $E_g$  from relatively simple quantities that are accessible in experiments. In chapter 3 it was shown that the statistical distribution of the energy gaps in a disordered system extracted by a numerical simulation of finite size systems is a significant property that can discriminate among different phases, thus it might be of importance to devise a way to detect such quantities in experiments with cold atoms. [64] In presence of the optical trap, it is usually not possible to have a Mott-insulating phase throughout the whole lattice and compressible regions intrude the system. This fact has been widely discussed both experimentally and theoretically and shows up through the typical “wedding-cake” profile of density. [19, 38, 87, 88, 90, 91] Therefore, the system always possesses regions that are locally compressible and a precise determination of the Mott gap is subtler than in the homogeneous case. Some preliminary attempts to measure the excitation spectrum of interacting

## 5.1 The formation of a Mott insulator in experiments with cold atoms

bosons have been performed by using Bragg spectroscopy. [39] Other approaches to characterize the appearance of Mott-insulating regions from experimentally accessible quantities have been also proposed. [65, 66] Here, we would like to propose an alternative approach that is based upon energy measurements only and could give important insights into the actual value of the gap.

For an *infinite and homogeneous* system, the excitation gap  $E_g$  can be calculated from the knowledge of the total energy for different particle numbers, namely  $E_g = \mu^+ - \mu^-$ , where  $\mu^\pm = \pm(E_{N\pm 1} - E_N)$ ,  $E_N$  being the ground-state energy with  $N$  particles. The Mott gap  $E_g$  is finite whenever  $\mu^+ \neq \mu^-$  and, therefore, it introduces a discontinuity in the first derivative of the energy with respect to the density. In a real experiment, it is not possible to consider adding or removing a single particle from a system with  $N$  particles in order to compute the energy gap. However, similar results may be obtained taking  $\mu^\pm = \pm(E_{N\pm M} - E_N)$ , with  $M \ll N$ , which could be considered in experiments.

In this chapter, we will show that the existence of incompressible Mott regions and the values of the corresponding gaps can be obtained from so-called *release energy*  $E^{rel}$ , which may be easily measured experimentally. [92] Indeed,  $E^{rel}$  is obtained by integrating the momentum distribution of the atoms after having switched off the confinement and let the atoms expand freely in a standard time-of-flight experiment. The release energy is given by the sum of the kinetic and interaction energies just before switching off the trap [92]

$$E^{rel} = E^{kin} + E^{int}. \quad (5.1)$$

We notice that it would be much more difficult to extract the total energy,

$$E^{tot} = E^{kin} + E^{int} + E^{pot}, \quad (5.2)$$

that also includes the potential term due to the trap, since this would require the knowledge of the density profile in the presence of the trap, which is harder to reconstruct. Specifically, we address two types of confinements *i)* the usual harmonic confinement and *ii)* a recently proposed off-diagonal confinement, [93] In such a confinement, the strength of the hopping parameter is varied across the lattice, being maximum at the center of the lattice and vanishing at its edges, which naturally induces a trapping of the particles.

We consider the bosonic case in one and two dimensions and use an insightful variational approach based upon the Gutzwiller wave function. [94, 95] However, similar results must hold also in fermionic systems. We find that the presence of Mott regions in the system is signaled by discontinuities in the derivative of the release-energy curve with respect to the total number of the bosons, reminiscent of the presence of a gap in infinite homogeneous system. In the case of harmonic confinement, the measured gap may be substantially smaller than the one of the uniform system, whereas a much closer agreement is achieved by considering the off-diagonal confinement. [96]

## 5.2 Model and Method

Our starting point is the Bose-Hubbard model which describes interacting bosons on a lattice: [38]

$$\hat{\mathcal{H}} = -\frac{1}{2} \sum_{\langle i,j \rangle} t_{i,j} \hat{b}_i^\dagger \hat{b}_j + h.c. + \frac{U}{2} \sum_i \hat{n}_i (\hat{n}_i - 1) + \sum_i \epsilon_i \hat{n}_i, \quad (5.3)$$

where  $\langle \dots \rangle$  indicates nearest-neighbor sites,  $\hat{b}_i^\dagger$  ( $\hat{b}_i$ ) creates (destroys) a boson on site  $i$ , and  $\hat{n}_i$  is the local density operator.  $U$  is the on-site interaction,  $t_{i,j}$  is the hopping amplitude, and  $\epsilon_i$  is a local energy offset due to an external trapping potential.

To study this model and describe its ground-state properties we use a mean-field approximation based on the Gutzwiller ansatz. [94, 95] This simple approach is able to capture important features of the true ground state and provides a correct description of local quantities, such as the local density or the total energy, even in presence of spatial inhomogeneities. [38, 91, 94, 95] More involved wave functions with a long-range Jastrow factor, [56] or numerically exact calculations [16] may be considered, but a much larger computational effort would be required. Instead, here we are just interested in showing that the Mott gap can be extracted from the behavior of the release energy as a function of the total number of particles.

Within the Gutzwiller ansatz the ground-state wave function is approximated as

$$|\Psi_G\rangle = \prod_i \left( \sum_{m=0}^{\infty} f_m^i |m\rangle_i \right), \quad (5.4)$$

where  $|m\rangle_i$  is the Fock state with  $m$  particles at site  $i$  and  $f_m^i$  are variational parameters which are to be determined by minimizing the expectation value of the Hamiltonian in Eq. (5.3). The sum in Eq. (5.4) runs from states with zero particles up to infinity, however, from a numerical point of view, we have to consider a cutoff and take only states up to a maximum number of particles (per site)  $M_{max}^i \gg \langle \Psi_G | \hat{n}_i | \Psi_G \rangle$  such that the contribution of those states with higher density are negligible and observables are converged to a certain desired precision. Equivalently, the Gutzwiller wave function can be introduced as the ground state of the following mean-field Hamiltonian: [54, 55]

$$\begin{aligned} \hat{\mathcal{H}}_{mf} = & -\frac{1}{2} \sum_{\langle i,j \rangle} t_{i,j} \left( \hat{b}_i^\dagger \Psi_j + \Psi_i^* \hat{b}_j - \Psi_i^* \Psi_j \right) + h.c. \\ & + \frac{U}{2} \sum_i \hat{n}_i (\hat{n}_i - 1) + \sum_i (\epsilon_i - \mu) \hat{n}_i, \end{aligned} \quad (5.5)$$

where  $\Psi_i$  is the mean-field potential which is self-consistently defined as  $\Psi_i = \langle \Psi_G | \hat{b}_i | \Psi_G \rangle$ ; it can be shown that  $f_m^i$  is related to the ground-state eigenvector components of the converged solution of the local Hamiltonian (5.5). [54] The parameter  $\mu$  is the chemical potential that fixes the number of bosons. A careful description on the implementation of the method is provided in chapter 2.

For the sake of simplicity and to simplify the presentation of the results, we first consider the one-dimensional (1D) case, which is the limiting case where a collection of non-interacting tubes is created. Finally, we also report some results for two dimensions (2D). We would like to stress that the results are valid in any dimension, since the Mott transition is always accompanied by the opening of a gap in the spectrum, thus also at the mean-field level. An almost 1D model may be easily generated by using different lasers in the three different spatial directions and has been experimentally considered. [39, 51] We mention that in 1D, within the Gutzwiller approach, the compressible phase has inevitably a finite condensate fraction. However, even in 1D this approach does correctly tell us that

a gap opens up whenever the Mott transition takes place, i.e., this fact does not have relevant qualitative differences on the estimation of the excitation gap with respect to an unbiased calculation. Therefore, we are confident that this approach is qualitatively correct for the quantities we are interested in.

We consider a lattice with a harmonic potential of the form  $\epsilon_i = V_0 r_i^2$ , where  $r_i$  is the distance of site  $i$  from the center of the lattice. In this case, the hopping amplitude is kept constant for all lattice sites  $t_{i,j} = t$ . In addition, we also analyze the case of off-diagonal confinement only in the one-dimensional case in which  $\epsilon_i = 0$  and  $t_{i,i+1} = 4t \times i \times (L - i)/L^2$ , where  $L$  is the total number of sites. In both cases, we evaluate local quantities which allow us to determine whether a certain region across the lattice is in a compressible or incompressible state, as well as the release-energy of the system. In particular, we will show, besides the release-energy, the local density  $n_i = \langle \Psi_G | \hat{n}_i | \Psi_G \rangle$  and its fluctuations  $\Delta_i = \langle \Psi_G | \hat{n}_i^2 | \Psi_G \rangle - n_i^2$ .

## 5.3 Results

Before showing the results for the confined system, which is relevant for experiments, let us briefly discuss the homogeneous case, with  $\epsilon_i = 0$  and  $t_{i,j} = t$ . In this case, a superfluid-Mott transition takes place at integer fillings whenever the on-site interaction  $U$  is large enough. On the other hand, for any non-integer fillings the ground state is always superfluid and, therefore, compressible. In Fig. 5.1, we report the energy curve as a function of the density  $n$ . Within the Gutzwiller approximation the values of the critical interaction may be determined analytically, i.e.,  $U_c/t = D(\sqrt{n} + \sqrt{n+1})^2$ , where  $n$  is an integer. [95] Whenever  $U < U_c$ , the energy curve is smooth with a positive curvature, implying a finite compressibility and a vanishing gap. On the contrary, for  $U > U_c$ , there is a clear discontinuity in the curve at integer fillings (the behavior in the vicinity of  $n = 1$  is reported in Fig. 5.1), signaling the presence of the Mott gap. The latter one can be estimated by considering the change of the slope close to the discontinuity.

Let us consider a harmonic confinement with  $V_0/t = 0.01$ . In Figs. 5.2 and 5.3, we present the results for the release energy as function of the total number of bosons, as well as the local quantities  $n_i$  and  $\Delta_i$  across the lattice sites. For

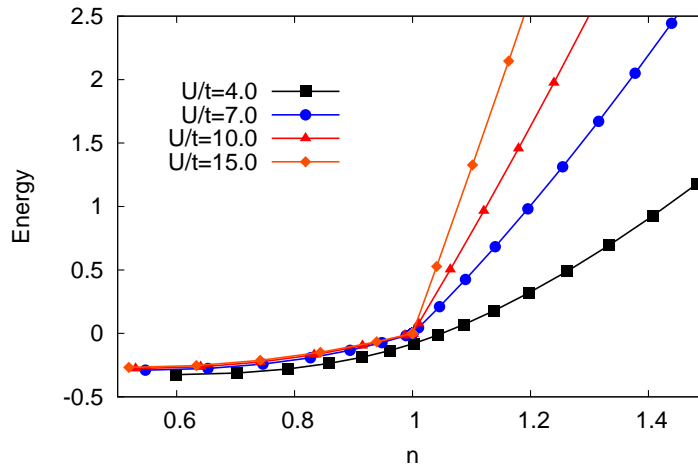


Figure 5.1: Energy per site versus density in the case of the homogeneous model for different values of  $U/t$ .

the case with  $U/t = 4$  (see Fig. 5.2) there are no insulating phases, no matter what the number of bosons is. The density profile is smooth, with a broad maximum at the center of the trap. In this case, all regions of the lattice are (locally) compressible and, therefore, the ground state is always gapless and both the energy and the release energy curves are smooth. This is not the case for  $U/t = 15$  (see Fig. 5.3), where insulating regions are expected. Indeed, what is found is the usual “wedding-cake” structure in the local density: the Mott regions with integer  $n_i$  and vanishing  $\Delta_i$  are surrounded by compressible regions which are locally gapless. We emphasize that the vanishing of  $\Delta_i$  is consequence of the Gutzwiller approach; in a more accurate description of a Mott insulator, this quantity is indeed finite, though it is strongly reduced with respect to its value in the superfluid regions. Here, the release-energy curve in Fig. 5.3 clearly exhibits discontinuities that are reminiscent of the presence of a Mott gap. A discontinuity in the derivative of the energy curve takes place whenever a new compressible region appears at the center of the trap, on top of the underlying Mott phase, see Fig. 5.3. The presence of such discontinuities allows us to define an energy gap for the confined system exactly as in the homogeneous system, namely  $E_g^{rel} = \mu_{rel}^+ - \mu_{rel}^-$ , where  $\mu_{rel}^\pm = \pm(E_{N\pm 1}^{rel} - E_N^{rel})$  ( $E_N^{rel}$  being the release

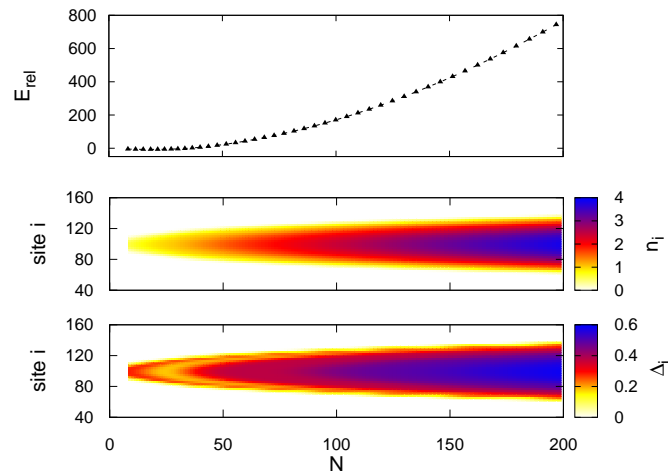


Figure 5.2: Results for the 1D Bose-Hubbard model with  $U/t = 4$  and  $V_0/t = 0.01$ . Upper panel: Release energy. Middle Panel: local density  $n_i$  across the lattice sites. Lower Panel: local density fluctuations  $\Delta_i$  across the lattice sites. All quantities are shown as a function of the total number of bosons  $N$ .

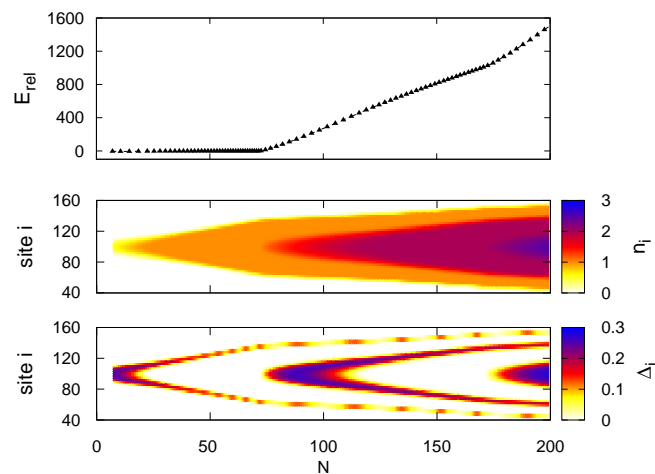


Figure 5.3: The same as in Fig. 5.2 for  $U/t = 15$ .

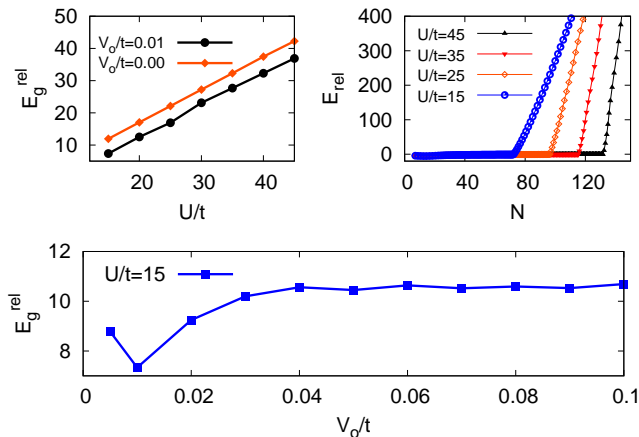


Figure 5.4: Results for the 1D Bose-Hubbard model. Upper panels: first Mott gap obtained from the release energy as function of  $U/t$  for  $V_0/t = 0.01$ , for comparison the homogeneous case is also reported (left); release-energy curves for different  $U/t$  and  $V_0/t = 0.01$  (right). Lower Panel: first Mott gap as function of  $V_0/t$  for  $U/t = 15$ .

energy with  $N$  particles). For the case shown in Fig. 5.3 (i.e., for  $V_0/t = 0.01$  and  $U/t = 15$ ), we obtain that the first Mott gap is  $E_g^{rel}/t \simeq 7.2$ , to be compared with the Mott gap with  $n = 1$  of the homogeneous case that gives  $E_g/t \simeq 11.8$ . The reduction of the measured gap comes from the fact that the release energy in the presence of the trap contains not only the information about the local creation of the new compressible region at the center of the trap, but also about all other sites of the lattice, which do not undergo the Mott transition. Therefore, the effect is spatially averaged over regions that are locally compressible and incompressible. Nevertheless, the effect that originates from the central sites is visible and provides an estimate of the gap associated with such a transition. A summary of the results is reported in Fig. 5.4, where we show  $E_g^{rel}$  (for the first Mott gap) as a function of  $U/t$  for  $V_0/t = 0.01$  and as a function of  $V_0/t$  for  $U/t = 15$ . We find that, when the harmonic trap is increased, the Mott gap saturates to  $E_g^{rel}/t \simeq 10.6$ , which is closer to the value of the homogeneous system. The initial depletion of the Mott gap as a function of  $V_0$  is due to the presence of (large) regions of compressible sites close to the boundaries of the system; by further increasing  $V_0$ , these regions

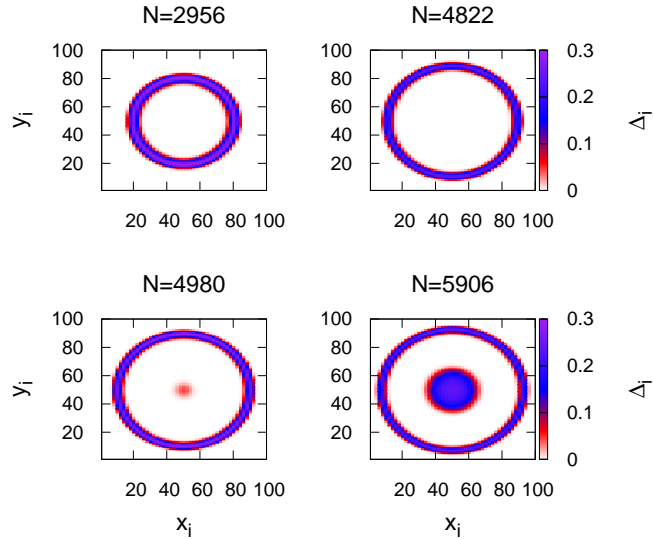


Figure 5.5: Results for the 2D Bose-Hubbard model with  $V_0/t = 0.01$ . Local density fluctuations  $\Delta_i$  across the lattice before (upper panels) and after (lower panels) the kink in the release energy for  $U/t = 20$ .

shrink and the gap eventually tends to approach the value of the uniform case.

We now turn our attention to the results on the 2D case. In Fig. 5.5 we show plots of the density fluctuations across the bidimensional lattice for  $U/t = 20$ . Just as it happens in one dimension, the system exhibits the wedding-cake structure of the density of coexisting superfluid and Mott-insulating regions. When the number of particles is increased, a new superfluid region emerges at the center of the trap between the system with  $N = 4822$  and the one with  $N = 4980$ . In Fig. 5.6, for  $U/t = 20$ , it is apparent that the appearance of the new superfluid region is accompanied with a kink in the release-energy curve. Therefore, similar conclusions to those in one dimension are obtained, confirming the appearance of kinks in 2D where the Gutzwiller mean-field approach is more reliable. Before moving to the off-diagonal confinement, we want to stress that the system with diagonal confinement we are dealing with is a system in which compressible and incompressible regions coexist. Therefore, the meaning of the measurement of gap we have performed has to be clarified. Indeed, the real gap of the overall confined system will be zero, as the global compressibility of the composed system

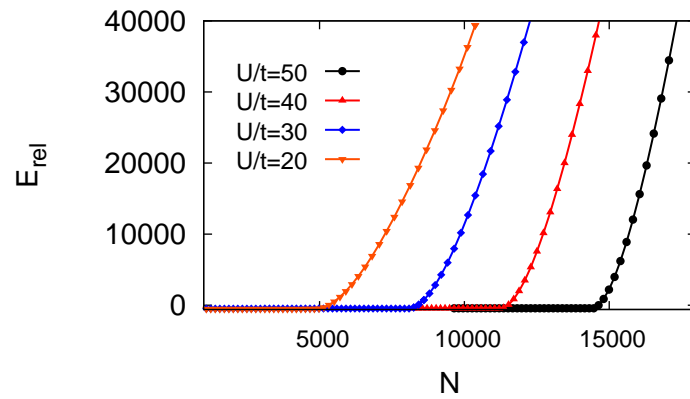


Figure 5.6: Release energy for different values of  $U/t$  across the kink

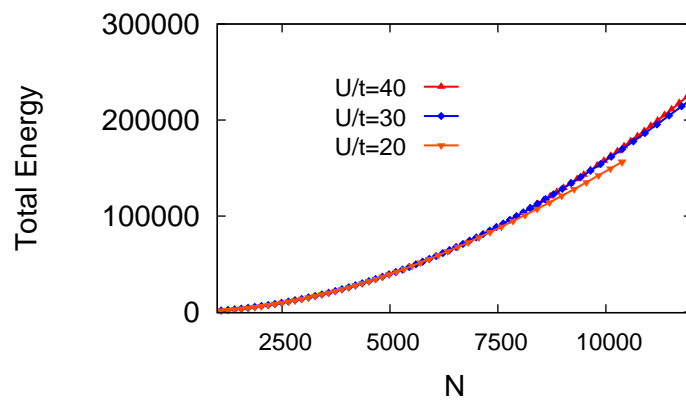


Figure 5.7: The two-dimensional results on total energy of the confined system as function of the number of particles for different values of  $U/t$ .

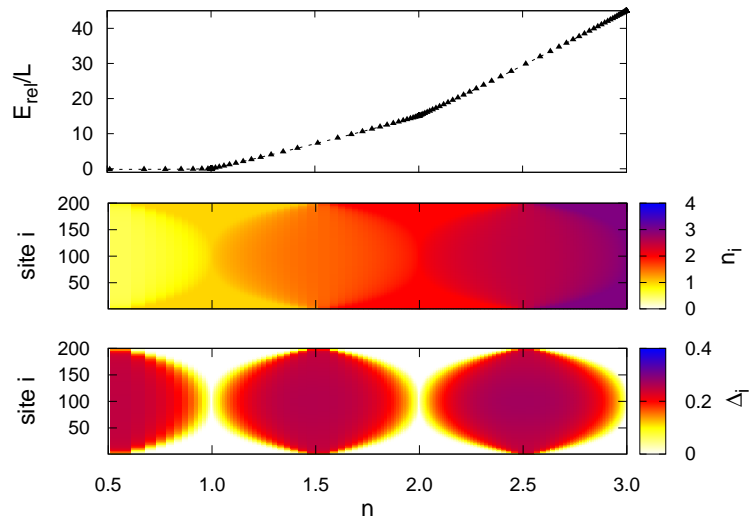


Figure 5.8: The same as in Fig. 5.3 but for an off-diagonal confinement. The number of sites is  $L = 200$  and  $n = N/L$  is the density.

is always finite. [65, 87] The idea is that in a confined system there will be always regions which are locally superfluid, making the overall system gapless. The total energy, as opposed to the release energy, gives a completely smooth curve with positive curvature (hence a vanishing real gap and finite compressibility). The total energy curve is shown in Fig. 5.7 which confirms that the total energy is completely smooth even if the system contains regions which are locally Mott insulating. Therefore, even though we know a priori that the overall system is gapless, our approach makes it possible to provide an estimate of the gap of the local Mott insulators emerging within the system which is in good agreement and behaves like the gap of the homogeneous system. Furthermore, the effect of the discontinuities on the derivatives of the release energy signals the presence of Mott insulating regions, so it serves as a simple detector of their presence.

Finally, let us analyze the case of off-diagonal confinement in 1D, recently proposed by Rousseau and collaborators. [93] In the experimental setup, the release-energy measurement corresponds to the actual total energy of the trapped system, since in this case there is no potential energy because the trapping is induced by reducing the kinetic energy of the bosons as the borders of the system

are approached. In Fig. 5.8, we present the results for the 1D system with  $U/t = 15$ . We observe that the kinks in the energy curve occur exactly at values of the total number of bosons  $N$  which are commensurate with  $L$ , i.e., for integer densities  $n = N/L$ , as in a homogeneous case. The advantage of this kind of confinement is that it is possible to have a Mott-insulating phase throughout the whole lattice, as discussed in Ref. [93]. By using the energy curve, we find that the value of the gap at  $n = 1$  is  $E_g^{rel}/t \simeq 11.9$ , remarkably close to the corresponding value in the homogeneous system ( $E_g/t \simeq 11.8$ ) but slightly larger. This is mainly due to the fact that regions towards the border of the lattice are effectively in a deeper Mott phase due to their reduced kinetic energy. Away from integer densities, the system shows coexistence of compressible and incompressible states as in the harmonic confinement, with compressible sites always at the center of the trap and Mott sites on the borders, again due to the reduced kinetic energy there. It is clear that in the off-diagonal confinement the renormalization of the gap is significantly less pronounced because the whole system can attain a Mott-insulating phase, such that the physical situation is closer to that of the infinite case where the kink comes from the addition of particles to a fully homogeneous Mott phase.

## 5.4 Conclusion

In this chapter we have proposed a method to estimate the value of the Mott gap in presence of the confinement potential that is present in experiments with ultracold gases. Even though confined systems are generally expected to be gapless because of the coexistence of superfluid and Mott-insulating phases, the presence of Mott regions are revealed by the kinks present in the derivative of the release-energy curve. On the contrary, the total energy is completely smooth and has positive curvature even if the system possesses regions that are Mott insulating. In principle, in order to perform such energy measurements, no further experimental developments are required. All the information required to compute the release energy can be extracted from the well established time-of-flight experiments. In relation to the disordered system discussed in chapter 3, this method could be applied to determine the distributions of the charge gap that contain

## 5.4 Conclusion

---

useful information about the structure of the phases of the disordered system in presence of the confinement potential.

# Chapter 6

## Conclusions and perspectives

In this thesis we have studied the Bose-Hubbard model in presence of disorder by using numerical simulations based on variational and Green's function Monte Carlo. The Bose-Hubbard model with disorder is relevant for the description of systems including ultracold atoms in disordered optical lattices, short-correlation-length superconductors, granular superconductors, Josephson arrays, the dynamics of flux lattices in type-II superconductors, critical behavior of  $^4\text{He}$  in porous media, and magnetic systems with random chemical substitution in presence of external magnetic field, among many others. All those systems exhibit a superfluid to insulator transition driven by disorder like the one studied in this thesis. We have discussed the emergence of the Bose-glass phase in disordered bosonic systems and shown that a proper characterization of the emerging phases on finite disordered clusters requires the knowledge of probability distributions of physical quantities rather than their averages. This holds in particular for determining the stability region of the Bose-glass phase, where we have calculated the distribution probability of the gap. We have found that on finite clusters, the Bose glass is characterized by a broad distribution of the gap that is peaked at finite energy but extends down to zero, a shape remarkably reminiscent of preformed Hubbard sidebands with the Mott gap completely filled by Lifshitz's tails. The Mott transition occurs when these tails terminate at finite energy. On the contrary, the gap distribution in the superfluid phase turns out to be strongly peaked at zero energy. These results are particularly appealing for experiments with ultracold atoms, limited as they are to finite lattice sizes, where a similar statistical anal-

---

ysis of the gap distribution could be performed. The disordered Bose-Hubbard model on  $N$ -leg ladder systems has been investigated, emphasizing that these geometries could be quite useful to study the evolution from one to two spatial dimensions. We found that the intervening Bose glass is shrunk as we go from one dimension to two dimensions. We expect this strong tendency to continue as the dimensionality of the system is increased further until infinite dimension. Indeed, in the infinite dimension (mean-field) limit, the Bose glass is unstable towards superfluidity for any arbitrarily weak hopping and a direct transition from the superfluid to the Mott insulator takes place. [9] We have also considered the effect of disorder on a two-leg ladder as function of density and interchain hopping in the limit of infinite interaction strength, i.e., a ladder of hardcore bosons. We have found a superfluid phase stable with respect to Anderson localization, as opposed to the decoupled chains which Anderson localize by any amount of disorder. This superfluid phase is stabilized by the hopping between otherwise insulating chains. We have investigated the low-density phase diagram and found that the frozen Mott insulator with zero (or one) boson per site is separated from the superfluid phase by the Bose glass. We have also verified that disorder tends to destroy the gap of the clean version of the rung Mott insulator, which is a kind of gapped Mott insulator at exactly half filling  $n = 1/2$ , i.e., one hardcore boson per rung. We have argued that this phase is always surrounded by the Bose glass, such that a direct transition from the superfluid is forbidden in presence of disorder.

In connection with the experimental determination of the distribution probability of the gap, we have proposed a method to perform such measurements in presence of the unavoidable confinement potential of experiments with ultracold atoms. We have shown that the measurement of the so-called release energy, which can be addressed experimentally, makes it possible to assess the value of the Mott gap. We found that the curve of the release energy as a function of the total number of particles shows kinks in the first derivative that are related to the excitation gaps associated to the formation of Mott-insulating regions within the system. The presence of kinks is remarkable because, even though confined systems are generally gapless, the presence of Mott regions are revealed through them. In principle, no further experimental developments are required in order

---

to perform such measurements and all the information required to compute the release energy can be extracted from the well established time-of-flight experiments.

We have successfully described the disordered Bose-Hubbard model in low-dimensional lattices. We have not studied the effect of the trapping potential on the disordered system. That constitutes a possible direction of research to which we could aim, as that understanding is relevant for a direct comparison with experiments. Including the effect of temperature would allow us to get closer to experiments as well as to study numerically some recently conjectured finite temperature phase transitions of disordered interacting bosons in one dimension. [97] It is also important for the studies of ultracold bosons where recent experiments have demonstrated Anderson localization and further experiments in denser clouds where the interplay between disorder and interaction plays a major role are underway. [23] Furthermore, the study of the dynamics of expansion of interacting disordered systems is important as this test is nowadays being used for detecting localized phases experimentally. In order to study the dynamics of such systems, a real-time approach based on a variational wave function could be devised as a straightforward (and powerful) generalization of the variational method used in this thesis. This will allow the possibility to study the real-time dynamics of a great variety of complex systems.

## Acknowledgements

I would like to take this opportunity to thank the many people who have helped and encouraged me during the completion of my PhD studies. First and foremost, I would like to thank my supervisors Dr. Federico Becca and Prof. Michele Fabrizio for their guidance and encouragement. I thank Federico for his patience, great deal of care, and positive criticisms. I want also to thank Andrea Trombettoni, I benefited from a lot of discussions with him. To Professors Erio Tosatti, Giuseppe Santoro and Sandro Sorella my gratitude for their useful discussions and care. Special thanks to Maria Elisabetta Pezzoli, she helped me a lot at the beginning of my studies. To Giuseppe Carleo my gratitude for these years of discussions about physics and other less important matters, his generosity has no boundaries. I would like to thank the many great friends I made during these years, not at least being: Yanier Crespo, Marco Schirò, Lorenzo Paulatto, Gabriele Sclauzero, Armin Maleki, Giovanni Borghi, Angus Prain, among many others. To Dora Astrid, thanks for your encouragement and love. Special thanks also to my family, they were very supportive of me during this period. Finally, I would like to thank SISSA and all the staff members for their hospitality and help during the years of my PhD.

# Bibliography

- [1] Anderson, P. (1958) Absence of diffusion in certain random lattices. *Phys. Rev*, **109**, 1492. [iii](#)
- [2] Kramer, B. and MacKinnon, A. (1993) Localization: theory and experiment. *Reports on Progress in Physics*, **56**, 1469. [iii](#)
- [3] Wiersma, D. S., Bartolini, P., Lagendijk, A., and Righini, R. (1997) Localization of light in a disordered medium. *Nature*, **390**, 671–673. [iii](#), [19](#)
- [4] Scheffold, F., Lenke, R., Tweer, R., and Maret, G. (1999) Localization or classical diffusion of light? *Nature*, **398**, 206–270. [iii](#), [19](#)
- [5] Dalichaouch, R., Armstrong, J. P., Schultz, S., Platzman, P. M., and McCall, S. L. (1991) Microwave localization by two-dimensional random scattering. *Nature*, **354**, 53–55. [iii](#), [19](#)
- [6] Weaver, R. L. (1990) Anderson localization of ultrasound. *Wave Motion*, **12**, 129–142. [iii](#), [19](#)
- [7] Akkermans, E. and Montambaux, G. (2006) *Mesoscopic Physics of Electrons and Photons*. Macmillan Publishers Limited. All rights reserved. [iii](#), [19](#)
- [8] Goldhirsch, I., Levich, E., and Yakhot, V. (1979) Exact boson representation of quantum spin systems and investigation of their critical behavior. *Phys. Rev. B*, **19**, 4780–4795. [iii](#)

- [9] Fisher, M. P. A., Weichman, P. B., Grinstein, G., and Fisher, D. S. (1989) Boson localization and the superfluid-insulator transition. *Phys. Rev. B*, **40**, 546–570. [iii](#), [8](#), [10](#), [11](#), [12](#), [14](#), [15](#), [16](#), [51](#), [59](#), [84](#), [100](#)
- [10] Giamarchi, T. and Schulz, H. J. (1987) Localization and interaction in one-dimensional quantum fluids. *Europhys.Lett*, **3**, 1287. [iii](#), [12](#), [51](#)
- [11] Freericks, J. K. and Monien, H. (1996) Strong-coupling expansions for the pure and disordered bose-hubbard model. *Phys. Rev. B*, **53**, 2691–2700. [iv](#), [11](#), [14](#), [15](#), [16](#), [51](#), [54](#)
- [12] Scalettar, R. T., Batrouni, G. G., and Zimanyi, G. T. (1991) Localization in interacting, disordered, bose systems. *Phys. Rev. Lett.*, **66**, 3144–3147. [iv](#), [51](#), [54](#)
- [13] Krauth, W., Trivedi, N., and Ceperley, D. (1991) Superfluid-insulator transition in disordered boson systems. *Phys. Rev. Lett.*, **67**, 2307–2310. [iv](#), [14](#), [51](#), [54](#)
- [14] Pai, R. V., Pandit, R., Krishnamurthy, H. R., and Ramasesha, S. (1996) One-dimensional disordered bosonic hubbard model: A density-matrix renormalization group study. *Phys. Rev. Lett.*, **76**, 2937–2940. [iv](#), [14](#), [51](#), [54](#)
- [15] Lee, J.-W., Cha, M.-C., and Kim, D. (2001) Phase diagram of a disordered boson hubbard model in two dimensions. *Phys. Rev. Lett.*, **87**, 247006. [iv](#), [51](#), [54](#)
- [16] Prokof'ev, N. and Svistunov, B. (2004) Superfluid-insulator transition in commensurate disordered bosonic systems: Large-scale worm algorithm simulations. *Phys. Rev. Lett.*, **92**, 015703. [iv](#), [51](#), [54](#), [88](#)
- [17] Pollet, L., Prokof'ev, N. V., Svistunov, B. V., and Troyer, M. (2009) Absence of a direct superfluid to mott insulator transition in disordered bose systems. *Phys. Rev. Lett.*, **103**, 140402. [iv](#), [15](#), [16](#), [18](#), [51](#), [54](#), [84](#)
- [18] Gurarie, V., Pollet, L., Prokof'ev, N. V., Svistunov, B. V., and Troyer, M. (2009) Phase diagram of the disordered bose-hubbard model. *Phys. Rev. B*, **80**, 214519. [iv](#), [18](#), [51](#), [54](#), [84](#)

- [19] Mandel, O., Esslinger, T., Hansch, T. E., Greiner, M., and Bloch, I. (2002) Quantum phase transition from a superfluid to a mott insulator in a gas of ultracold atoms. *Nature*, **415**, 39–44. [v](#), [8](#), [11](#), [56](#), [86](#)
- [20] Billy, J., Josse, V., Zuo, Z., Bernard, A., Hambrecht, B., Lugan, P., Clément, D., Sanchez-Palencia, L., Bouyer, P., and Aspect, A. (2008) Direct observation of anderson localization of matter waves in a controlled disorder. *Nature*, **453**, 891–894. [v](#), [19](#), [21](#), [23](#)
- [21] D’errico, C., Fallani, L., Fattori, M., Fort, C., Zaccanti, M., Modugno, G., Modugno, M., Roati, G., and Inguscio, M. (2008) Anderson localization of a non-interacting bose–einstein condensate. *Nature*, **453**, 895–898. [v](#), [19](#), [21](#)
- [22] Lye, J. E., Guarrera, V., Fort, C., Fallani, L., and Inguscio, M. (2007) Ultracold atoms in a disordered crystal of light: Towards a bose glass. *Phys. Rev. Lett*, **98**, 130404. [v](#)
- [23] Zaccanti, M., Roati, G., D’errico, C., Fattori, M., Modugno, M., Modugno, G., Deissler, B., and Inguscio, M. (2010) Delocalization of a disordered bosonic system by repulsive interactions. *Nature physics*, **6**, 354–358. [v](#), [101](#)
- [24] McMillan, W. L. (1965) Ground state of liquid he<sup>4</sup>. *Phys. Rev.*, **138**, A442–A451. [v](#)
- [25] Chester, G. V., Ceperley, D., and Kalos, M. H. (1977) Monte carlo simulation of a many-fermion study. *Phys. Rev. B*, **16**, 3081–3099. [v](#)
- [26] Kalos, M. H. (1962) Monte carlo calculations of the ground state of three- and four-body nuclei. *Phys. Rev.*, **128**, 1791–1795. [v](#)
- [27] Buonaura, M. C. and Sorella, S. (1998) Numerical study of the two-dimensional heisenberg model using a green function monte carlo technique with a fixed number of walkers. *Phys. Rev. B*, **57**, 11446–11456. [v](#)
- [28] Greiner, M. and Folling, S. (2008) Condensed-matter physics: Optical lattices. *Nature*, **453**, 736–738. [2](#), [3](#), [86](#)

- [29] Grimm, R., Weidemüller, M., and Ovchinnikov, Y. N. (2000) Optical dipole traps for neutral atoms. *Adv. At. Mol. Opt. Phys*, **42**, 95. [2](#), [3](#)
- [30] Becker, C., Soltan-Panahi, P., Kronjäger, J., Dörscher, S., Bongs, K., and Sengstock, K. (2010) Ultracold quantum gases in triangular optical lattices. *New Journal of Physics*, **12**, 065025. [3](#)
- [31] Santos, L., Baranov, M. A., Cirac, J. I., Everts, H.-U., Fehrmann, H., and Lewenstein, M. (2004) Atomic quantum gases in kagomé lattices. *Phys. Rev. Lett.*, **93**, 030601. [3](#)
- [32] Bloch, I., Dalibard, J., and Zwerger, W. (2008) Many-body physics with ultracold gases. *Rev. Mod. Phys.*, **80**, 885–964. [5](#)
- [33] Chin, C., Grimm, R., Julienne, P., and Tiesinga, E. (2010) Feshbach resonances in ultracold gases. *Rev. Mod. Phys.*, **82**, 1225–1286. [5](#), [6](#)
- [34] Moerdijk, A. J., Verhaar, B. J., and Axelsson, A. (1995) Resonances in ultracold collisions of *li6*, *li7*, and *na23*. *Phys. Rev. A*, **51**, 4852–4861. [5](#)
- [35] Abraham, E. R. I., McAlexander, W. I., Sackett, C. A., and Hulet, R. G. (1995) Spectroscopic determination of the s-wave scattering length of lithium. *Phys. Rev. Lett.*, **74**, 1315. [6](#)
- [36] Zwierlein, M. W., Abo-Shaeer, J. R., Schirotzek, A., Schunck, C. H., and Ketterle, W. (2005) Vortices and superfluidity in a strongly interacting fermi gas. *Nature*, **435**, 1047–1051. [6](#)
- [37] Viverit, L. (2002) Boson-induced s-wave pairing in dilute boson-fermion mixtures. *Phys. Rev. A*, **66**, 023605. [6](#)
- [38] Jaksch, D., Bruder, C., Cirac, J. I., Gardiner, C. W., and Zoller, P. (1998) Cold bosonic atoms in optical lattices. *Phys. Rev. Lett.*, **81**, 3108–3111. [8](#), [11](#), [86](#), [88](#)
- [39] Stoferle, T., Moritz, H., Schori, C., Kohl, M., and Esslinger, T. (2004) Transition from a strongly interacting 1d superfluid to a mott insulator. *Phys. Rev. Lett.*, **92**, 130403. [12](#), [56](#), [71](#), [87](#), [89](#)

- [40] Spielman, I. B., Phillips, W. D., and Porto, J. V. (2007) Mott-insulator transition in a two-dimensional atomic bose gas. *Phys. Rev. Lett.*, **98**, 080404. [12](#)
- [41] C., B., Crooker, Hebral, H., Smith, E. N., Takano, Y., and Reppy, J. D. (1983) Superfluidity in a dilute bose gas. *Phys. Rev. Lett.*, **51**, 666. [12](#)
- [42] Weichman, P. B. (2008) Dirty bosons: Twenty years later. *Mod. Phys. Lett. B*, **22**, 2623–2647. [14](#), [16](#), [54](#)
- [43] Makivić, M., Trivedi, N., and Ullah, S. (1993) Disordered bosons: Critical phenomena and evidence for new low energy excitations. *Phys. Rev. Lett.*, **71**, 2307–2310. [14](#)
- [44] Svistunov, B. V. (1996) Superfluid–bose-glass transition in weakly disordered commensurate one-dimensional system. *Phys. Rev. B*, **54**, 16131–16134. [14](#)
- [45] Bissbort, U. and Hofstetter, W. (2009) Stochastic mean-field theory for the disordered bose-hubbard model. *EPL (Europhysics Letters)*, **86**, 50007. [14](#)
- [46] Krüger, F., Wu, J., and Phillips, P. (2009) Anomalous suppression of the bose glass at commensurate fillings in the disordered bose-hubbard model. *Phys. Rev. B*, **80**, 094526. [14](#), [16](#)
- [47] Hong, T., Zheludev, A., Manaka, H., and Regnault, L.-P. (2010) Evidence of a magnetic bose glass in  $(\text{CH}_3)_2\text{CHNH}_3\text{Cu}(\text{Cl}_{0.95}\text{Br}_{0.05})_3$  from neutron diffraction. *Phys. Rev. B*, **81**, 060410. [19](#), [25](#), [52](#), [72](#)
- [48] Aubry, S. and Andre, G. (1980) Analyticity breaking and anderson localization in incommensurate lattices. *Ann. Israel Phys. Soc.*, **3**, 133–140. [19](#), [20](#)
- [49] Goodman, J. W. (2007) *Speckle Phenomena in Optics*. Macmillan Publishers Limited. [21](#)
- [50] Clément, D., Varón, A. F., Retter, J. A., Sanchez-Palencia, L., Aspect, A., and Bouyer, P. (2006) Experimental study of the transport of coherent

- interacting matter-waves in a 1d random potential induced by laser speckle. *New Journal of Physics*, **8**, 165. [21](#)
- [51] Fallani, L., Lye, J. E., Guarrera, V., Fort, C., and Inguscio, M. (2007) Ultracold atoms in a disordered crystal of light: Towards a bose glass. *Phys. Rev. Lett.*, **98**, 130404. [23](#), [56](#), [89](#)
- [52] Fazekas, P. (1999) *Lecture notes on electron correlation and magnetism*. World Scientific. [24](#)
- [53] Giamarchi, T., Rugg, C., and Tchernyshyov, O. (2008) Bose-einstein condensation in magnetic insulators. *Nat Phys*, **4**, 198–204. [24](#), [72](#)
- [54] Sheshadri, K., Krishnamurthy, H. R., Pandit, R., and Ramakrishnan, T. V. (1993) Superfluid and insulating phases in an interacting-boson model: Mean-field theory and the rpa. *EPL (Europhysics Letters)*, **22**, 257. [28](#), [29](#), [89](#)
- [55] Buonsante, P., Massel, F., Penna, V., and Vezzani, A. (2009) Gutzwiller approach to the bose-hubbard model with random local impurities. *Phys. Rev. A*, **79**, 013623. [28](#), [89](#)
- [56] Capello, M., Becca, F., Fabrizio, M., and Sorella, S. (2008) Mott transition in bosonic systems: Insights from the variational approach. *Phys. Rev. B*, **77**, 144517. [30](#), [31](#), [53](#), [63](#), [88](#)
- [57] Pezzoli, M. E., Becca, F., Fabrizio, M., and Santoro, G. (2009) Local moments and magnetic order in the two-dimensional anderson-mott transition. *Phys. Rev. B*, **79**, 033111. [32](#), [54](#)
- [58] Metropolis, N., Rosenbluth, A. W., Rosenbluth, M. N., Teller, A. H., and Teller, E. (1953) Equation of state calculations by fast computing machines. *The Journal of Chemical Physics*, **21**, 1087–1092. [34](#)
- [59] Sorella, S., Santoro, G., and Becca, F. (2010) Sissa lecture notes on numerical methods for strongly correlated electrons, [www.sissa.it/~sorella/Simulazioni.pdf](http://www.sissa.it/~sorella/Simulazioni.pdf). [35](#), [43](#)

- [60] Sorella, S. (2005) Wave function optimization in the variational monte carlo method. *Phys. Rev. B*, **71**, 241103. [36](#)
- [61] Calandra Buonaura, M. and Sorella, S. (1998) Numerical study of the two-dimensional heisenberg model using a green function monte carlo technique with a fixed number of walkers. *Phys. Rev. B*, **57**, 11446–11456. [41](#), [46](#)
- [62] Trivedi, N. and Ceperley, D. M. (1990) Ground-state correlations of quantum antiferromagnets: A green-function monte carlo study. *Phys. Rev. B*, **41**, 4552–4569. [41](#)
- [63] Pollock, E. L. and Ceperley, D. M. (1987) Path-integral computation of superfluid densities. *Phys. Rev. B*, **36**, 8343–8352. [48](#)
- [64] Carrasquilla, J., Becca, F., Trombettoni, A., and Fabrizio, M. (2010) Characterization of the bose-glass phase in low-dimensional lattices. *Phys. Rev. B*, **81**, 195129. [52](#), [86](#)
- [65] Roscilde, T. (2009) Probing correlated phases of bosons in optical lattices via trap squeezing. *New Journal of Physics*, **11**, 023019. [56](#), [87](#), [96](#)
- [66] Rigol, M., Scalettar, R. T., Sengupta, P., and Batrouni, G. G. (2006) Time-of-flight observables and the formation of mott domains of fermions and bosons on optical lattices. *Phys. Rev. B*, **73**, 121103. [56](#), [87](#)
- [67] Rapsch, S., Schollwöck, U., and Zwerger, W. (1999) Density matrix renormalization group for disordered bosons in one dimension. *EPL (Europhysics Letters)*, **46**, 559. [56](#), [57](#)
- [68] Albiez, M., Gati, R., Fölling, J., Hunsmann, S., Cristiani, M., and Oberthaler, M. K. (2005) Direct observation of tunneling and nonlinear self-trapping in a single bosonic josephson junction. *Phys. Rev. Lett.*, **95**, 010402. [61](#)
- [69] Gemelke, N., Zhang, X., Hung, C.-L., and Chin, C. (2009) In situ observation of incompressible mott-insulating domains in ultracold atomic gases. *Nature*, **460**, 995–998. [62](#)

- [70] Bakr, W. S., Peng, A., Tai, M. E., Ma, R., Simon, J., Gillen, J. I., Folling, S., Pollet, L., and Greiner, M. (2010) Probing the Superfluid-to-Mott Insulator Transition at the Single-Atom Level. *Science*, **329**, 547–550. [62](#)
- [71] Sherson, J. F., Weitenberg, C., Endres, M., Cheneau, M., Bloch, I., and Kuhr, S. (2010) Single-atom-resolved fluorescence imaging of an atomic mott insulator. *Nature*, **467**, 68–72. [62](#)
- [72] Jordan, P. and Wigner, E. (1928) Über das paulische äquivalenzverbot. *Zeitschrift für Physik A Hadrons and Nuclei*, **47**, 631–651. [67](#), [71](#)
- [73] Carmona, R. and Lacroix, J. (1990) *Spectral Theory Of Random Schrödinger operators*. Birkhauser. [68](#)
- [74] Fazio, R. and van der Zant, H. (2001) Quantum phase transitions and vortex dynamics in superconducting networks. *Physics Reports*, **355**, 235 – 334. [71](#)
- [75] Paredes, B., Widera, A., Murg, V., Mandel, O., Folling, S., Cirac, I., Shlyapnikov, G. V., Hansch, T. W., and Bloch, I. (2004) Tonks-girardeau gas of ultracold atoms in an optical lattice. *Nature*, **429**, 277–281. [71](#)
- [76] Kinoshita, T., Wenger, T., and Weiss, D. S. (2004) Observation of a One-Dimensional Tonks-Girardeau Gas. *Science*, **305**, 1125–1128. [71](#)
- [77] Rigol, M. and Muramatsu, A. (2004) Universal properties of hard-core bosons confined on one-dimensional lattices. *Phys. Rev. A*, **70**, 031603. [71](#)
- [78] Orignac, E. and Giamarchi, T. (1998) Vortices in coupled planes with columnar disorder and bosonic ladders. *Phys. Rev. B*, **57**, 11713–11729. [71](#), [72](#), [78](#)
- [79] Orignac, E. and Giamarchi, T. (1997) Effects of disorder on two strongly correlated coupled chains. *Phys. Rev. B*, **56**, 7167–7188. [71](#)
- [80] Danshita, I., Williams, J., S de Melo, C., and Clark, C. (2008) Quantum phase transition of ultracold bosons in double-well optical lattices. *Laser Physics*, **18**, 318–321. [72](#)

- [81] Danshita, I., Williams, J. E., Sá de Melo, C. A. R., and Clark, C. W. (2007) Quantum phases of bosons in double-well optical lattices. *Phys. Rev. A*, **76**, 043606. [72](#)
- [82] Albiez, M., Gati, R., Fölling, J., Hunsmann, S., Cristiani, M., and Oberthaler, M. K. (2005) Direct observation of tunneling and nonlinear self-trapping in a single bosonic josephson junction. *Phys. Rev. Lett.*, **95**, 010402. [72](#)
- [83] Carrasquilla, J., Becca, F., Laflorencie, N., and Fabrizio, M. (2010) The onset of superfluidity of hardcore bosons in disordered ladders. *In preparation*. [73](#)
- [84] Laflorencie, N. and Rieger, H. (2004) Scaling of the spin stiffness in random spin- $\frac{1}{2}$  chains; crossover from pure-metallic behaviour to random singlet-localized regime. *The European Physical Journal B - Condensed Matter and Complex Systems*, **40**, 201–207. [75](#)
- [85] Block, M. S., Mishmash, R. V., Kaul, R. K., Sheng, D. N., Motrunich, O. I., and Fisher, M. P. A. (2010) Exotic gapless mott insulators of bosons on multi-leg ladders. <http://arxiv.org/abs/1008.4105>. [75](#)
- [86] Lewenstein, M., Sanpera, A., Ahufinger, V., Damski, B., Sen, A., and Sen, U. (2007) Ultracold atomic gases in optical lattices: mimicking condensed matter physics and beyond. *Advances In Physics*, **56**, 243–379(137). [86](#)
- [87] Batrouni, G. G., Rousseau, V., Scalettar, R. T., Rigol, M., Muramatsu, A., Denteneer, P. J. H., and Troyer, M. (2002) Mott domains of bosons confined on optical lattices. *Phys. Rev. Lett.*, **89**, 117203. [86](#), [96](#)
- [88] Wessel, S., Alet, F., Troyer, M., and Batrouni, G. G. (2004) Quantum monte carlo simulations of confined bosonic atoms in optical lattices. *Phys. Rev. A*, **70**, 053615. [86](#)
- [89] Pupillo, G., Williams, C. J., and Prokof'ev, N. V. (2006) Effects of finite temperature on the mott-insulator state. *Phys. Rev. A*, **73**, 013408. [86](#)

- [90] Rigol, M., Batrouni, G. G., Rousseau, V. G., and Scalettar, R. T. (2009) State diagrams for harmonically trapped bosons in optical lattices. *Phys. Rev. A*, **79**, 053605. [86](#)
- [91] Schroll, C., Marquardt, F., and Bruder, C. (2004) Perturbative corrections to the gutzwiller mean-field solution of the mott-hubbard model. *Phys. Rev. A*, **70**, 053609. [86](#), [88](#)
- [92] Dalfovo, F., Giorgini, S., Pitaevskii, L. P., and Stringari, S. (1999) Theory of bose-einstein condensation in trapped gases. *Rev. Mod. Phys.*, **71**, 463–512. [87](#)
- [93] Rousseau, V. G., Batrouni, G. G., Sheehy, D. E., Moreno, J., and Jarrell, M. (2010) Pure mott phases in confined ultracold atomic systems. *Phys. Rev. Lett.*, **104**, 167201. [87](#), [96](#), [97](#)
- [94] Rokhsar, D. S. and Kotliar, B. G. (1991) Gutzwiller projection for bosons. *Phys. Rev. B*, **44**, 10328–10332. [88](#)
- [95] Krauth, W., Caffarel, M., and Bouchaud, J.-P. (1992) Gutzwiller wave function for a model of strongly interacting bosons. *Phys. Rev. B*, **45**, 3137–3140. [88](#), [90](#)
- [96] Carrasquilla, J. and Becca, F. (2010) Extracting the mott gap from energy measurements in trapped atomic gases. *Phys. Rev. A*, **82**, 053609. [88](#)
- [97] Aleiner, I. L., Altshuler, B. L., and Shlyapnikov, G. V. (2010) A finite-temperature phase transition for disordered weakly interacting bosons in one dimension. *Nat Phys.* [101](#)